Investigation of Lipid-based Drug Delivery Vehicle using Molecular Dynamics Simulations

Xie, Joanna

Awarding institution:
King's College London

Investigation of Lipid-based Drug Delivery Vehicle using Molecular Dynamics Simulations

Jun Xie

Department of Physics
King's College London

This dissertation is submitted for the degree of
Doctor of Philosophy

October 2024

Acknowledgements

I would like to express my deepest gratitude to my supervisor, Prof. Chris Lorenz, for his exceptional mentorship, unwavering support, and invaluable guidance throughout this research endeavor. I am really grateful for the encouragement, and constructive feedback from him and all these have been pivotal in shaping this thesis and my academic growth. And also would like to extend my appreciation for the computational resources from King's College London and EPSRC.

I extend heartfelt thanks to all amazing people in Lorenz Lab for their insightful suggestions, critical evaluation, and scholarly input, which have significantly enriched the quality of this work. Special appreciation goes to Paul Smith, Hrachya Ishkhanyan, Sze May Yee, Raquel Lopez-Rios De Castro, Jirawat Assawkhajornsak, Rob Ziolek, Dr Alejandro Santana-Bonilla and Melissa Jade Mitchell for their assistance in various aspects of this research, including data collection, analysis and python script preparation. Their expertise and dedication have been instrumental in achieving the objectives of this study. To Natasha Rhys, Javier Garcia-Ruiz, Alice Pettitt, Miruna Serian, Zhiwen Zhong and Xilan Wang, I am so grateful to for your encouragement, support, and stimulating discussions. Your friendship have provided me with a conducive environment for intellectual growth and personal development.

My deepest appreciation goes to my family. Thank you to my parents, my dad Yongqiang, and my mom Wuliang, who have shown unwavering love, encouragement, and made sacrifices throughout this journey. Their belief in me has been a constant source of motivation, and I am profoundly grateful for their enduring support. And also my grandparent, for their unconditional love and support along the way.

Last but not least, I extend my sincere thanks to all the participants who generously contributed their time and insights to this study. Their willingness to participate and share their experiences have been invaluable and have contributed significantly to the outcomes of this research.

Abstract

The development of nanoparticle formulations, particularly lipid-based nanoformulations, holds immense potential in drug delivery applications owing to their biocompatibility and versatility. Recent successes, such as lipid nanoparticles (LNPs) in delivering COVID vaccines, underscore their significance. Phosphatidylcholine (PC) lipids, major constituents of cell membranes, possess self-assembling properties, forming various nanostructures including bilayers and micelles. However, understanding the dynamics of lipid-based nanoformulations is crucial for optimizing drug delivery efficiency. One challenge in computational studies of drug targets has been the determination of membrane protein structures. Achieving high drug loading efficiency while maintaining the stability of the micelles is a significant challenge. The ability of the micelles to effectively encapsulate and retain drugs can vary depending on factors such as drug hydrophobicity, micelle composition, and preparation methods.

In this thesis, extensive atomistic molecular dynamics simulations were conducted to investigate various lipid-based drug delivery systems, aiming to elucidate the underlying mechanisms governing their behavior and interactions. The focus was on understanding the internal and interfacial structures and properties of micelles, as well as exploring the influence of different lipid compositions on micellar dynamic systems and drug localization within micelles. Our findings elucidate the unique effects of different micelle components on membrane properties, shedding light on the molec-

ular mechanisms underlying drug delivery processes. Understanding how drugs interact with micelles is crucial for optimizing drug delivery systems.

In the subsequent chapter, the complex interplay between drugs and lipid-based micelles was investigated, revealing distinct preferences of Camptothecin (CAMPT) and Doxorubicin (DOX) within micellar environments. Disparities between PP-micelle and PL-micelle systems underscore the significance of lipid composition in dictating micellar stability and dynamics. Detailed analyses of micelle composition, internal structure, and hydration behaviors provide insights for optimizing drug delivery systems. Further investigations in subsequent chapters focus on drug orientation, localization, and hydration behavior within Solid Lipid Nanoparticles (SLN) and Liquid Lipid Nanoparticles (LLN) systems. Results highlight differences between SLN and LLN in drug encapsulation and distribution, offering implications for nanoparticle design and drug delivery efficacy.

In conclusion, the comprehensive exploration of lipid-based drug delivery systems through atomistic molecular dynamics simulations offers valuable insights into their behavior and interactions. Emphasizing the influence of lipid composition on micellar stability and dynamics, this research provides a foundation for the design of lipid-based drug delivery vehicles. Furthermore, the importance of tailoring drug-micelle interactions to specific drug properties is highlighted, with implications for the advancement of drug delivery systems, particularly in the realm of cancer therapy.

Publication

Jun Xie Demi L Pink, M Jayne Lawrence, and Christian D Lorenz. Digestion of lipid micelles leads to increased membrane permeability. Nanoscale, 16(5):2642–2653, 2024.

Table of contents

List of figures

List of tables

Chapter 1

Introduction

1.1 Lipids

Lipids, in broad terms, can be classified as hydrophobic or amphiphilic small molecules. The amphiphilic nature of certain lipids grants them the ability to organize into structures such as vesicles, liposomes, or membranes when placed in an aqueous environment. This characteristic reflects the dual affinity of amphiphilic lipids, possessing both hydrophobic and hydrophilic properties, enabling them to arrange in specific configurations that are vital for various biological functions. Lipids encompass a wide range of organic compounds, including fats, waxes, sterols, fat-soluble vitamins (A, D, E, K), monoglycerides, diglycerides, phospholipids, etc. They play crucial roles in storing energy, signaling, and as structural components in cell membranes and they have applications in the cosmetic and food industries, as well as in nanotechnology.[3–6]

The lipid bilayer, a fundamental structural component of cells, serves as a functional barrier that provides subcellullar compartments and separates the cell from its external environment. Lipids extend beyond their structural role in membranes; they serve as energy sources, signaling molecules, plat-

forms for protein recruitment, and substrates for post-translational protein-lipid modifications.[7–9] For instance, the signalling lipids have diverse structures so that it can mediate specific ligand-receptor interactions.[10]

The lipid composition also plays a crucial role in facilitating membrane deformation through spontaneous curvature, which refers to the preferred curvature of a membrane or interface based on the intrinsic properties of its constituent molecules. This tendency is determined by the molecular shape and the balance between the sizes of the hydrophobic and hydrophilic regions. Positive spontaneous curvature leads to structures like spherical micelles, which minimize the exposure of hydrophobic tails to water by clustering them together inside a spherical formation. Zero spontaneous curvature leads to flat bilayers and negative spontaneous curvature can lead to inverse structures, such as inverted micelles.[11, 12] Lipids containing long and saturated fatty acids, such as sphingolipids, contribute to thicker and less fluid membranes. This effect is because of the tight packing of their hydrophobic tails and the resulting stronger lipid–lipid interactions. In contrast, unsaturated lipids have the opposite impact due to kinks in their acyl chains, which prevent tight packing amongst these chains and lead to increased membrane fluidity. In artificial lipid membranes, the interplay of saturated lipids, unsaturated lipids, and cholesterol is dynamic and influenced by their ratio. This dynamic interplay results in the formation of distinct regions characterized by high lipid packing, known as liquid-ordered domains, and regions with less lipid packing, referred to as liquid-disordered domains. [13–16]

1.1.1 Phospholipids

Phospholipids are the main components of the cellular membrane. A typical phospholipid is composed of two hydrophrobic fatty acid tails, glycerol

and a phosphate-linked head group thus it is renowned for the amphiphlilic structures (in Figure 1.1). Due to their ability to self-assemble into other structures (e.g. lysosomes and micelles), they are also commonly used in drug delivery vehicles at various concentrations. Phospholipids are also very important components of the structure for the lipid nanoparticles(LNPs) and also help the process of endosomal escape.[17] Self-assembled phosphopilids in an aqueous milieu are able to produce various supermolecular structures. Small changes in the length of lipid tail can noticeably alter not only the concentration that lipids self-assemble in solution but also the nature of aggregation. Lipid nanoparticles were used along with mRNA strands encoding the SARS-CoV-2 Spike glycoprotein in the COVID-19 mRNA vaccines.[18] In recent years, phospholipid-based DDS have been found to be effective in delivering a variety of drugs, such as Silybin Phytosomem[19], Doxorubicin etc.[20] One type of phosphpilid that has attracted great interest is phosphatidylcholine (PC). Just like many other lipids, it can be modified to self-assemble into micelles or other nanoparticles for specific uses, which have excellent biocompatibility and an amphiphilic characteristic for transporting both hydrophilic and hydrophobic agents.

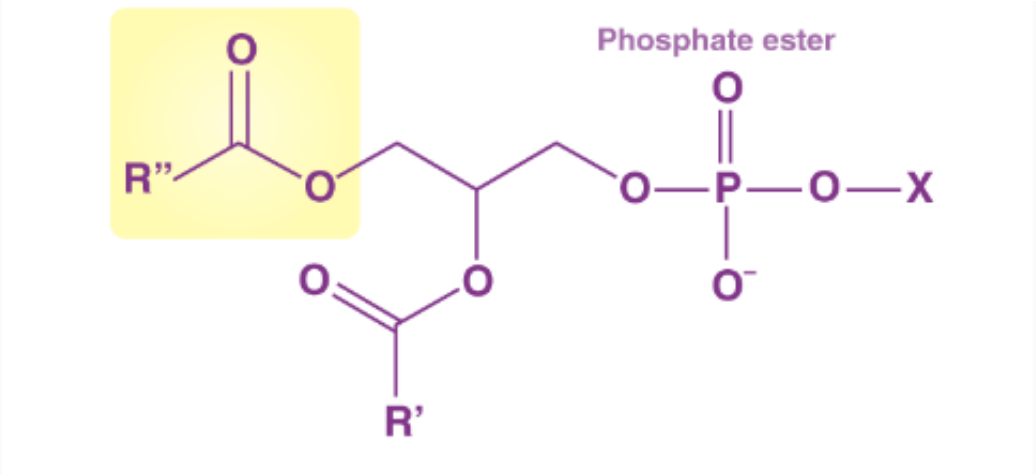

Fig. 1.1 Phospholipids structure: the fatty acid esters highlighted in yellow.

Phospholipids are classified based on their head groups, giving rise to subclasses like phosphatidylcholine (PC), phosphatidylethanolamine (PE), phosphatidylserine (PS), and phosphatidylinositol (PI). Phospholipids are crucial for forming lipid bilayers, providing structural integrity to biological membranes and influencing their fluidity. The lipid bilayer acts as a selective barrier, regulating the passage of substances into and out of cells based on the hydrophobic or hydrophilic nature of the molecules.[21–23] It also participates in intracellular signaling, serving as platforms for signaling proteins and activating pathways that control cell division, growth, and calcium signaling.[24] Additionally the fatty acid tails of phospholipids can be enzymatically cleaved for energy production through β-oxidation and certain phospholipids serve as precursors for bioactive lipid mediators involved in inflammation, immunological responses, and blood coagulation. The saturated and unsaturated fatty acids' structures in Figure 1.2 display different properties as stated previously.[25]

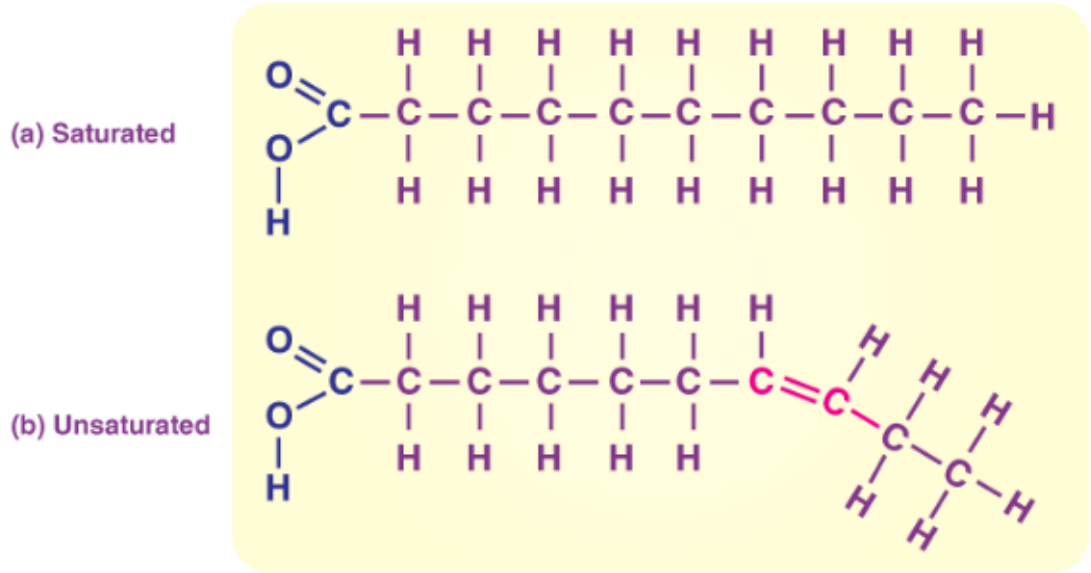

Fig. 1.2 The lipid structure - Saturated (a) and Unsaturated fatty acids (b). Adapted with permission from ref.[26]

1.1.2 Triglycerides

Triglycerides are a type of lipid, which are the most common form of fat in the human body and in food. It is normally composed of three fatty acid molecules covalently bonded to a glycerol molecule. The fatty acids can be different types, including saturated or unsaturated.[27, 28] Glycerol is a three-carbon alcohol that serves as the backbone of triglyerides and each carbon in the glycerol molecule forms an ester bond with a fatty acid. Through a process called esterification, triglycerides can be formed, where the hydroxyl (OH) groups of glycerol react with the carboxyl groups of fatty acids. This reaction release three water molecules and forms ester bonds between glycerol and the fatty acids. [29]

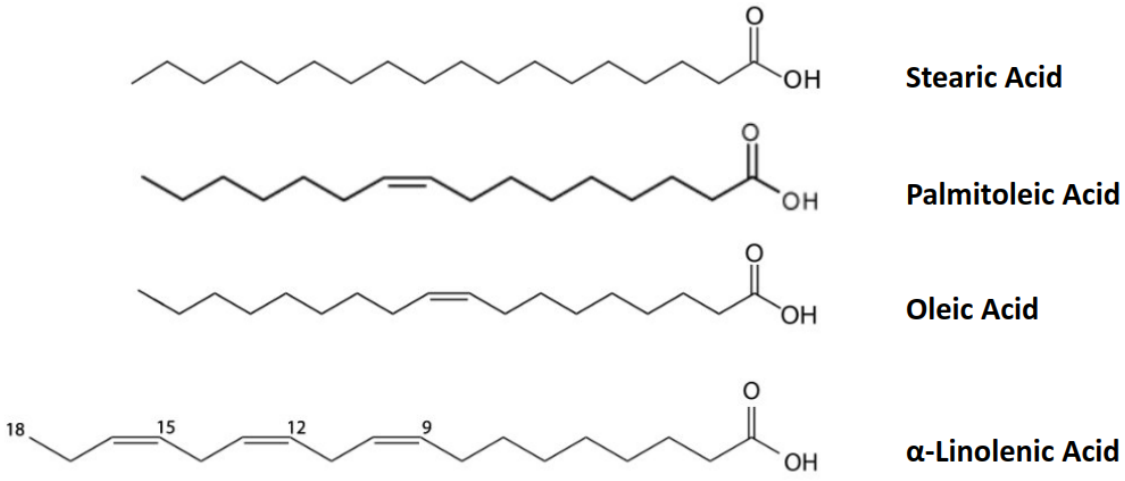

Fig. 1.3 Illustrations of some examples for the saturated and unsaturated triglycerides.

The saturated acids have no double bonds between carbon atoms in the fatty acid chain so they are typically solid at room temperature and commonly found in animals fats, such as stearic acid shown in Figure 1.3. In contrast, the unsaturated triglycerides have one or more double bonds between carbon atoms in the fatty acid chain (palmitoleic acid in Figure 1.3. Depending on the number of double bonds, they are classified as

monounsaturated or polyunsaturated, such as oleic acid and α-linolenic acid respectively in Figure 1.3. Unsaturated fats are usually liquid at room temperature and are commonly found in plant oils. [30–32]

Self-assembled Structures

As phospholipids are amphiphilic molecules, meaning they have both hydrohilic (water-loving) and hydrophobic (water-repelling) regions, spontaneously organize into various structures, driven by the interactions between their different components (in Figure 1.4).

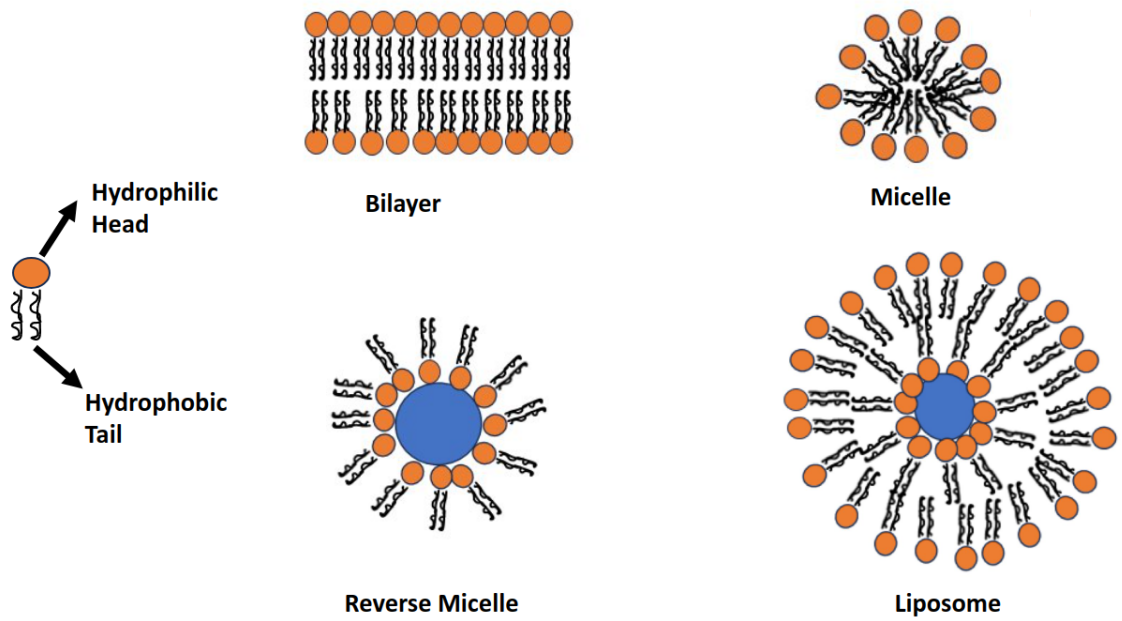

Fig. 1.4 The self-organization of phospholipids results in the formation of distinct structures with unique properties and functions. These structures are liposomes, micelles, reverse micelle and lipid bilayers.

The most crucial self-organization of phospholipids occurs in cell membranes. Cell membranes are primarily composed of a lipid bilayer, where phospholipids arrange themselves into two layers with hydrophilic heads facing outward and hydrophobic tails facing inward, shown in Figure 1.4.

This lipid bilayer provides a selective barrier, controlling the passage of ions and molecules into and out of the cell. [33, 34, 8]

In an aqueous solution, phospholipids can organize themselves into micelles. Micelles are spherical structures where the hydrophilic heads of phospholipids face outward, interacting with water, while the hydrophobic tails are tucked in the core, shielded from the surrounding aqueous environment. This formation is driven by the hydrophobic effect, which is a fundamental driving force for the self-assembly of molecules in aqueous environments. This effect arises from the tendency of hydrophobic (water-repelling) molecules to minimize their contact with water. When hydrophobic molecules aggregate, they reduce the overall free energy of the system by decreasing the entropy loss associated with the structured water molecules that surround them.[35–37] Micelles are used in drug delivery to solubilize hydrophobic drugs in their core. The hydrophilic shell helps in stabilizing the micelle and improving its circulation time in the bloodstream. In contrast, a reverse micelle forms in a nonpolar or less polar polar solvent, which the hydrophilic heads face inwards, creating a water core surrounded by the hydrophobic tails.[38–40]

Liposomes are another common self-organized structure formed by phospholipids (Figure 1.4). They are essentially a lipid bilayer assembled into a spherical nanoparticle. Similar to micelles, the hydrophilic heads of phospholipids are oriented toward the aqueous environment, both on the inner and outer leaflet of the bilayer which makes up the vesicle, while the hydrophobic tails are sandwiched between the lipid layers. Additionally, liposomes are versatile drug delivery vehicles, which they can encapsulate both hydrophobic drugs within the lipid bilayer and hydrophilic drugs in the aqueous core. They can be used to improve drug targeting, reduce toxicity, and enhance the stability of certain drugs.[41–43]

The critical micelle concentration (CMC) is a crucial parameter in the self-organization of phospholipids.[44] It represents the concentration at which micelles start to form in a solution. Below the CMC, phospholipids exist as individual molecules, but above this concentration, they aggregate to form micelles or other self-organized structures. Eccentially, the self-organization of phospholipids into liposomes, micelles, and lipid bilayers highlights their ability to spontaneously form diverse structures with specific functionalities. These structures play critical roles in biological systems, technological applications, and pharmaceutical advancements.

1.2 Drug Delivery Systems

Effective drug delivery is primary for ensuring optimal therapeutic outcomes. However, achieving efficient oral exposure poses significant challenges, especially in terms of drug absorption across the gastrointestinal tract (GIT). Various factors contribute to the success of drug absorption, including stability and solubility in gastrointestinal fluids, adequate intestinal permeability, and resistance to metabolism within both the enterocyte and the liver. In recent years, there has been a notable surge in the development of new chemical entities (NCE) where low aqueous solubility emerges as a significant obstacle to absorption. Addressing these challenges requires innovative drug delivery systems that can enhance drug bioavailability and therapeutic efficacy.[45–47]

Drug delivery systems (DDS) are designed to enhance the therapeutic efficacy of drugs by improving their pharmacokinetic and pharmacodynamic properties.[48] Traditional DDS face challenges related to unpredictable mechanisms of absorption, distribution, metabolism, and excretion within

the body, leading to suboptimal drug levels at the intended site or negative impacts on healthy tissues.

To address these limitations, various DDS have been developed to control drug release and bioavaibility, ensuring targeted drug delivery to specific cells or tissues. Oral DDS like enteric-coated tablets[49] or sustained-release formulations[50] are some examples that designed to deliver drugs optimally in the GIT. Nanotechnology-based DDSs, utilizing nanoparticles, liposomes, dentrimers, and other nanoscale materials, have gained attention. These systems encapsulate drugs, improving solubility and protecting them from degradation or elimination by the body. Additionally, nanotechnology enables targeted drug delivery to specific cells or tissues, such as cancer cells, by leveraging unique features of the tumor micro-environment or cell surface receptors.[51–53]

Advanced DDSs aim to precisely deliver drugs to the intended target while minimizing adverse effects. The continuous evolution of technologies and approaches in this field is expected to play a crucial role in enhancing the efficacy safety, and convenience of drug therapies in modern medicine. Although there has been extensive exploration of both polymeric and lipid-based nanoparticles for delivering drugs, the works that are presented in this thesis will specifically delve into lipid-based nanocarriers.

1.2.1 Nanocarriers Explored for Drug Delivery

Nanomedicine represents a rapidly advancing field with profound implications for cancer diagnosis and treatment. Nanoparticles, characterized by their small diameter size (typically 1-100 nm) and large surface area relative to volume, possess distinctive biological attributes. This unique combination enables them to efficiently bind, absorb, and transport anticancer agents,

including drugs, DNA, RNA, and proteins, as well as imaging agents. In chemotherapy, nanocarriers fall into two primary categories based on their intended mode of drug delivery: targeted and non-targeted. These vehicles utilize organic molecules as a major building block and inorganic elements (often metals) as their core materials. Organic nanocarriers are found in variety of structures such as liposomes, lipids, dendrimers, carbon nanotubes, synthetic polymers and emulsions.[54, 55] The advantages of these nanocarrier formulations are summarised in Figure .1.5 show.

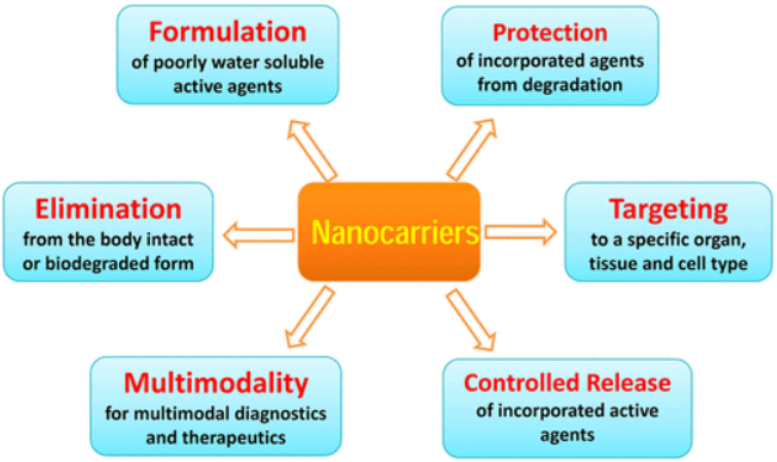

Fig. 1.5 Advantages of nanocarrier formulations in medicine field

Lipid nanoparticles (LNPs) have revolutionized drug delivery systems through their applications in delivering siRNA to the liver (in the case of Onpattro[56]), and being integral components in the development of mRNA vaccines by Pfizer-BioNTech and Moderna for COVID-19.[57, 58]

1.2.2 Lipid Nanoparticles (LNPs)

Nanostructed lipid carriers are composed of a blend of solid and liquid lipids, typically in ratios ranging from 70:30 or 99.9:0.1.[59] By mixing solid and liquid lipids in different ratios, the combination allows for the

creation of a less order (liquid) lipid nanoparticles (LLN), providing more space for the active components. Lipid-based nanoparticles, including liposomes, solid lipid nanoparticles (SLN), and nanostructured lipid carriers (NLC), have garnered significant attention in drug discovery and cancer treatment. These lipid nanosystems can incorporate chemical modification to avoid immune detection (utilizing substances like gangliosides or polyethylene glycol (PEG)) and enhencing drug solubility. Furthermore, lipid-based nanoparticles can be synergistically employed with other therapeutic strategies to enhance patient responses. Numerous antitumor agents, including cisplatin, irinotecan (IRI), paclitaxel (PTX), doxorubicin (DOX), oxaliplatin, daunorubicin, cytarabine, or vincristine, have been investigated in nanoformulations. Some of these formulations have undergone analysis in clinical trials and/or are commercially available for clinical use in patients.[60, 61]

General Composition and Structure of LNPs

The origin of lipid nanoprticles (LNPs) can be traced back to the 1990s, with significant contributions from Cullins group, who pioneered research on pH-sensitive LNPs.[62] LNPs are constructed with an outer layer comprising a mixture of functional and helper lipids. Functional lipids are primarily represented by an ionizable cationic lipid, while helper lipids encompass substances, like distearoyl phosphatidylcholine (DSPC), dioleoyl phosphatidylcholine (DOPC), dioleoyl phosphatidylethanolamine (DOPE), stearoyl oleoyl phosphocholine (SOPC), polyethylene glycol-lipid (PEG-lipid), and cholesterol.[63, 64] Figure.1.6 shows that a typical lipid nanoparticles structure allows modular encapsulation of both small and large mass drugs. It is often designed to encapsulate various types of cargoes for drug delivery.

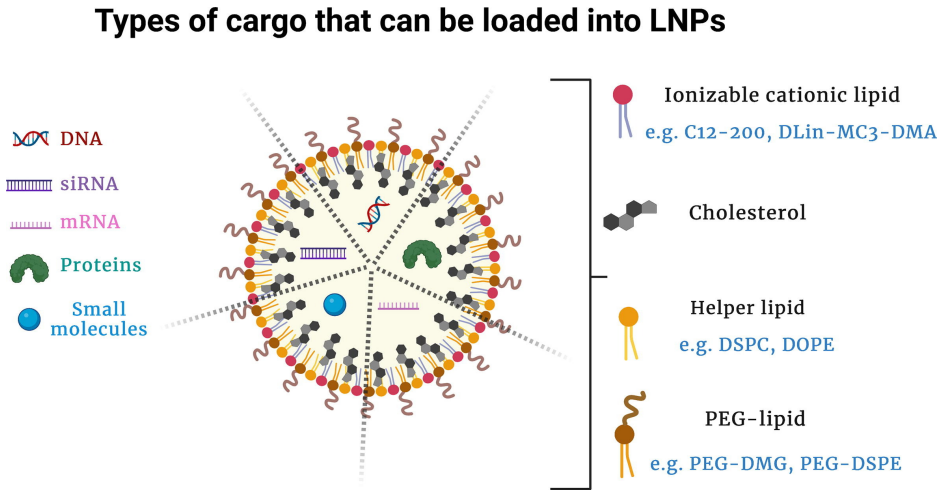

Fig. 1.6 The general structure and composition of LNPs (Lipid Nanoparticles) with various lipid components. Reproduced with permission from ref. [65]

These lipidic components play a crucial role in maintaining the structural integrity of LNPs, thereby their enhancing their stability and ensuring the effective intracellular delivery of the payload. PEG-lipid components like polyethylene glycol-dimyristoyl glycerol (PEG-DMG), polyethylene glycol-distearoyl phosphoethanolamine (PEG-DSPE), polyethylene glycol-distearoylglycerol (PEG-DSG), PEG-cholesterol, PEG-chondroitin sulfate, and others provide steric stability to LNPs by limiting particle aggregation, maintaining low particle diameters, and promoting the long-term colloidal stability of LNPs.[66, 67]

LNPs as Drug Delivery Vehicles

While the scaling up of formations remains a challenge in the clinical translation of many nanotherapeutics, LNPs stand out as they have successfully overcome this hurdle. Unlike most nanoparticles, LNPs have undergone scale-up with predictable colloidal attributes and demonstrated in viva efficacy, enhancing their clinical translatability.[68] Thus, this subsection

provides the most significant advances made in recent years about the used of LNPs in the treatment of the most common types of cancer.

A number of anticancer drugs have been encapsulated in solid lipid nanoparticles (SLNs) and investigated in both in vitro and in vivo studies since the 1990s. These drug classes include anthracyclines, taxanes, camptothecins, etoposide, fluorodeoxyuridine, and retinoic acid.[69–72] Animal experiments have demonstrated that SLNs can increase the area under the curve (AUC) of encapsulated drugs by 3- to 20-fold, along with a significant extension of the half-life of the encapsulated agent compared to the corresponding free drug. The AUC provides valuable information about the overall exposure of the body to a drug, taking into account both the extent (how much) and the duration (how long) the drug remains in the bloodstream. A larger AUC generally indicates greater drug exposure.[73, 74] Additionally, the stealth form of SLNs, achieved through PEGylation, further enhances the AUC and the half-life of encapsulated drugs more than non-stealth SLNs. Previous investigations on the cytotoxicity of cholesteryl butyrate, doxorubicin (DOX), and paclitaxel (PTX) encapsulated SLNs were conducted in the human colorectal HT-28 cancer cell line.[72]

Nanostructured lipid carriers (NLPs) is a second generation of lipid-based nanoparticles, building upon the foundation of SLPs. NLCs are developed from SLPs to address their limitations by combining solid and liquid lipids, such as glyceryl tricaprylate, ethy oleate, isopropyl myristate, and glyceryl dioleate. This combination provides flexibility in formation and improve the stability of encapsulated drugs. Thus, NLCs aim to enhance drug loading capacity and prevent drug expulsion during storage, which can occur due to lipid crystallization in SLNs. The mean particle size is comparable to SLPs, typically ranging from 10 to 1000 nm. The particle size can vary depending on the lipid composition and the manufacturing process

utilized. Despite their advantages, NLCs may still face challenges such as drug expulsion after polymorphic transitions of lipids during storage and relatively lower drug loading capacity compared to other nanocarriers.[75]

There are several notable contributions in the field of nanoparticle-based drug delivery systems, particularly the application of NLCs. Fluvastatin, when combined with lipoic acid and ellagic acid in an NLC formulation, demonstrates potential for prostate cancer therapy.[76] The combination shows enhanced efficacy in inducing cell death compared to free drugs, suggesting promising prospects for cancer treatment. Artesunate nanoparticles, modified with hyaluronic acid and cell-penetrating peptides, demonstrated efficient targeting and penetration of tThe properties of polymeric micelles, including their ability to load drugs and their fate in vivo, are influenced by the design of the amphiphilic block copolymers. Ideally, polymeric micelles should efficiently load, protect, deliver, and release the entrapped cargo at the targeted site with favorable pharmacokinetic characteristics. Amphiphilic polymers can be structured in various ways, such as having randomly combined monomer units with different hydrophobicities represented by two conjugated blocks (A-B type copolymers) or alternating blocks with different hydrophobicities (A-B-A type copolymers). Alternatively, the hydrophilic backbone chain of a polymer can be grafted with hydrophobic blocks (graft copolymers)umor cell membranes. This targeted delivery system showed promising results against cancer HepG2 cells, indicating its potential in cancer therapy with enhanced efficacy and specificity.[77] NLCs loaded with orcinol-glycoside and coated with polyethylene glycol (PEG) exhibited anticancer activity against gastrointestinal cancer cell lines and hepatoma.[78] This nanoformulation shows promise for oral delivery, suggesting its potential as an effective and convenient treatment option for certain types of cancer.[79]

Recently, a diverse range of liposomally encapsulated anticancer drugs has obtained clinical approval and is commercially available, with numerous other formulations under investigation across various stages of clinical trials or awaiting approval. Advancements in liposomal design have given rise to the next generation of lipid-based nanoparticles, such as lipid micelles, solid lipid nanoparticles, nanostructured lipid carriers, and lipid-polymer hybrid nanoparticles. These innovations are believed to address current limitations observed in liposome technology. Nevertheless, further research is needed to optimize their capabilities as drug delivery systems. Alongside other forms of targeted drug delivery systems, liposomes and lipid-based nanoparticles are poised to enhance the efficacy and safety profile of anticancer agents, thereby influencing the outcomes for cancer patients.[80]

1.2.3 Micelles as a Drug Carrier

Micelles are effective drug delivery vehicles, characterized by their spherical colloidal nanostructures formed through the self-assembly of amphiphilic molecules in an aqueous environment. Micelles belong to a class of amphiphilic colloids that spontaneously form at specific concentrations (CMC) and temperatures. The hydrophobic core functions as reservoir for hydrophobic drugs, while the hydrophilic shell stabilizes the core and enhances the water solubility of both the polymer and hydrophobic drugs, making them suitable for intravenous administration. Drugs are incorporated into micelles through chemical, physical and electrostatic interactions.[81, 82]

Lipid-core micelles are another category of lipid-based nanoparticles that can be produced from phospholipids. The lipid-core micelles was initially observed when mixtures of polyethylene glycol-phosphatidylethanolamine conjugate (PEG-PE) reached a critical concentration, resulting in the for-

mation of micelles rather than PEGylated liposomes. Recognizing the potential of PEG-PE micelles as a lipid-based nanoparticle drug delivery system followed shortly thereafter. PEG-PE not only extends the circulation time of micelles but also contributes to their stability when used as the hydrophobic block of copolymers, rendering these micelles highly stable. This enhanced stability arises from the hydrophobic interaction between the double acyl chains of phospholipids, enabling the solubilization of hydrophobic drugs.[83, 84]

For instance, Genexol-PM (PEG-poly (D, L-lactide)-paclitaxel) represents the first polymeric micelle formation of paclitaxel, offering a Cremophor-free option that can be administered without adverse reactions, with a favorable toxicity profile observed in patients with advanced refractory malignancies.[85] Multifunctional star-shaped polymeric micelles, based on four-arm disculfide-linked poly (ε- caprolactone)-poly (ethylene glycol) emphiphilic copolymers coupled with folate ligands, exhibit high stability and sustained release, with the potential for prompt release in acidic environments.[86] (shows in Fig.1.7) The drug doxorubicin is encapsulated into cationic 1,2-dioleoyl-3-trimethylammonium propane/methoxy poly (ethylene glycol) (DPP) nanoparticles to form micelles for intravesical drug delivery, demonstrating anticancer efficacy against bladder cancer. [87] Additionally, cholesterol-modified mPEG-PLA micelles (mPEG-PLA-Ch) show high encapsulation efficiency and significantly reduce tumor size compared to the pure drug (curcumin).[88]

Phenylboronic acid (PBA) can selectively recognize sialic acid (SA), thereby targeting sialylated epitopes over expressed on cancer cells. Micelles incorporating oxaliplatin exhibit enhanced tumor-targeting abilities through specific interactions with SA, offering a promising strategy for improving chemotherapy efficacy. Furthermore, lipid- and polyion complex-

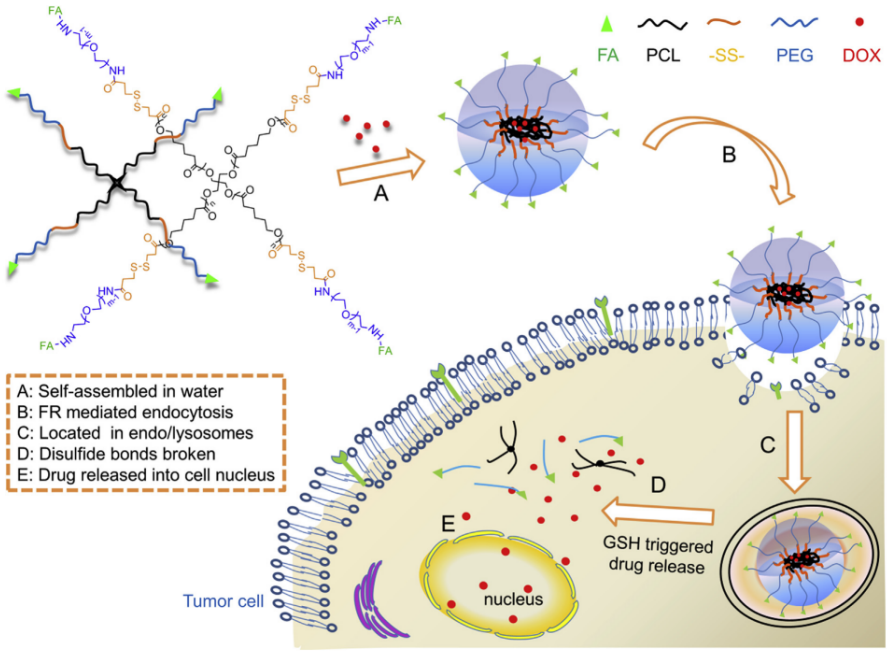

Fig. 1.7 Schematic illustration of DOX-loaded star-shaped micelles functionalized with folate and responsive to intracellular redox conditions. Reproduced with premission from ref. [86]

based micelles have been explored for the rapid generation of multivalent agonists targeting tumor necrosis factor receptors, showing promising therapeutic efficacy.[89, 90]

When utilized as carriers for drugs in water-based solutions, micelles have the capability to encapsulate poorly soluble non-polar pharmaceuticals within their core. Polar molecules can adhere to the surface of micelles, while substances with intermediate polarity are distributed along the surfactant molecules at intermediate positions. The micelle's corona provides effective steric protection for the core and influences the micelle's hydrophilicity and charge, which depend on factors such as the length and surface density of its hydrophilic blocks and the presence of reactive groups suitable for further modification, such as the attachment of targeting moieties.[91–93]

The properties of polymeric micelles, including their ability to load drugs and their fate in vivo, are influenced by the design of the amphiphilic block copolymers. Ideally, polymeric micelles should efficiently load, protect, deliver, and release the entrapped cargo at the targeted site with favorable pharmacokinetic characteristics. Amphiphilic polymers can be structured in various ways, such as having randomly combined monomer units with different hydrophobicities represented by two conjugated blocks (A-B type copolymers) or alternating blocks with different hydrophobicities (A-B-A type copolymers). Alternatively, the hydrophilic backbone chain of a polymer can be grafted with hydrophobic blocks (graft copolymers).[94–96]

The hydrophilic shell of polymeric micelles, responsible for stabilization and interaction with plasma proteins and cell membranes, typically comprises poly(ethylene glycol) (PEG) blocks with molecular weights ranging from 1 to 15 kDa. Other polymers like poly(N-isopropylacrylamide) and poly(alkylacrylic acid) impart temperature or pH-sensitivity to the micelles. The hydrophobic core usually consists of biodegradable polymers such as poly(β-benzyl-L-aspartate), poly(DL-lactide), or poly(ε-caprolactone), or non-biodegradable polymers like polystyrene or poly(methyl methacrylate). Phospholipid residues or chitosan-grafted with hydrophobic groups are utilized as core-forming compounds in some cases.[97–99, 83, 100] Using simple model systems involving peptides solubilized in micelles and single-component membranes, they provided insights into the interactions and structures of the Neu and Neu* TM domains and their disruptive mutants, shedding light on previous findings obtained in E. coli membranes. And analysis of the peptides' behavior in model membranes indicated that they are shielded from solvent exchange, likely due to interactions with the lipid headgroups. The mutants exhibited altered secondary structures and tilt angles, indicating changes in their interactions with the lipid bilayer.[101]

1.2.4 Self-assembly as a Drug Carrier

Self-assembly serves as a promising strategy for drug delivery, wherein molecules organize themselves into ordered structures spontaneously driven by free energy. This process offers a straightforward approach to constructing nanoscale bioactive materials, making it highly attractive for various biomedical applications, including tissue engineering, regenerative medicine, and drug delivery. One of the key advantages of self-assemblies lies in their tunable structural features, which can be adjusted through molecular chemistry and environmental conditions such as pH, ionic strength, solvents, and temperature.[102]

In the context of cancer therapy, self-assembly can be utilized to design drug carriers that inhibit tumor recurrence. For instance, the self-assembly of the photosensitizer chlorine e6 (Ce6) and the chemotherapeutic agent doxorubicin is achieved through electrostatic, $\pi - \pi$ stacking, and hydrophobic interactions. When administered intravenously, both free Ce6 and nanoparticles (NPs) are distributed throughout the body. However, self-assembly drugs exhibit exclusive accumulation at the tumor site. Ex vivo imaging of excised tumors further confirms higher drug accumulation in tumors with NPs compared to free Ce6 solution, highlighting the effectiveness of self-assembly-based drug delivery systems in targeting tumors.[103]

1.2.5 Molecular Dynamics Simulations in Drug delivery

Lipid-based nanocarriers, particularly solid lipid nanoparticles (SLNs), and micelles have gained significant attention in the field of drug delivery. SLNs offer advantages such as efficient encapsulation and controlled release of pharmaceuticals and lipophilic compounds. These carriers are

known for their ability to protect chemically unstable compounds from degradation, contributing to enhanced stability. It's important to acknowledge the reported disadvantages associated with SLNs. The highly ordered recrystallization of the lipid matrix after cooling can pose challenges. This phenomenon may lead to lower encapsulation efficiency, poor controlled release, and physical instability of the nanoparticles. These issues can impact the overall effectiveness of SLNs as drug delivery systems.

Understanding the internal structure of these lipid-based carriers is crucial for optimizing their performance in drug delivery. The homogeneous distribution, heterogeneous structure with lipid bilayers, and core–shell structures, reflect the complexity of lipid-based nanocarriers and the need for detailed characterization. Through molecular dynamics simulations, the evolution of nanoparticle formation can be detailed and displayed (like the Figure 1.8 shows) In the work by Chaban and Khandelia [104], MD simulations offer a valuable tool to explore the internal structure of nanostructured drug carriers at the molecular level. In their study using coarse-grained molecular dynamics within the MARTINI framework, they focused on lipid droplets composed of triolein and cholesteryl oleate. The presence of a phospholipid monolayer formed by a mixture of POPC and POPE phospholipid molecules adds an additional layer of complexity. The simulation results provided insights into the molecular structure of lipid droplets, indicating that cholesteryl oleate molecules tend to be located within the hydrophobic core of the droplets, with limited penetration into the monolayer. This suggests the retention of a single phase between triolein and cholesteryl oleate, forming the hydrophobic core of the lipid droplets.[104] The findings from the study by Chaban and Khandelia (2014) provide valuable insights into the formation and internal structure of lipid droplets in systems comprising triolein, cholesterol, POPC, and POPE in a water medium. These insights contribute to the broader knowledge base on lipid-

based nanocarriers, aiding in the rational design and optimization of such systems for drug delivery applications.[105]

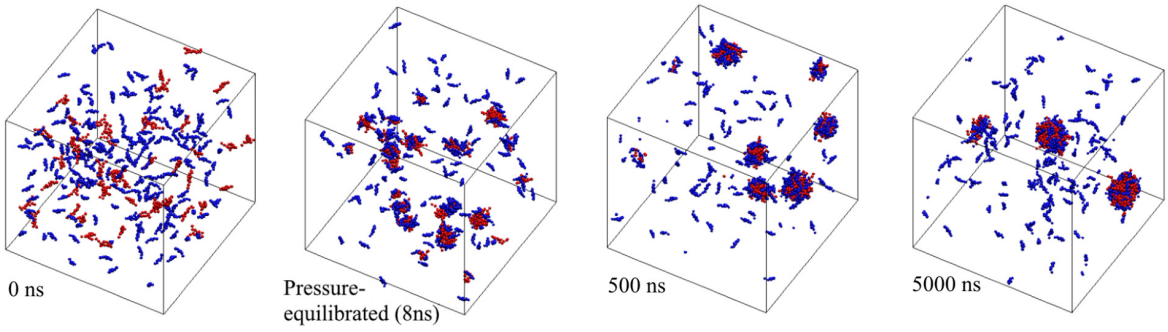

Fig. 1.8 Snapshots from MD simulation systems showing the evolution of self-assembly mixed micelles. Reproduced with permission from ref. [106]

Understanding the interactions between micelles, membranes, and drugs is fundamental to improving drug delivery systems. The interaction of membrane with their surrounding environments is significantly influenced by the type of micelles or lipid bilayers present. Studies have shown that detergents such as dodecylmaltoside (DDM) closely mimic lipid bilayers in their interactions with proteins, whereas short-tailed detergents like dihexanoylphosphatidylcholine (DHPC) can form non-physiological interactions with protein termini. This suggests that selecting appropriate detergents for experimental studies is crucial for maintaining protein integrity and functionality.[107] MD simulations of Dodecylphosphocholine (DPC) micelles have provided detailed insights into their structural and dynamic properties. DPC micelles are found to be slightly prolate in shape with limited water penetration into the micelle interior. The interaction of water is mainly with the head groups, and the micelle's dynamic behavior aligns well with experimental NMR data. These findings highlight the importance of head group interactions in defining micelle behavior.[108] Simulations involving Poly-ε-caprolactone (PCL) and Methoxy-polyethylene glycol (MePEG) block copolymers interacting with lipid bilayers reveal significant morphological changes in the micelles. The hydrophilic-to-hydrophobic

ratio plays a critical role in these interactions, demonstrating phenomena such as the 'snorkeling effect,' where hydrophilic segments penetrate into the bilayer while hydrophobic segments remain in the micelle core.[109]

Polymer micelles have been shown to enhance the solubilization of lipophilic, poorly water-soluble drugs. MD simulations combined with experimental validations suggest that calculating Flory-Huggins interaction parameters can predict drug incorporation efficiency into polymer micelles. This theoretical approach aids in optimizing drug delivery formulations, reducing the reliance on extensive experimental trials.[110] Coarse-grained MD simulations have explored the self-assembly of paclitaxel-loaded polymeric micelles, focusing on the effects of drug-polymer ratio and process parameters. The simulations reveal that increasing the drug content can lead to a transition from spherical to ellipsoidal micelle shapes, with larger micelles demonstrating improved structural stability and reduced solvent accessibility. These insights can inform the design of more stable drug delivery vehicles.[111] Investigations into smart nano-drug delivery systems using modified PNIPAAm-b-PEG block copolymers have shown promising results for curcumin encapsulation. The MD simulations predict favorable encapsulation processes, increased drug solubility, and polymer phase transitions that align well with experimental data. This suggests that smart polymers can significantly enhance the therapeutic efficacy of hydrophobic drugs.[112] Detailed studies of drug-micelle interactions, such as those involving dodecyl--D-maltoside (DDM) micelles, show that micelle hydration is limited but dynamically influenced by the acyl chains' flexibility. This dynamic interaction between the micelle's core and the solvated outer shell provides a nuanced understanding of micelle hydration and stability.[113] MD simulations investigating drug delivery mechanisms, such as the interaction of bile micelles with lipid membranes, have proposed models like the shuttle and elevator hypotheses. These models explain how micelles

facilitate drug incorporation into cellular membranes, providing a molecular basis for observed drug absorption patterns. The simulations reveal that amorphous drug aggregates solubilize more quickly than crystalline nanostructures, enhancing drug absorption efficiency.[114–118]

These simulation studies contribute valuable information about the behavior of lipid-based carriers at the molecular level, aiding in the understanding of their internal structure and interactions. Integrating experimental observations with molecular dynamics simulations enhances our ability to design and engineer lipid-based nanocarriers with specific properties for drug delivery applications.

1.3 Lipid Digestion on Drug Delivery

The role of enzymes in controlling structural changes in biomaterials, particularly lipids, within the body, is crucial. Lipids serve various functions, including providing energy and acting as carriers for lipophilic nutrients and drugs. Enzymes, such as lipases and phospholipases, play a crucial role in transforming dietary lipid species into absorbable components. In oral drug delivery, lipases are responsible for cleaving fatty acid moieties from triglycerides, the primary lipid consumed in the diet. Triglycerides are essential for transporting lipophilic nutrients through the blood and lymphatic systems. However, due to their poor solubility in aqueous environments, triglycerides are broken down by lipases in the gut into more polar 2-monoglycerides and fatty acids. These absorbed components are then reassembled into triglycerides by intracellular enzymes for transport throughout the body. Phospholipases disassemble specific parts of phospholipid molecules, primarily removing one fatty acid residue to produce lysophospholipids with different surfactant properties. Similar to triacyl-

glycerol lipases, the cleavage of fatty acids from phospholipids enables the absorption of phospholipid components for reuse by the body.[119, 120]

Although the biochemical process of lipid digestion is well understood, the physical-chemical and structural aspects of lipid fate are less well-known. During lipid digestion, the production of polar amphiphilic lipids at lipid-aqueous interfaces of fat droplets impacts lipid self-assembly in the gut. The critical packing parameter concept predicts structural transitions based on the polar lipid compositions. These transitions involve changes in the curvature of lipid-aqueous interfaces, progressing from lamellar and vesicular structures to inverse bicontinuous cubic phases and inverse micellar phases with increasing critical packing parameter values.

1.3.1 Lipid composition during digestion

Lipids serve various functions, including providing energy and acting as carriers for lipophilic nutrients and drugs. Enzymes, such as lipases and phospholipases, play a crucial role in transforming dietary lipid species into absorbable components. [121] During lipid digestion, the production of polar amphiphilic lipids at lipid-aqueous interfaces of fat droplets impacts lipid self-assembly in the gut. The critical packing parameter concept predicts structural transitions based on the polar lipid compositions. These transitions involve changes in the curvature of lipid-aqueous interfaces, progressing from lamellar and vesicular structures to inverse bicontinuous cubic phases and inverse micellar phases with increasing critical packing parameter values.[122]

1.3.2 Effect on Drugs by Lipid Digestion

The process of lipid digestion plays a crucial role in drug, delivery by facilitating the dissolution and transportation of lipophilic compounds through the GIT, thereby enabling the absorption of otherwise insoluble substances. Synchrotron sources offer high flux and large area detectors, allowing for the rapid measurement of X-ray diffraction patterns from very low concentrations of crystalline material dispersed in a formulation.[123] This capability enables the study of dissolution, amorphization, precipitation, and polymorphic transformation of drugs in dilute suspension on timescales relevant to digestion processes.

In some cases, the drug may exhibit higher solubility in the undigested formulation lipids compared to the digestion products. This can lead to drug precipitation during digestion, as evidenced by characteristic diffraction peaks growing over time in powder X-ray diffraction (XRD) measurements. The precipitation occurs rapidly, making it challenging to obtain kinetic information using traditional analytical methods. Such behavior often indicates poor performance of the formulation in vivo, as the presence of precipitated crystalline drug is typically associated with reduced oral bioavailability.

Alternatively, the antimalarial drug artefenomel (OZ439), when paired with ferroquine, shows promise as a single-dose cure for malaria.[124] Artefenomel, being amphiphilic, forms micelles and other aggregate structures in aqueous solution. However, its precipitation risk upon exposure to gastrointestinal environments necessitates careful formulation. Time-resolved X-ray scattering studies during digestion of milk and infant formula, potential lipid-based formulations for low-income settings, have revealed rapid formation of the poorly soluble hydrochloride salt or free base form

of artefenomel. This transformation occurs concurrently with solubilization, highlighting the intricate interplay between drug precipitation and solubilization during lipid digestion.[125]

Lipid digestion serves not only to absorb lipids for energy and structural purposes but also facilitates the absorption of lipophilic nutrients. Instead of resisting digestion to maintain an unfavorable state, there's potential in leveraging lipid digestion to enable the absorption of otherwise insoluble drugs. Studies have shown that administering the drug and lipid separately can be as effective as combining them in a lipid-based formulation. Co-administration offers opportunities, especially for drugs with poor solubility in undigested lipids or stability issues in lipid formulations. Fatty acids formed during digestion play a crucial role in solubilizing weakly basic drugs by forming lipophilic ion pairs.[126] Various studies have demonstrated the solubilization of solid crystalline drugs during lipid digestion using pharmaceutical lipids, milk, and infant formula. These studies highlight the evolving perspective on lipid-based formulations, the potential benefits of leveraging lipid digestion, and the various factors influencing drug solubilization during digestion.[127, 128]

1.4 Motivation

The development of nanoparticle formulations, particularly lipid-based nanoformulations, holds immense potential in drug delivery applications due to their biocompatibility and versatility. Lipid nanoparticles have garnered increasing interest, especially with the success of lipid nanoparticles (LNPs) in delivering COVID vaccines. Phosphatidylcholine (PC) lipids, major constituents of cell membranes, exhibit self-assembling properties, forming various nanostructures such as bilayers and micelles.[129]

Understanding the dynamics of lipid-based nanoformulations is crucial for optimizing drug delivery efficiency. Molecular dynamics (MD) simulations offer a powerful tool to investigate the interactions of lipid-based nanoformulations with model lipid membranes. By exploring the dynamics of lipid micelles at various stages of digestion with model membranes, our study aims to provide insights into the enhanced permeability of these nanoformulations and their potential to improve drug delivery to cells. Our findings highlight the unique effects of different micelle components on membrane properties, shedding light on the molecular mechanisms underlying drug delivery processes. Understanding how these drugs interact with micelles is crucial for optimizing drug delivery systems. Our research also explores the influence of lipid composition on micellar dynamics and drug localization within micelles.

1.4.1 Structure of Thesis

The structure of this thesis is as follows:

In Chapter 2, I provide a detailed description of the molecular dynamics (MD) method utilized as the primary technique in our research. This chapter outlines the theoretical framework and computational procedures employed to simulate the dynamics of lipid micelles and drug interactions within lipid-based nanoformulations.

Chapter 3 focuses on exploring the dynamics of lipid micelles at various stages of digestion with model membranes. The aim is to provide insights into the enhanced permeability of these micelles and their potential to improve drug delivery to cells. Through a combination of MD simulations and detailed analyses, we investigate the behavior of lipid micelles within model membranes to understand their interactions and transport properties.

In Chapter 4, delves into the behavior of different drugs, specifically CAMPT and DOX, within lipid-based micelle environments. The objective is to understand how these drugs interact with micelles to optimize drug delivery systems. Through comprehensive analyses of drug-micelle interactions using MD simulations, aim to elucidate the mechanisms underlying drug localization and release within lipid-based nanoformulations.

Chapter 5 serves as the conclusion of our research, summarizing the key findings and insights gained from our investigations into lipid micelle dynamics and drug interactions. The implications of our findings for the field of drug delivery and propose avenues for future research are discussed

In Chapter 6, outlines potential directions for further research building upon the findings presented in this thesis.

Chapter 2

Methods

2.1 Molecular Dynamics Simulations

Molecular dynamics (MD) simulations are a powerful computational technique employed in the field of molecular modeling to study the dynamic behavior of atoms and molecules. These simulations provide valuable insights into the motions, interactions, and structural alterations of systems at the atomic and molecular scales. The first MD simulation can trace its origins to the late 1950s, reported by Alder and Wainwright.[130] The method has been applied to systems with hard spheres and particles who interact via a square well potential of attraction. Notably, it successfully calculated equilibrium properties, revealing the differences in the equation of state between hard spheres and previous Monte Carlo results.[130, 131] Over the past decades, researchers have developed and summarized a number of techniques in order to improve MD simulations, and some of these have become crucial foundations for the MD software packages of today, such as time integration algorithms, neighbor list periodic boundary conditions etc.[132–134]

Ideally, the time-dependent Schrödinger equation is able to predict all properties of all molecules with absolute precision ab initio. However, it is necessary to introduce approximations when dealing with a larger number of particles in larger systems.[135] In many biomolecular systems, empirical models that are parameterized on experimental data or on data from ab initio or semi-empirical quantum mechanical calculations, are commonly chosen, such as classic Coulomb interactions between atomic charges, instead of employing a quantum description of the electrons.[136] These models perform better when it comes to observations over larger time, such as microsecond.[137]

The macroscopic properties obtained through experimental measurements do not constitute direct observations; instead, they are averages derived from billions of molecules reflecting a statistical mechanics ensemble. The two predominant methods for generating equilibrium ensembles with statistical accuracy are molecular dynamics simulation and Monte Carlo simulations. MD simulations have the advantages of reproducing the kinetics associated with non-equilibrium properties, including processes like diffusion or folding times.[138]

MD is a deterministic way to simulate the movement of all atoms and the principle behind MD simulations is relatively simple. The required input includes the positions, velocities and masses of all atoms. The simulation is divided into sequential time steps, usually on the order of femtoseconds, and the general workflow summary can be found in Figure 2.1 . In each step, forces between each atoms are computed, and the results are integrated to derive new positions and velocities. This process is iterated until the simulation ends. Throughout all theses time steps, material properties can be computed based on the atoms' positions, forces and velocities.[137]

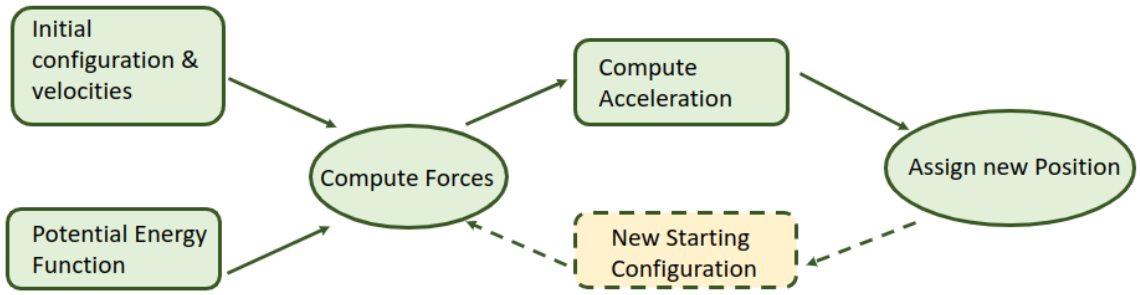

Fig. 2.1 A typical workflow of molecular dynamic simulations algorithm summary.

2.1.1 Force Fields

As discussed previously, while molecular dynamics (MD) simulations offer advantages in reproducing kinetics associated with non-equilibrium properties, such as diffusion or folding times, their applicability can be limited by the spatial or time scales required, often due to the expensive computational costs associated with ab initio methods. In such cases, we need to employ a higher level of approximation and turn to empirical force field (FF) based methods. These models allow comprising of hundreds of thousands of atoms to be studied over timescales ranging from several nanoseconds to even microseconds. Many different experimental results can be used to validate the quality of a force field as it plays a particularly important role in MD simulations. A force field is a mathematical expression that defines how the energy of a system depends on the coordinates of its particles. It comprises an analytical expression for the interatomic potential energy, denoted as $U(\mathbf{r}_1,\mathbf{r}_2, ..., \mathbf{r}_i)$ and a collection of parameters associated with this expression, where $\mathbf{r}$ represents a point in microscopic phase space.[139, 140] The forces on particle i can be determined by taking the derivative of the potential energy with respect to the position of particle i:

$$\boldsymbol{f}_i = -\frac{\partial U}{\partial \mathbf{r}_i} \tag{2.1}$$

To simplify the calculations, the electronic effects are ignored completely in this method and it only account for positions of the nuclei of the atoms. The parameters within the force fields are generally derived from quantum approaches like density functional theory. There are a variety of force fields which exist, including CHARMM[141], AMBER[142] and GROMOS[143]. Even though these different force fields are similar in their functional forms, there are some differences in the terms and parameters for these force fields. The potential energy commonly comprises both bonded and non-bonded terms as follows:

$$U(\mathbf{r}) = U_{bonded}(\mathbf{r}) + U_{non-bonded}(\mathbf{r}) \tag{2.2}$$

In this work, the CHARMM36 all-atom force field[144] was used where the potential energy is classically modelled as follows:

$$\begin{aligned} U = & \sum_{bonds} k_b(r_{ij} - r_0)^2 + \sum_{angles} k_\theta(\theta_{ijk} - \theta_0)^2 + \sum_{dihedrals} k_\phi[1 + (\cos n\phi_{ijjl} - \delta)] \\ & + \sum_{impropers} k_\omega(\omega_{ijkl} - \omega_0)^2 + \sum_{Urey-Bradley} k_u(l_{ik} - l_0)^2 \\ & + \sum_{non-bonded} \left(4\varepsilon \left[\left(\frac{\sigma}{r_{ij}} \right)^{12} - \left(\frac{\sigma}{r_{ij}} \right)^{6} \right] + k_e \frac{q_i q_j}{r_{ij}} \right) \end{aligned} \tag{2.3}$$

Bonded Terms

The first five terms in Equation 2.3 are bonded interaction potential terms (Figure2.2), standing for bond stretching, angle bending, dihedrals and improper dihedrals respectively, where k_b, k_θ, k_ϕ, k_ω, and k_u are their respective force constants. The last of the five bonded interaction terms is the Urey-Bradly potential, which is an extra special term used in CHARMM force-field for 1,3 atom interactions.[145]

The bonding stretching term is a harmonic potential used to model the interaction between two atoms *i, j* connected by a single covalent bond, (r_{ij} - r_0) describes the deviation from the equilibrium distance. The bond angle potential in the second term is characterized by a harmonic approximation and serve as indicators of the deviation from ideal geometry, similarly, where θ_{ijk} - θ_0 stands for the deviation from the equilibrium bond angle. The torsional angles in the third term, *n* represents the dihedral multiplicity, the number of energy minima found in the rotation of the *ijkl* dihedral angle, ϕ_{ijkl} is the dihedral angle formed between the planes of *i-j-k* and the *j-k-l* (in Figure 2.2(c)), and δ is the phrase shift. The improper dihedral term is implemented in the CHARMM force field to preserve the chiralities in chemical structures and ensure the planarity of ring structures, where ω_{ijkl} - ω_0 signifies the deviation in the out-of-plane angle. The Urey-Bradly potential was introduced as an extra correction to the 1, 3 angle potential, where l_{ik} - l_0 is the distance from the 1, 3 bonded atom to the equilibrium distance. By using this additional harmonic potential, it can be used to describe the bending motions within bonded angles.

Overall, the terms representing bonded interactions aim to account for the stretching of bonds, the bending of valence angles and the rotation

between planes. By summing them, it can give the total bonded energy of entire system.[146]

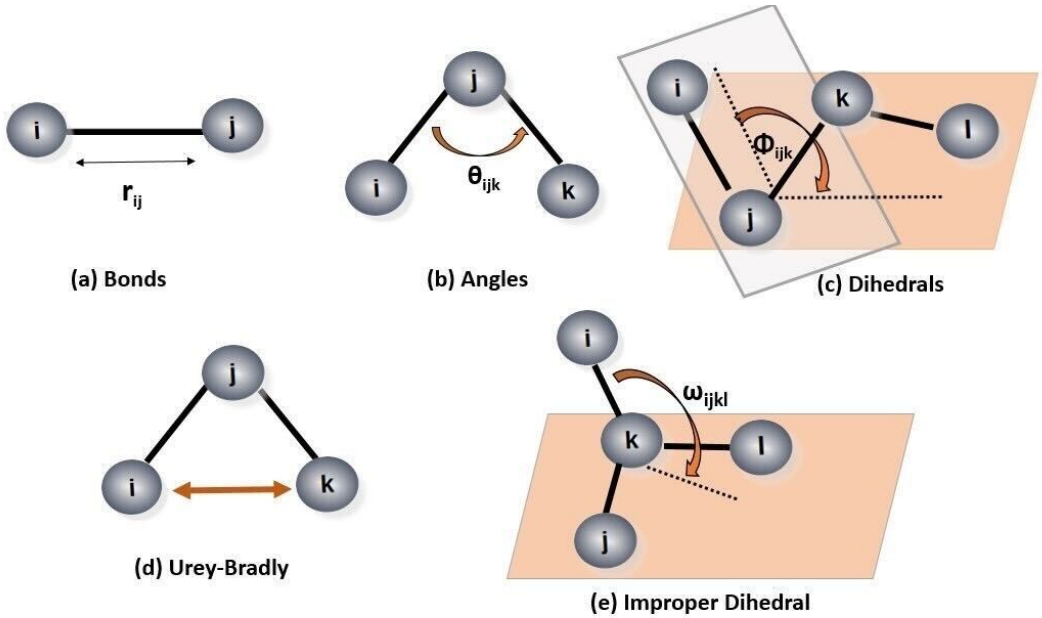

Fig. 2.2 Bonded potential terms used in classical MD force field

Non-Bonded Terms

$$U(\mathbf{r})_{Non-Bonded} = \sum_{Lennard-Jones} 4\varepsilon \left[\left(\frac{\sigma}{r_{ij}} \right)^{12} - \left(\frac{\sigma}{r_{ij}} \right)^{6} \right] + \sum_{Coulomb} \frac{q_i q_j}{4\pi\varepsilon_0 r_{ij}} \tag{2.4}$$

The non-bonded terms characterize the van der Waal and Coulomb (electrostatic) interactions (last two terms in Eq. 2.3) between atoms not directly connected by bond angles or covalent bonds. The van der Waal interactions are typically represented using 12-6 Lennard-Jones (LJ) functional form, where r_{ij} is the distance between two atoms, $R_{min,ij}$ is the distance at which the LJ potential decreases to it's minimum value and ε is the depth of the potential well (Figure 2.3). It is the LJ potential energy as a function of the

distance r between two interacting particles, which commonly include both attractive interactions r_{ij}^{-6}, which dominate at larger distances, and repulsive interactions r_{ij}^{-12} which dominate at small distances. These parameters are commonly derived from simulations based on quantum mechanics or through the process of fitting experimental data. As depicted in Figure 2.3, as $r_{ij} \to \infty$, $U_{LJ} \to 0$. Thus, the cutoff radius is normally applied at r_{cut} = 1.2 nm from organic forcefields, which is approximately 2.5 times the sigma value for the interactions of carbon atoms. In CHARMM each single particle has its unique parameters of ε_{ij} and σ_{ij}. For CHARMM force field, the standard Lorentz-Berthelot combination rule was used. The ε_{ij} and σ_{ij} are generated by calculating the following form equations:

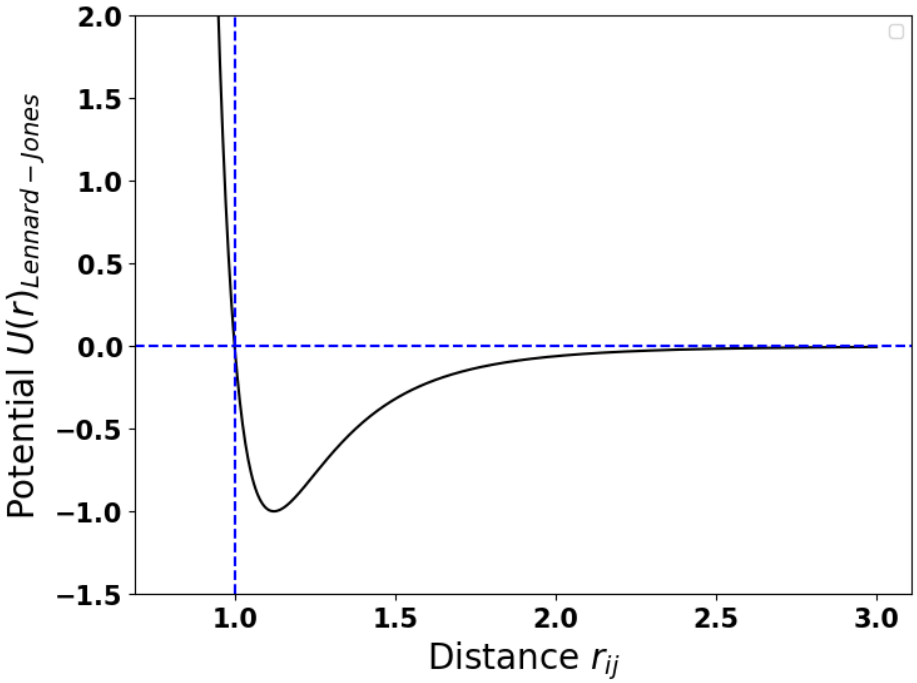

Fig. 2.3 The Lennard-Jones potential as function of distance between two atoms r and j.

$$\begin{aligned} \varepsilon_{ij} &= \sqrt{\varepsilon_i \times \varepsilon_j} \\ \sigma_{ij} &= \frac{\sigma_i + \sigma_j}{2} \end{aligned} \tag{2.5}$$

As for the electrostatic interaction, in classical fixed-charge force fields, only pairwise Coulomb interactions between atom i and atom j are considered, where q_{ij} is partial charge for q_i and q_j, and ε is the dielectric constant between the distance from atom i to the atom j. The electrostatic interaction between atoms is calculated in a pair-wise manner using the Coulomb equation for atoms that generally are at a distance less than the LJ cutoff distance ($r_{\text{cutoff}} = 1.2 \quad \text{nm}$). [140, 147, 148] The Particle-Mesh Ewald (PME) technique is a method used in computational chemistry and molecular dynamics simulations to efficiently calculate long-range electrostatic interactions in periodic systems. It relies on Fast Fourier Transform (FFT) algorithm to transform the charge distribution from real space to reciprocal space. The charge distribution is represented on a mesh grid in real space then the FFT is used to convert this grid representation to reciprocal space, where the long-range interactions are calculated. The PME technique substantially accelerates the computation of electrostatic forces and energies in simulations involving charged particles, such as ions or molecules with net charges.

The Verlet cutoff scheme[149] is particularly useful for systems where the majority of interactions are short-ranged, such as in many molecular and biomolecular simulations. The simulation system is divided into short-range and long-range regions based on a cutoff distance, often denoted as r_{cutoff}. Interactions between particles within r_{cutoff} are computed explicitly shown in yellow in Fig.2.4, while interactions beyond this distance shown in black are handled separately.

The sum of the bonded and non-bonded terms can provide an approximation value for the potential energy of the whole system. Then the forces acting on every atom can be calculated from the negative gradient of the potential energy function so we can solve classical equation of motion and

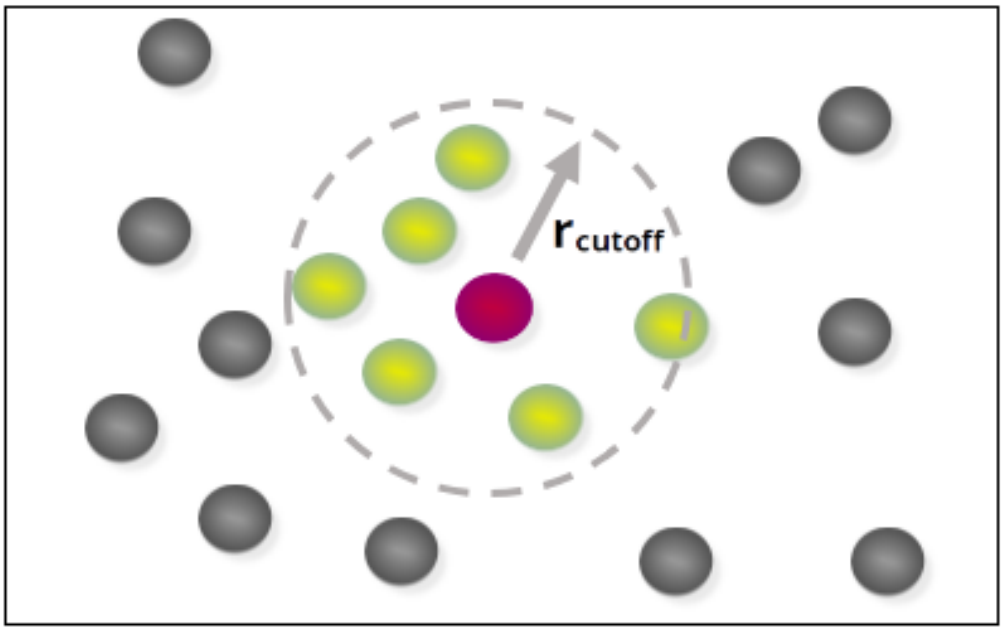

Fig. 2.4 Illustration of Verlet cutoff scheme method used in MD simulations.

the atoms' position at each time step can be consequently determined later on. This provides a detailed picture and better understanding of the dynamic behaviour and interactions of each molecule in the typical simulated systems at the atomic scale. [131, 137, 150]

2.1.2 Force Calculation and Simulation Integrator

Once the potential energy function $U(\mathbf{r}^N)$ has been defined, the next step is to calculate the forces ($\mathbf{f}_i$) acting on the atom i:

$$\mathbf{f}_i = -\frac{\partial U(\mathbf{r}^N)}{\partial \mathbf{r}_i} \tag{2.6}$$

Time integration algorithms play a crucial role in MD simulation engines, responsible for providing the trajectories of interacting atoms. These algorithms are developed using the finite difference method, where time is

discretized on a finite grid with a timestep denoted as δt. Given the atomic positions, velocities, and accelerations at time t, the integration scheme calculates these quantities for a later time t + δt. There are some common MD simulations, such as the Verlet algorithm[149] and the Leap-Frog algorithm[151] etc.. Both the Leap-Frog and Verlet algorithms are effective choices for time integration in MD simulations, and the choice between them may depend on factors such as ease of implementation and specific requirements of the simulation. The Verlet algorithm is more commonly used in practice due to its good energy conservation properties. For the velocity Verlet algorithm, it can be written as:

$$\mathbf{v}_i\left(t+\frac{1}{2}\delta t\right) = \mathbf{v}_i(t) + \frac{1}{2}\frac{\mathbf{f}_i}{m_i}\delta t \tag{2.7}$$

$$\mathbf{r}_i(t+\delta t) = \mathbf{r}_i(t) + \delta t\, \mathbf{v}_i(t+\frac{1}{2}\delta t) \tag{2.8}$$

$$\mathbf{v}_i(t+\delta t) = \mathbf{v}_i(t+\frac{1}{2}\delta t) + \frac{1}{2}$$

Chapter 3

Digestion of lipid micelles leads to increased membrane permeability

Nanoparticles, particularly lipid-based formulations, are gaining prominence in diverse applications, notably as drug-delivery vehicles (DDVs). Phosphatidylcholine (PC) lipids, major constituents of cell membranes, exhibit self-assembly into various nanostructures, making them attractive for drug delivery. This chapter focuses on the interplay between dihexanoylphosphatidylcholine (2C6PC) micelles and model lipid membranes, representing ordered (DPPC:CHOL) and disordered (DOPC) states.

Building upon our prior work on the structure of micelles containing 2C6PC digestion molecules by the calcium-dependent secreted phospholipase A2 ($sPLA_2$) enzyme, this research explores how the natural digestion process of lipid-based micelles influences interactions with lipid membranes. Elevated $sPLA_2$ levels in inflammatory diseases and cancers provide a targeted release mechanism for PC lipid-based DDVs. The enzymatic digestion produces lysolipids and fatty acids, known enhancers of drug transport across membranes.

This study utilizes all-atom molecular dynamics simulations to unravel the dynamics of 2C6PC micelle interactions at various digestion stages with two different model membranes. The investigation aims to provide insights into enhanced permeability and its implications for drug delivery. The unique effects of micellar components on membrane properties are examined, offering valuable perspectives on the dynamics of membrane interactions.

The research presented in this chapter is derived from an article published in *Nanoscale*, where I am the first author, undertaking data curation, formal analysis, investigation, methodology, software development, validation, visualization, and drafting of the original manuscript. I carried out all of the molecular dynamics simulations. The collaborative effort involved Demi L. Pinke and M. Jayne Lawrence, who contributed to the conceptualization and participated in the review and editing process.

3.1 Publication

Jun Xie, Demi L Pink, M Jayne Lawrence, and Christian D Lorenz. Digestion of lipid micelles leads to increased membrane permeability. Nanoscale, 16(5):2642–2653, 2024.[152]

Nanoscale

PAPER

View Article Online
View Journal | View Issue

Cite this: *Nanoscale*, 2024, **16**, 2642

Digestion of lipid micelles leads to increased membrane permeability†

Jun Xie,[a] Demi L. Pink,[a] M. Jayne Lawrence [b] and Christian D. Lorenz *[a]

Received 9th October 2023,
Accepted 31st December 2023

DOI: 10.1039/d3nr05083a

rsc.li/nanoscale

Lipid-based drug carriers are an attractive option to solubilise poorly water soluble therapeutics. Previously, we reported that the digestion of a short tail PC lipid (2C6PC) by the PLA2 enzyme has a significant effect on the structure and stability of the micelles it forms. Here, we studied the interactions of micelles of varying composition representing various degrees of digestion with a model ordered (70 mol% DPPC & 30 mol% cholesterol) and disordered (100% DOPC) lipid membrane. Micelles of all compositions disassociated when interacting with the two different membranes. As the percentage of digestion products (C6FA and C6LYSO) in the micelle increased, the disassociation occurred more rapidly. The C6FA inserts preferentially into both membranes. We find that all micelle components increase the area per lipid, increase the disorder and decrease the thickness of the membranes, and the 2C6PC lipid molecules have the most significant impact. Additionally, there is an increase in permeation of water into the membrane that accompanies the insertion of C6FA into the DOPC membranes. We show that the natural digestion of lipid micelles result in molecular species that can enhance the permeability of lipid membranes that in turn result in an enhanced delivery of drugs.

1 Introduction

Nanoparticle formulations consisting of a range of materials are being developed for a range of applications including use as drug-delivery vehicles (DDVs).[1–14] Lipid-based nanoformulations are of particular importance due to their biocompatability,[15–17] and they have been of increasing interest over the past few years as a result of the success of the various lipid nanoparticles (LNPs) used to deliver the COVID vaccines.[18]

Phosphatidylcholine (PC) lipids are the major components of cell membranes. Due to their amphiphilic nature, PC lipids are able to self-assemble into a variety of nanostructures including bilayers and micelles. The molecular architecture of the lipids can be tailored in order to generate a variety of different self-assembled structures. For example, small changes in the lipid tail length can alter the concentration at which the lipid self-assembles (called the critical micelle concentration (CMC)) as well as the structure of the aggregates formed, with the size of the aggregates formed increasing with the length of the hydrophobic tails of the lipid molecules?

Within the body, PC molecules are degraded *via* the hydrolysis of the PC sn-2 ester bond, a process which is mediated by the calcium-dependent secreted phospholipase A2 ($sPLA_2$) enzyme.[19] This hydrolysis results in the production of lysophosphocholine and fatty acid molecules.[20,21] Previously we have combined static and time-resolved small angle neutron scattering with all-atom molecular dynamics simulations to characterise how the structure of micelles containing dihexanoylphosphatidylcholine (2C6PC) changes as the molecule is digested by $sPLA_2$ into 1-hexanoyl-lysophosphocholine (C6LYSO) and hexanoic acid (C6FA) (Fig. S1†).[2] Our results show that as the degradation progresses the cmc of the resulting micelles decreases and therefore potentially affect the release of any payload that they are carrying.[2]

The concentration of $sPLA_2$ is elevated in various inflammatory diseases, atherosclerosis and cancers, specifically prostate, breast and pancreatic cancer.[22–30] As a result, the release of anti-cancer agents contained in PC lipid-based DDVs can be triggered by an enzyme that is upregulated in the targeted

[a]*Biological & Soft Matter Research Group, Department of Physics, Faculty of Natural, Mathematical & Engineering Sciences, King's College London, London, UK. E-mail: chris.lorenz@kcl.ac.uk*
[b]*Division of Pharmacy and Optometry, School of Health Sciences, Faculty of Biology, Medicine and Health, University of Manchester, Stopford Building, Oxford Road, Manchester, UK*

† Electronic supplementary information (ESI) available: (i) A detailed description of the analysis carried out for the various simulations, (ii) plots of the R_G and eccentricity of the micelles as a function of time (iii) the contacts between the EO monomers and the hydration of the EO monomers on the polymers within each micelle (iv) the intrinsic density of the various components within the simulations for each micelle and (v) the outputs of the dimensionality reduction and clustering of the molecules within each micelle. See DOI: **https://doi.org/10.1039/d3nr05083a**

tissue and therefore would not require any external stimuli to trigger the drug release.[31–34] Such enzyme triggered release cxould be beneficial in a clinical setting,[35] as the localised release of encapsulated drug(s) would reduce their side effects.

The action of the sPLA2 enzyme on these phospholipid-based DDVs will result in the production of bioactive molecules in the form of the lysolipids and fatty acids. As free fatty acids and lysolipids have been shown to enhance drug transport across lipid membranes,[36–39] the natural production of these molecules is an attractive way to overcome various biological barriers, to drug absorption which is one of the most significant challenges faced when developing an effective DDV. Specifically, for anticancer DDVs, delivering the drug to the exterior of a solid tumor is not sufficient as the drug has to diffuse through the tumor microenvironment and get into the tumor cells to exert its therapeutic effect.

In this manuscript, we present the results of all-atom molecular dynamics simulations that were used to investigate the interactions of 2C6PC micelles at various stages of digestion with two model lipid membranes: an ordered membrane (70 : 30 mole ratio 1,2-dipalmitoyl-*sn-glycero*-3-phosphocholine (DPPC):Cholesterol (CHOL)) and a disordered membrane (pure 1,2-dioleoyl-*sn-glycero*-3-phosphocholine (DOPC)). Our findings provide insight into how the natural digestion of the 2C6PC molecules in the micelles lead to their enhanced permeability and in turn may increase the delivery of any encapsulated drugs to the cell. In particular, we demonstrate the unique effects that each of the different components of the micelles has on the interfacial and structural properties of the two different membranes. Additionally, we show the different dynamical properties of the various molecules comprising the micelles have once they have inserted into each of the membranes.

2 Results

2.1 Interaction of micelles with membranes

The micelles in each of the simulated systems remained intact throughout the equilibration stages of the simulations, and therefore are still whole in the snapshots taken from the beginning of the production simulations (0 ns snapshot of Fig. 1 and 2). However, in all six of the simulated systems investigated, the micelles were found to disassociate to varying degrees during the production simulations of the micelles interacting with the membranes. Fig. 1 and 2 show the interaction and penetration of the constituent molecules of the three different micelles in the DOPC and DPPC-CHOL lipid membranes, respectively.

As each of the micelles begin to disassociate while interacting with the DOPC bilayer, the different molecular species approach the interface of the lipid bilayer and then penetrate into the membranes (see Fig. 1). The snapshots show that the C6FA, C6LYSO and 2C6PC molecules penetrate the pure DOPC lipid bilayer in differing amounts and to different depths. During this penetration, the C6FA molecules were the first species to insert into the lipid bilayer as they are small in size and are the most hydrophobic. We have extended the simulations with the product containing micelles in order to allow more time for various components to interact with the membranes.

We observed a significantly different behaviour of the micelles when they were interacting with the DPPC-CHOL membrane. Fig. 2 shows typical snapshots of the micelles during their interaction with the more ordered membrane over 1 μs. The three main differences are: (i) fewer molecules penetrate into the membrane than in the DOPC membrane and in particular there are very few C6LYSO or 2C6PC molecules inserted into lipid bilayer even after 1 μs; (ii) aggregates of the molecules in the Mixed and Pure-Lipids systems are observed throughout the production simulations, which is not the case when the micelles interacted with the pure DOPC membranes; and (iii) Pure-Lipids micelles are more likely to remain predominantly whole as some molecules are released and have less impact on the DPPC-CHOL membrane than they did on the DOPC membrane. The micelles destabilise as they begin interacting with the lipid membranes. *Via* visual inspection, we observe the micelles go through different aggregated states during their destabilization. As 2C6PC and C6FA molecules leave the micelles they interact with the lipid bilayers, while the C6LYS molecules remain isolated in solution. As a result, the different micelles demonstrate different rates of destabilization. For instance, the pure-lipid micelles demonstrated a longer duration of remaining intact compared to the other two, indicating its higher stability, which is in line with our previous findings.

The plots in the bottom row of Fig. 1 and 2 show the extent to which the various constituent molecules comprising the micelles insert into the lipid membranes. The trends shown in the plots are consistent with the trends observed visually in the snapshots for each system. In the DOPC membrane systems, nearly all of the C6FA molecules are fully inserted into the membrane after approximately 200 ns, indicating that the C6FA can easily penetrate into the membrane. As the 2C6PC molecules are larger and have a preference to interact with one another as opposed to inserting into the membrane, they are observed to more slowly migrate to the membrane's interface and penetrate into the membrane until an equilibrium was reached after ~1.2 μs, as seen in Fig. 1(c) and (d). However, due to the more hydrophilic nature of C6LYS is the least likely molecule to penetrate the membrane, and as such seems to generally prefer to remain isolated in solution. In the DPPC-CHOL membrane, we find that approximately 40% less of the C6FA has inserted for the Pure-Products and Mixed systems than observed in the DOPC membrane (Fig. 2(b), (c) and Table 1). Additionally we observe that very few C6LYSO (~8%) and 2C6PC (~4%) molecules penetrate into the DPPC-CHOL membrane (Fig. 2(b–d) and Table 1).

The behaviour of the various molecules that comprise the micelles observed in our simulations are consistent with the critical micelle concentrations (cmc) that have been measured

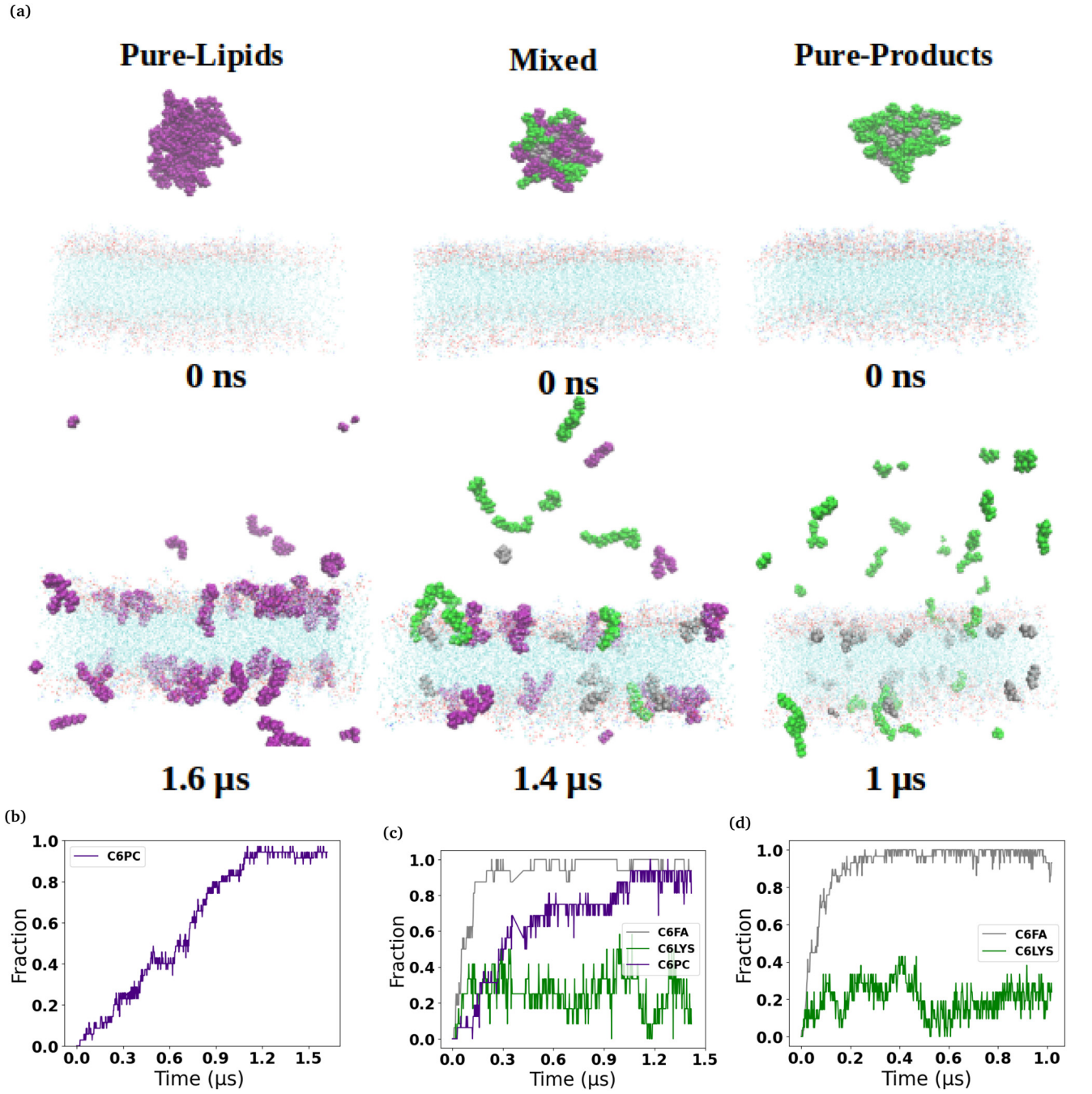

Fig. 1 Interactions of micelles with the DOPC membrane. (a) Representative snapshots of three different lipid-based micelles (C6PC purple, C6FA sliver, C6LYS green) interacting with DOPC (cyan) membrane over time. From left to right, they are the Pure-Lipids, Mixed and Pure-Product systems, respectively. Water molecules and ions were removed for clarity. The fraction of the micelle molecules that have inserted into the membranes are shown in the bottom row for each of the three micelles (b–d).

for these molecules experimentally. While there is not any published cmc values for C6LYSO, there are cmc values published for C8LYSO (57 mM), C10LYSO (5.7 mM) and C12LYSO (0.6 mM),[40] so the cmc for C6LYSO would be greater than 57 mM. The cmc for 2C6PC was found to be ≈14 mM.[41,42] As we have studied the free hexanoic acid (C6FA), there are no experimentally obtained cmc values, but a coarse-grain molecular dynamics simulation study reported a cmc of 9.26 mM at 50 °C, which is an order of magnitude larger than the cmc found for the sodium salt of hexanoic acid.[43] Therefore the fact that we find that the C6LYSO is the least likely of the molecules to remain in the micelle or insert into the membrane, and that C6FA is the most likely to be in either environment agrees with the rank order of these cmc values.

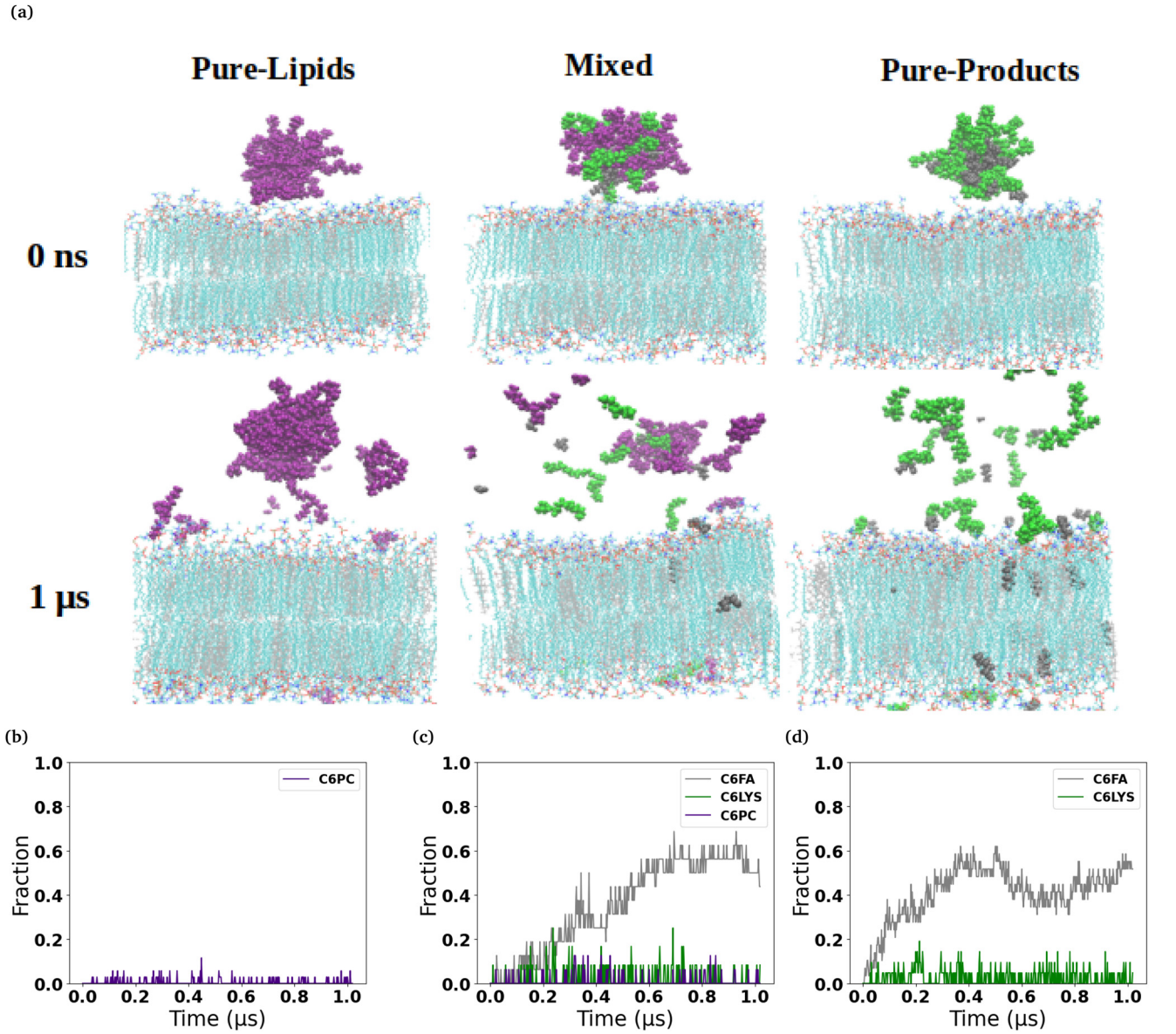

Fig. 2 Interactions of micelles with DPPC-CHOL membrane. (a) Representative snapshots of three different lipid-based micelles (C6PC purple, C6FA sliver, C6LYS green) interacting with DPPC-CHOL (DPPC cyan, CHOL grey) membrane over time. From left to right, they are the Pure-Lipids, Mixed and Pure-Product systems, respectively. Water molecules and ions were removed for clarity. The fraction of the micelle molecules that have inserted into the membranes are shown in the bottom row for each of the three micelles (b–d).

2.2 Effect of micelles on membranes' structural properties

In order to determine how the insertion of the micelle components into the membranes effect the structure of the lipid membranes, we measured the area per lipid for each lipid species, the membrane thickness, and the lipid order parameters. The area per lipid for the pure DOPC and DPPC-CHOL membrane systems are 0.68 nm^2 and 0.57 nm^2, respectively, which are consistent with those reported elsewhere.[44–46] The area per lipid and membrane thickness for each simulated system as the micelles interact with the membranes are shown in Fig. 3. In the three DOPC systems, we observe that the area per lipid increases and the thickness decreases as more and more 2C6PC inserts into the membrane. In all three systems, the area per lipid is larger and the membrane thickness is smaller than those measured in the pure DOPC membrane (Fig. S13†). The same general trends are observed for the DPPC-CHOL membrane as well, where even the minimal amount of 2C6PC that is able to insert into the membrane results in a noticeable difference in the area and thickness of the membrane. Table 1 summarises the calculated values of area per lipid for all of the systems with the micelles.

Table 1 Structural properties of lipid membranes. The properties of the DOPC and DPPC-CHOL membranes alone (Bilayer) and when they interact with the Pure-Lipids (PL), Mixed (Mixed) and Pure-Products (PP) listed here include: (i) the thickness (nm) and area per lipid (nm^2 per lipid) for the PC (APL_{PC}) and cholesterol (APL_{CHOL}) lipids in each system; (ii) the fraction of the micellar component molecules ($f_{xtrmC6FA}$, f_{C6LYSO} & f_{2C6PC}) that inserted into the membrane during the final 100 ns of the simulations; (iii) the average order parameter per tail of the PC lipids ($\langle -S_{CH,sn1} \rangle$ & $\langle -S_{CH,sn2} \rangle$); and (iv) the average number of water molecules within the bilayers per lipid (n_{H_2O}) in each of the systems. Standard deviations for various quantities are shown within parentheses

	DOPC				DPPC-CHOL			
	Bilayer	PL	Mixed	PP	Bilayer	PL	Mixed	PP
Thickness	3.89 (0.04)	3.73 (0.05)	3.76 (0.04)	3.83 (0.04)	4.87 (0.06)	4.60 (0.07)	4.94 (0.03)	4.85 (0.06)
APL_{PC}	0.68 (0.02)	0.74 (0.02)	0.72 (0.01)	0.71 (0.01)	0.58 (0.02)	0.57 (0.01)	0.59 (0.04)	0.58 (0.03)
APL_{CHOL}	—	—	—	—	0.40 (0.03)	0.41 (0.13)	0.40 (0.07)	0.40 (0.04)
f_{2C6PC}	—	0.95	0.95	—	—	0.03	0.04	—
f_{C6FA}	—	—	0.98	0.98	0.57	0.55	—	—
f_{C6LYSO}	—	—	0.35	0.23	—	—	0.07	0.08
$\langle -S_{CH,sn1} \rangle$	0.122	0.115	0.115	0.117	0.425	0.422	0.421	0.422
$\langle -S_{CH,sn2} \rangle$	0.121	0.105	0.106	0.107	0.412	0.398	0.398	0.399
n_{H_2O}	14.7 (0.3)	17.3 (0.6)	15.9 (0.7)	16.6 (0.4)	7.8 (0.1)	6.5 (0.1)	7.2 (0.1)	6.9 (0.1)

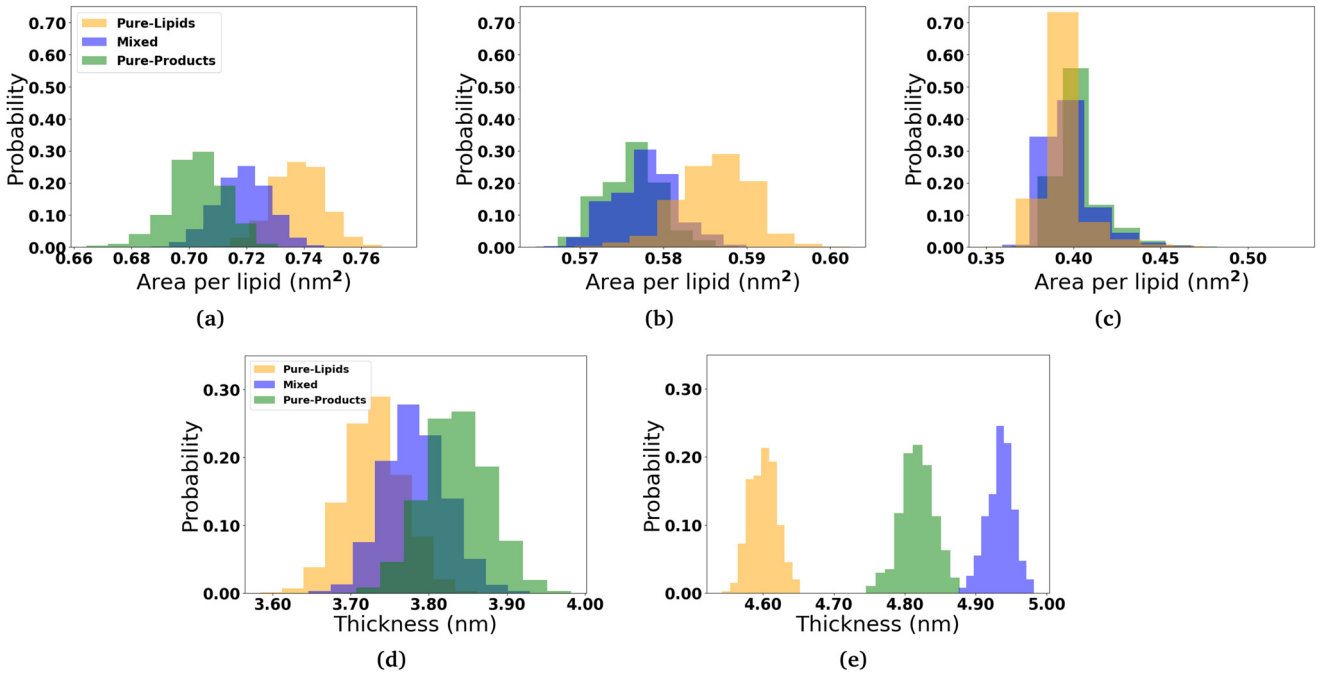

Fig. 3 Effects of the micelles on the structure of the bilayers. The distribution of the area per lipid for the (a) DOPC lipids in the DOPC membrane and the (b) DPPC and (c) CHOL lipids in the DPPC-CHOL membrane are displayed. Also the distribution of the thickness of the (d) DOPC and (e) DPPC-CHOL membranes is also plotted. Analysis of micelle-membrane was calculated over the last 200 ns of the production simulations.

2.3 Effect of micelles on the structure of lipid bilayers

To better understand the internal structure of the different bilayers after they interact with the molecules comprising the micelles, mass density profiles along the *z*-coordinate have been calculated (Fig. 4). In the DOPC membrane, of the three molecules comprising the micelles, the C6FA molecules insert the deepest into the membrane and are generally found amongst the ester groups of the lipids. Meanwhile, the 2C6PC molecules are found amongst the PC headgroups and the ester groups of the DOPC lipids, while the C6LYSO molecules are found amongst the PC headgroups.

In the DPPC-CHOL membrane, only C6FA inserts into the membrane to a significant extent. The C6FA molecules insert slightly further into the hydrophobic region of the lipid membrane. It is note worthy that in the mixed micelle system, we do find some C6FA at the boundary of the two leaflets of the DPPC-CHOL membrane.

To understand the orientation of the C6FA molecules that have inserted into the DOPC membrane, we measured the angle formed by the vector which connects the terminal carbon (C2) in the hydrocarbon chain of the fatty acid to the double-bonded oxygen (O2) on the other end of the molecule and the *z*-axis that is normal to the membrane's interface

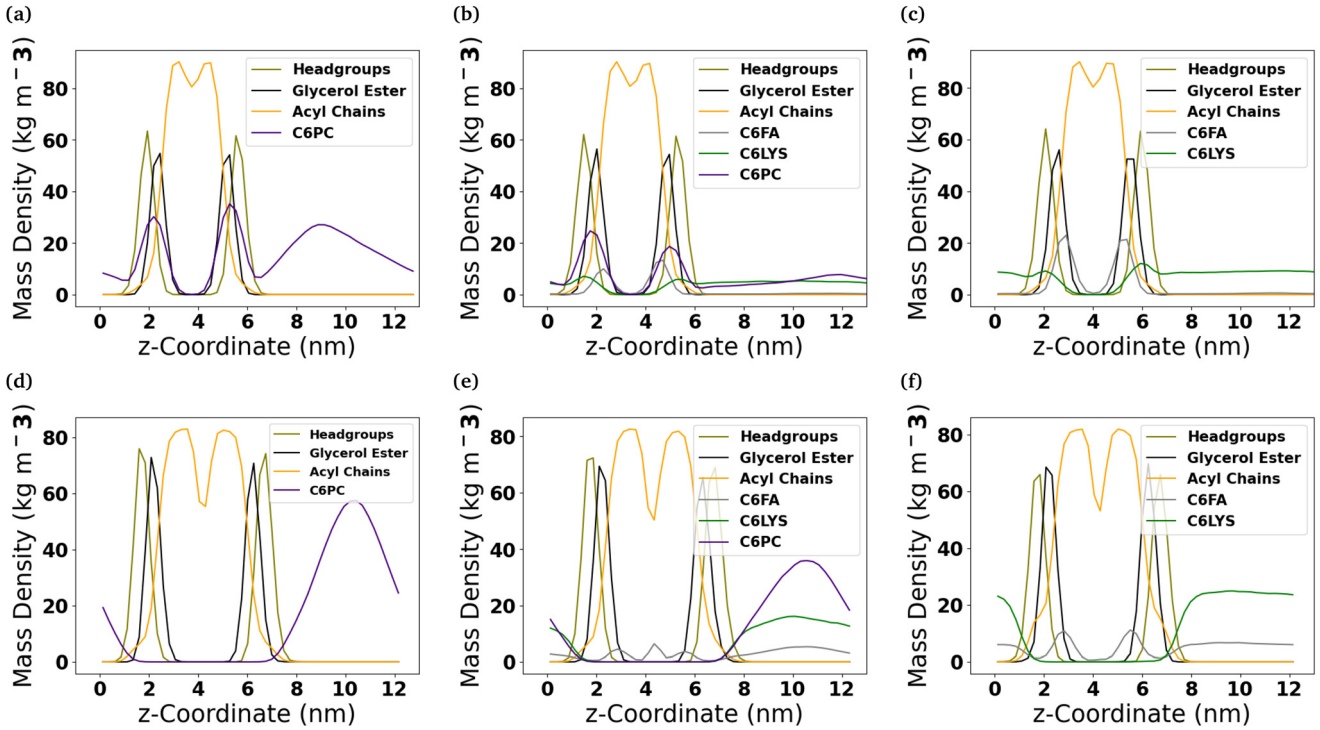

Fig. 4 Location of molecules comprising the micelles within lipid membranes. Mass density profiles of the DOPC ((a)–(c)) and DPPC-CHOL ((d)–(f)) membrane systems which have interacted with the three micelles that were studied (Pure-Lipids, Mixed and Pure-Products, respectively). Headgroups refers to the choline and phosphate groups in the PC lipids.

(Fig. 5 and Table S2†). The C6FA molecules are primarily oriented with their carboxylic acid groups located in the same plane within the membrane as the ester groups of the phospholipids with water and their hydrocarbon tails in the hydrophobic core of the DOPC bilayer ($\cos\theta \sim 0.9$). The mass density profiles of the –COOH and C2 groups in the C6FA molecules in the Pure-Products and Mixed micelle systems help to identify the depth and orientation after penetration. Fig. S8† shows that the C2 groups are closer to the mid-plane of the DOPC bilayer while the hydrophobic tails prefer to reside closer to the mid-plane than the COOH groups, indicating that the orientation of inserted C6FA tends to be parallel to the *z*-axis. The same behaviour is observed for C6FA when present in the DPPC-CHOL membrane, with there being a more significant difference in the mean *z*-positions of the –COOH and C2 groups indicating that the C6FA are less tilted in the DPPC-CHOL membrane. Also in the DPPC-CHOL membrane we observe that those C6FA molecules found in the bilayer's midplane are oriented parallel to the bilayer's interface.

The 2C6PC molecules are also found to insert with their tails within the hydrophobic core of the bilayer and the headgroups are solvated. The headgroups of the 2C6PC molecules inserted into the DOPC membrane are generally found to possess similar tilt angles as found for the DOPC lipids ($\cos\theta \sim 0.34$) themselves. The tilt angle distribution measured for the DOPC lipids is similar to those reported elsewhere for DOPC membranes.[47]

The order parameter has been calculated to study the lipid tail flexibility and is also related to the membrane thickness. It was computed over the trajectories for both saturated and unsaturated acyl chain carbon atoms from the lipid molecules in the upper and lower leaflets separately. The results for the mixed micelle system are shown in Fig. S4,† and the behaviour in the other systems are nearly identical. Similar values of the lipid order parameter for DOPC (liquid-ordered) and DPPC-CHOL (liquid-disordered) membranes have been reported elsewhere.[48,49] Interactions with the molecules from the various micelles result in a more significant disordering of the DOPC bilayer than the DPPC-CHOL bilayer as can be seen from the average values of the lipid order parameter for both of the sn1 ($\langle -S_{CH,sn1}\rangle$) and sn2 ($\langle -S_{CH,sn2}\rangle$) tails shown in Table 1. Recent studies have shown that the increased free volume in the middle of lipid bilayers is a result of the decreasing the values of the lipid order parameters.[50,51] In our case, the localization of the molecules comprising the micelles within the middle of the bilayer promotes a slight disorganization of the carbons in both tails, which leads to the lateral expansion of the membranes.

The radial distribution functions (RDFs) were used to determine the distribution of water molecules around the PC headgroups of the DOPC and DPPC lipid molecules and around the oxygen in the hydroxyl group of the cholesterol molecules in our membranes. By calculating the integral of the RDF from 0 to a distance corresponding to the first peak minimum, the

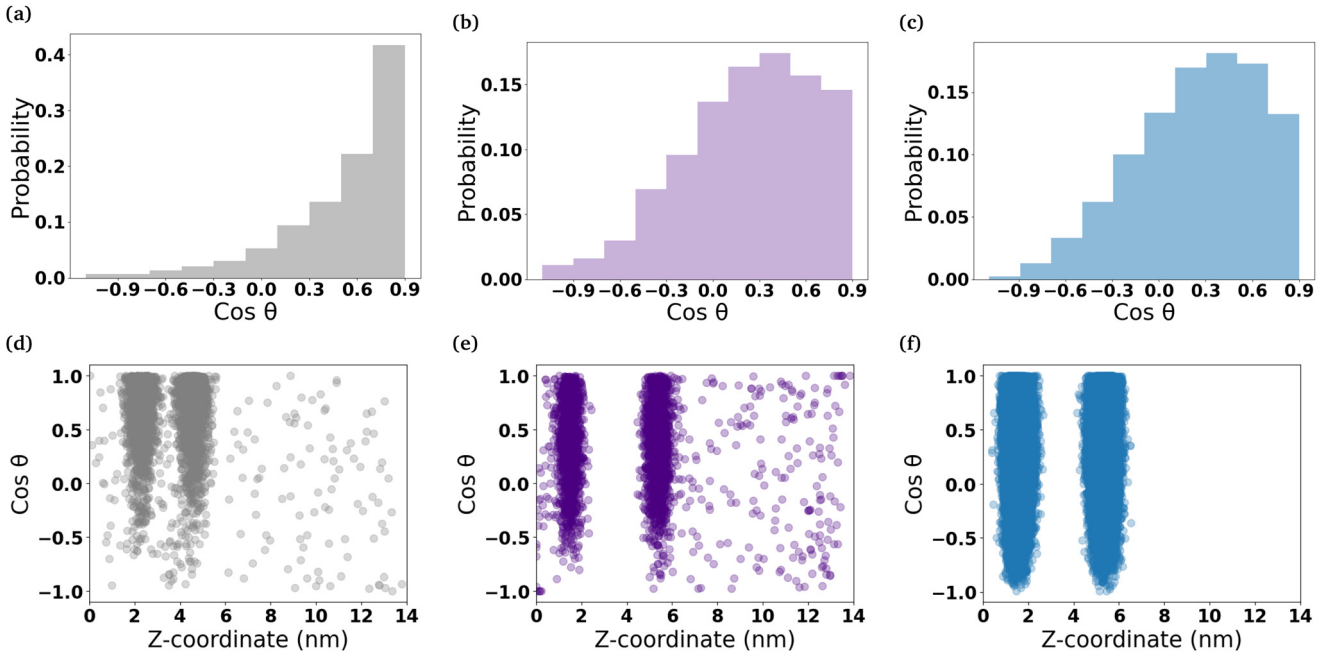

Fig. 5 Orientation of micelle components within DOPC membranes. The histograms show the cosine of the tilt angles of the (a) C6FA molecules that have inserted into the DOPC bilayer. (b) and (c) show the distribution of the cosine of the head group tilt angles of the 2C6PC molecules that have inserted into the DOPC bilayers and the head group tilt angles for DOPC lipids in the membrane, respectively. The scatter plots show how the distribution of the orientation of the (d) C6FA molecules, (e) the 2C6PC lipid head group and (f) the DOPC lipid head group changes with the molecule's location in the *z*-dimension.

average number of waters in the first hydration shell can be estimated. The RDFs are shown in Fig. S5 and S6.† The calculated coordination numbers for the first shell and the coordination number of waters are reported in Table S3.† The insertion of 2C6PC in the various membrane systems was seen to result in a dehydration of the choline group within the headgroup of DOPC. This dehydration of the nitrogen atom in the choline group of the DOPC molecules is likely due to the large steric barrier that exists between the headgroups when more and more molecules were inserted into membranes. Whereas the hydration of the phosphate group is unchanged by the presence of the molecules comprising the micelles within the lipid bilayer. While significantly less 2C6PC inserts into the DPPC-CHOL membrane, there is still a slight dehydration observed of the choline group of the DPPC lipids.

We have also determined the amount of water that is found between the phosphorous atoms in the lipid headgroups in the upper and lower leaflets of the bilayers. The number of water molecules within the bilayer per lipid molecule in the bilayer is reported in Table 1. We see that in the DOPC membrane there is an increased amount of water molecules that permeate into the bilayer when the various components of the micelle are present. While, in contrast, in the case of the DPPC-CHOL membranes, there is a slight decrease in the amount of water present in the bilayer after interaction with the various molecules comprising the micelles. As the penetration of water molecules into lipid bilayers is regularly used to investigate the permeability of a membrane,[52–54] these results demonstrate that as the micelle components partition into the membrane they increase the permeability of the disordered (DOPC) membranes.

2.4 Dynamics of micelle components within lipid bilayers

The motion of each molecule that was initially in a micelle was tracked in the *z*-dimension in each of the simulated systems (Fig. S10 and S11†). This allowed us to see that the C6FA molecules generally move to membranes' interface quickly. 2C6PC molecules were also found to adsorb to the membrane interface, while the C6LYSO molecules, which are more hydrophilic than the other molecules comprising the micelles, remain isolated in solution for longer and when they do come to the membrane interface they only remain there for a relatively short period of time.

Interestingly, we found that all of the micelle components have the ability to flip-flop across the lipid membranes, although we only observed the flip-flop of C6FA molecules across the DPPC-CHOL membrane. Table 2 contains the total number of flip-flops observed and the flip-flop rate for each molecule type in both membranes. The flip-flop rate is unchanged by the presence of the different molecules from the micelles within the membranes. However, as would be expected, we observe significantly less flip-flop of C6FA molecules within the more ordered DPPC-CHOL membrane than within the DOPC membrane.

In order to determine whether the micelle components aggregate with one another within the DOPC membrane, we

Table 2 Flip flop of micelle components across model bilayers. The total number of flip-flip events and the flip-flop rates (number per microseconds, in parentheses) across the DOPC and DPPC-CHOL membranes when they interact with the Pure-Lipids (PL), Mixed (Mixed) and Pure-Products (PP)

	DOPC			DPPC-CHOL		
System	PL	Mixed	PP	PL	Mixed	PP
2C6PC	3 (0.1)	2 (0.2)	—	0 (0)	0 (0)	—
C6FA	—	42 (1.8)	54 (1.9)	—	11 (0.7)	22 (0.8)
C6LYSO	—	16 (0.8)	18 (0.9)	—	0 (0)	0 (0)

have calculated the lipid enrichment index over the final 200 ns of each of those simulations. The lipid enrichment values are representative of the local environment in the membranes.[55] Fig. S12† shows that none of the micelle components (2C6PC, C6FA & C6LYSO) aggregate with one another within the membrane, as generally their respective enrichment indices are lower than 1.

3 Conclusion

In this manuscript, we have used all-atom molecular dynamics simulations to investigate how the C6 phosphocholine micelles at various stages of digestion after exposure to the $sPLA_2$ enzyme interact with a disordered and an ordered lipid bilayer. We observed that as the micelles begin to interact with the bilayers they disassociate and release the various components of the micelles although each of the molecules comprising the micelles behaves differently. The 2C6PC molecules are more preferably found within a micelle and therefore we observe an aggregate remaining as the disassociation progresses, although as the molecules are released they diffuse to the interface of the membranes and insert into the bilayers. In contrast, the lysophosphocholine (C6LYSO) molecules become solvated in the aqueous environment and commonly remain isolated in solution, but occasionally they adsorb reversibly to the interface of the bilayers. The C6FA molecules are found to disassociate from the micelles as they appear to prefer to absorb into the lipid bilayers.

The various types of molecules in the micelles then penetrate the two different lipid bilayers to differing degrees with more of each component inserting into the disordered DOPC membrane than into the ordered DPPC-CHOL membrane. This is due to the fact that there is less free volume available for the molecules to insert into the DPPC-CHOL membrane than in the DOPC membrane. Similar trends in the absorption of lysolipids and fatty acids with 10–16 carbons in their hydrocarbon chains have been observedexperimentally.[56]

We found that each of the micelle components impact the structural properties of the lipid membranes to differing degrees. However, the insertion of the molecules have the same general effect on both membranes. Specifically, the products of the lipid digestion (C6FA & C6LYSO) result in a small increase in the area per lipid of the phosphocholine lipids in each membrane and a slight thinning of both membranes. This is consistent with various studies that found that when fatty acids and lysolipids are added together to liquid ordered and liquid disordered membranes they have little to no effect on the permeation of small molecules into the membranes.[36,38,39,57] However, the 2C6PC molecules have more of an impact on the area per lipid and the thinning of the membranes.

In addition to the difference in the structural properties caused by each micelle component, we also found that they demonstrate different dynamic properties within the bilayers. The C6FA molecules are found to flip-flop across the bilayers significantly more and more frequently than either the C6LYSO and 2C6PC molecules. This results from the C6FA being the least hydrated of any of the micelle components when inserted into the membrane and also they are significantly smaller than the 2C6PC molecules. Previously, longer fatty acid chains have been observed to flip-flop across lipid membranes of varying composition.[58–61]

The findings presented in this manuscript provide the first atomistic understanding of how a combination of lipids and their digestion products affects model lipid membranes. In doing so, we have shown that each micellar component has differing degrees of effect on the interfacial and structural properties of the two model membranes studied. Additionally we have shown that the molecules comprising the micelles have significantly different dynamic properties once they are inserted within the two bilayers. These results will be of particular interest when considering the design of novel lipid-based drug delivery vehicles.

This is of particular interest when considering the application of phospholipid drug delivery vehicles for anticancer therapeutics. The concentration of the $sPLA_2$ enzyme is elevated in cancerous cells which would then lead to a more rapid digestion of the phospholipids into the corresponding lysolipids and fatty acids. Our previous work[2] showed that the phospholipid micelles were stable and as the amount of lysolipids and fatty acids increased in the micelles, they became increasingly dynamic. Therefore these phospholipid micelles would then preferentially release their payload near cancerous cells where the action of $sPLA_2$ would be enhanced. In this manuscript, we have gone on to show that the lysolipids and fatty acids produced during the digestion of the phospholipids then result in the increased permeability of lipid membranes which would result in faster diffusion of the therapeutics into the cancerous cells. Therefore phospholipid drug delivery vehicles may prove to be promising anti-cancer formulations moving forward.

4 Methods

4.1 System setup

In this study, we used all-atom molecular dynamics simulations to investigate the interactions between micelles con-

taining 2C6PC and its hydrolysis products and a model disordered and ordered lipid membranes. Firstly, two model lipid membranes were equilibrated: (i) a DOPC membrane (disordered) and (ii) a membrane consisting of 70 mol% DPPC and 30 mol% cholesterol (ordered). In order to insure that the micelles would not interact with themselves through the periodic boundary conditions, the interfacial area of each membrane was chosen such that it was greater than twice the diameter of the largest micelle we planned to investigate in subsequent simulations. The chemical structures of the various lipid molecules comprising the membranes are shown in Fig. S2† while snapshots of the two membranes are shown in Fig. S3.†

Both of the lipid bilayers studied were generated by using the CHARMM-GUI Membrane Builder.[62] The bilayers were neutralised using a salt concentration of 150 mM NaCl to mimic the physiological environment. Table S1† contains the molecular composition of both types of bilayers. The initial dimensions of the simulated lipid bilayer systems were 10.8 nm × 10.8 nm × 9.0 nm ($x \times y \times z$ dimensions).

These bilayers were equilibrated using the simulation protocol prescribed by CHARMM-GUI, whereby (i) initial structures were energy minimized using steepest descent, (ii) systems were equilibrated using the NVT (constant number of particles, volume, and temperature) followed by the NPT (constant number of particles, pressure, and temperature) ensembles for at least 1.8 ns, and (iii) finally, MD production simulations were performed using the NPT ensemble for 200 ns.

Subsequently, we investigated the interactions between micelles representing varying degrees of digestion of the 2C6PC molecules and each of the two lipid membranes. Three different micelle compositions (namely, Pure-Lipid, Mixed & Pure-Products system) were investigated according to the percentage of 2C6PC that had been degraded. The Pure-Lipid micelle system contains only 2C6PC. The Mixed micelle represents the state where approximately half of the 2C6PC have been digested and therefore contains a mixture of the parent molecule and both of the hydrolysis products (C6FA & C6LYSO). Finally the Pure-Products micelle represents the aggregate formed when after all of the 2C6PC has been hydrolysed and as a consequence contains only C6FA and C6LYSO. The equilibrated structure of each micelle as reported in our previous study[2] was used as an initial state of the micelle in the simulations reported here. The number of each type of molecule in the various micelles is given in Table S1.† We then created six different systems, each one contained a single micelle inserted into the aqueous environment approximately 2 nm above the surface of the equilibrated ordered or disordered membrane. Additional water and ions were added to fully solvate the system and to maintain an ionic concentration of 150 mM NaCl. Each of the micelle and bilayer systems had initial dimensions of 11 nm × 11 nm × 13 nm. A detailed description of the molecular components found in the simulations of the two pure lipid membranes, and the six different micelle and membrane systems is given in Table S1† and their chemical structures can be found in Fig. S1 and S2.† The six resulting systems were then simulated by using the same protocol as described above for the two pure membrane systems, and the parameters suggested by CHARMM-GUI. The starting configurations were first energy minimized in order to remove any possible bad contacts and then six short equilibration simulations (a mixture of NVT and NPT) were performed before the production simulations of at least 1 μs was conducted.

The TIP3P and the CHARMM36 forcefields[63] were used for water and all of the lipid molecules, respectively. Periodic boundary conditions were applied in all three dimensions for the simulated systems. All simulations were carried out using the GROMACS MD engine.[64] In the production simulations, the temperature was maintained at 310 K with the Nosé–Hoover thermostat with a time constant of 5 ps.[65,66] Semi-isotropic pressure coupling was used to maintain a pressure of 1 bar with the Parrinello–Rahman barostat,[67,68] using a time constant of 5 ps and a standard compressibility of 4.5×10^{-5} per bar. The Verlet cutoff scheme was employed. Electrostatic interactions were calculated using the particle-mesh Ewald algorithm. Both electrostatic and van der Waals interactions were cut off beyond 1.2 nm. All bonds involving hydrogen atoms were constrained using the LINCS algorithm.[69]

4.2 Analysis

In the simulated systems, the membranes are oriented such that their component molecules lie in the xy-plane with their normal vector in the z-direction and their hydrophilic head groups on the exterior surfaces of the membrane. The membrane thickness therefore was determined by calculating the difference between the average z position of the phosphorous atoms of the PC lipid headgroups in the upper leaflet of the membrane and the average z position of the phosphorous atoms of the PC lipids in the membrane's lower leaflet.

The area per lipid (APL) was calculated using the Voronoi tessellation scheme found in the FATSLiM python package.[70] The mass density profile for the membrane systems was obtained utilizing the gmx density tool in the Gromacs package. Using this tool we are able to find the average distribution of different atom/molecules as a function of the z-axis.

The lipid order parameter of each chain S_{CH} was calculated using eqn (1):

$$S_{CH} = \frac{1}{2}\left(3\cos^2\theta - 1\right) \quad (1)$$

where θ is the angle between carbon–hydrogen (C–H) bond and the normal vector for the lipid leaflet. S_{CH} is used to describe the orientation of the C–H bond vector with respect to the z-axis over all lipids and the sampling time. When S_{CH} = 1, it means that the C–H bond is completely aligned with the bilayer normal, whereas S_{CH} = −0.5 means the C–H bond is oriented perpendicular to the z-axis.[71,72]

In order to investigate if there was any preferential interaction of the various components of the micelles with each

other or with components of the lipid membranes, a lipid enrichment index was used, which was defined as:

$$E_{AB} = \frac{N_{AB}}{N_B} \quad (2)$$

where E_{AB} is the enrichment index of species B around species A, N_{AB} is the number of molecules of species B around species A and N_B is the average total number of species B around any species. When the value is below 1, it corresponds to depletion of species B in the local environment of species A. On the other hand, if E_{AB} is larger than 1 it corresponds to an enrichment of species B within the local environment of A.[73]

The tilt angles of the headgroups of the PC lipid molecules are defined as the angle between the vector formed between the atom P and N in the PC headgroup and the z-axis (see Fig. S2†). Meanwhile, the tilt angle of hexanoic acid (C6FA) is measured from the angle between the vector connecting the C2 and O2 atoms (see Fig. S8†) and the z-axis.[74] Moreover, the z-coordinates of each molecule has been measured as a function of time in order to track each molecules' position.

Finally, radial distribution functions (RDFs) were calculated by using the gmx rdf command. The RDF measures the probability of finding a specific particle (B) at a distance r from another particle (A) as shown in eqn (3):

$$g_{AB}(r) = \frac{1}{\langle \rho_B \rangle} \frac{1}{N_A} \sum_{i \epsilon A}^{N_A} \sum_{j \epsilon B}^{N_B} \frac{\delta(r_{ij} - r)}{4\pi r^2} \quad (3)$$

where $\langle \rho_B \rangle$ is the bulk density of B.

Snapshots of the simulation systems were created using Visual Molecular Dynamics (VMD).[75] In addition to using the gromacs tools noted above, all other analysis was carried out with a mixture of python scripts developed in house and functions found in LiPyphilic.[74]

Author contributions

Jun Xie: data curation, formal analysis, investigation, methodology, software, validation, visualisation, writing – original draft, writing – review & editing. Demi L. Pinke: conceptualization, writing – review & editing. M. Jayne Lawrence: conceptualization, supervision, writing – review & editing. Christian D. Lorenz: conceptualization, funding acquisition, project administration, resources, supervision, writing – review & editing.

Conflicts of interest

There are no conflicts to declare.

Acknowledgements

We are grateful to the UK Materials and Molecular Modelling Hub for computational resources, which is partially funded by EPSRC (EP/T022213/1, EP/W032260/1 and EP/P020194/1), and the UK HPC Materials Chemistry Consortium, which is also funded by EPSRC (EP/R029431), for providing us access to computational resources. This work also benefited from access to the King's Computational Research, Engineering and Technology Environment (CREATE) at King's College London.[76] J. X. acknowledges the support by King's-China Scholarship Council PhD studentship (KCL-CSC). For the purpose of open access, the author has applied a Creative Commons Attribution (CC BY) licence (where permitted by UKRI, 'Open Government Licence' or 'Creative Commons Attribution No-derivatives (CC BY-ND) public copyright licence' may be stated instead) to any Author Accepted Manuscript version arising.

References

1 H. Ishkhanyan, R. M. Ziolek, D. J. Barlow, M. J. Lawrence and C. D. Lorenz, *Nanoscale*, 2022, **14**, 5392–5403.
2 D. L. Pink, F. Foglia, D. J. Barlow, M. J. Lawrence and C. D. Lorenz, *Small*, 2021, **17**, 2004761.
3 D. L. Pink, O. Loruthai, R. M. Ziolek, A. E. Terry, D. J. Barlow, M. J. Lawrence and C. D. Lorenz, *J. Colloid Interface Sci.*, 2021, **597**, 278–288.
4 D. L. Pink, O. Loruthai, R. M. Ziolek, P. Wasutrasawat, A. E. Terry, M. J. Lawrence and C. D. Lorenz, *Small*, 2019, **15**, 1903156.
5 D. T. Allen, Y. Aaaka, M. J. Lawrence and C. D. Lorenz, *J. Phys. Chem. B*, 2014, **118**, 13192–13201.
6 S. Senapati, A. K. Mahanta, S. Kumar and P. Maiti, *Signal Transduction Targeted Ther.*, 2018, **3**, 7.
7 D. E. Large, J. R. Soucy, J. Hebert and D. T. Auguste, *Adv. Ther.*, 2019, **2**, 1800091.
8 A. P. Singh, A. Biswas, A. Shukla and P. Maiti, *Signal Transduction Targeted Ther.*, 2019, **4**, 33.
9 B. Das, D. Chattopadhyay and D. Rana, *Biomater. Sci.*, 2020, **8**, 4665–4691.
10 A. S. Piotrowski-Daspit, A. C. Kauffman, L. G. Bracaglia and W. M. Saltzman, *Adv. Drug Delivery Rev.*, 2020, **156**, 119–132.
11 Y.-B. Miao, Y.-J. Lin, K.-H. Chen, P.-K. Luo, S.-H. Chuang, Y.-T. Yu, H.-M. Tai, C.-T. Chen, K.-J. Lin and H.-W. Sung, *Adv. Mater.*, 2021, **33**, 2104139.
12 D. E. Large, R. G. Abdelmessih, E. A. Fink and D. T. Auguste, *Adv. Drug Delivery Rev.*, 2021, **176**, 113851.
13 K. Paunovska, D. Loughrey and J. E. Dahlman, *Nat. Rev. Genet.*, 2022, **23**, 265–280.
14 L. Xu, X. Wang, Y. Liu, G. Yang, R. J. Falconer and C.-X. Zhao, *Adv. NanoBiomed Res.*, 2022, **2**, 2100109.
15 R. R. Sawant and V. P. Torchilin, *Mol. Membr. Biol.*, 2010, **27**, 232–246.
16 J. Li, X. Wang, T. Zhang, C. Wang, Z. Huang, X. Luo and Y. Deng, *Asian J. Pharm. Sci.*, 2015, **10**, 81–98.
17 Z. Gao, A. N. Lukyanov, A. R. Chakilam and V. P. Torchilin, *J. Drug Targeting*, 2003, **11**, 87–92.

18 C. Zimmer, J. Corum, S.-L. Wee and M. Kristoffersen, *Coronavirus vaccine tracker*, 2020, **https://www.nytimes.com/interactive/2020/science/coronavirus-vaccine-tracker.html**.
19 E. A. Dennis, P. L. Darke, R. A. Deems, C. R. Kensil and A. Plückthun, *Mol. Cell. Biochem.*, 1981, **36**, 37–45.
20 D. A. Six and E. A. Dennis, *Biochim. Biophys. Acta, Mol. Cell Biol. Lipids*, 2000, **1488**, 1–19.
21 G. Lambeau and M. H. Gelb, *Annu. Rev. Biochem.*, 2008, **77**, 495–520.
22 W. Pruzanski and P. Vadas, *J. Rheumatol.*, 1988, **15**, 1601–1603.
23 S. Yamashita, J. Yamashita and M. Ogawa, *Br. J. Cancer*, 1994, **69**, 1166–1170.
24 H. Kiyohara, H. Egami, H. Kako, Y. Shibata, K. Murata, S. Ohshima, K. Sei, S. Suko, R. Kurano and M. Ogawa, *Int. J. Pancreatol.*, 1994, **13**, 49–57.
25 S. Yamashita, J. Yamashita, K. Sakamoto, K. Inada, Y. Nakashima, K. Murata, T. Saishoji, K. Nomura and M. Ogawa, *Cancer*, 1993, **71**, 3058–3064.
26 J. R. Graff, B. W. Konicek, J. A. Deddens, M. Chedid, B. M. Hurst, B. Colligan, B. L. Neubauer, H. W. Carter and J. H. Carter, *Clin. Cancer Res.*, 2001, **7**, 3857–3861.
27 L. Leistad, A. J. Feuerherm, M. Ostensen, A. Faxvaag and B. Johansen, *Clin. Chem. Lab. Med.*, 2004, **42**, 602–610.
28 B. Rosengren, A. C. Jonsson-Rylander, H. Peilot, G. Camejo and E. Hurt-Camejo, *Biochim. Biophys. Acta, Mol. Cell Biol. Lipids*, 2006, **1761**, 1301–1308.
29 Q. Dong, M. Patel, K. F. Scott, G. G. Graham, P. J. Russell and P. Sved, *Cancer Lett.*, 2006, **240**, 9–16.
30 E. A. Dennis, J. Cao, Y.-H. Hsu, V. Magrioti and G. Kokotos, *Chem. Rev.*, 2011, **111**, 6130–6185.
31 K. Jørgensen, J. Davidsen and O. G. Mouritsen, *FEBS Lett.*, 2002, **531**, 23–27.
32 T. L. Andresen, J. Davidsen, M. Begtrup, O. G. Mouritsen and K. Jørgensen, *J. Med. Chem.*, 2004, **47**, 1694–1703.
33 G. Zhu, J. N. Mock, I. Aljuffali, B. S. Cummings and R. D. Arnold, *J. Pharm. Sci.*, 2011, **100**, 3146–3159.
34 F. Fouladi, K. J. Steffen and S. Mallik, *Bioconjugate Chem.*, 2017, **28**, 857–868.
35 F. Movahedi, R. G. Hu, D. L. Becker and X. Xu, *Nanomedicine*, 2015, **11**, 1575–1584.
36 J. Davidsen, O. G. Mouritsen and K. Jørgensen, *Biochim. Biophys. Acta*, 2002, **1564**, 256–262.
37 R. de la Rica, D. Aili and M. M. Stevens, *Adv. Drug Delivery Rev.*, 2012, **64**, 967–978.
38 H. Jespersen, J. H. Andersen, H. J. Ditzel and O. G. Mouritsen, *Biochimie*, 2012, **94**, 2–10.
39 A. Arouri, K. E. Lauritsen, H. L. Nielsen and O. G. Mouritsen, *Chem. Phys. Lipids*, 2016, **200**, 139–146.
40 V. V. Kumar and W. J. Baumann, *Biophys. J.*, 1991, **59**, 103–107.
41 P. Martinez-Landeira, J. L. Lopez-Fontan, J. M. Ruso, G. Prieto and F. Sarmiento, *Colloids Surf., A*, 2003, **216**, 91–96.
42 R. J. M. Tausk and J. T. G. Overbeek, *Biophys. Chem.*, 1974, **2**, 175–179.
43 M. S. Hossain, S. Berg, C. A. S. Bergstrom and P. Larsson, *AAPS PharmSciTech*, 2019, **20**, 61.
44 O. Edholm and J. F. Nagle, *Biophys. J.*, 2005, **89**, 1827–1832.
45 N. Kučerka, S. Tristram-Nagle and J. F. Nagle, *Biophys. J.*, 2006, **90**, L83–L85.
46 A. I. Greenwood, S. Tristram-Nagle and J. F. Nagle, *Chem. Phys. Lipids*, 2006, **143**, 1–10.
47 S. M. Yee, R. J. Gillams, S. E. McLain and C. D. Lorenz, *Soft Matter*, 2021, **17**, 126–135.
48 A. Suhaj, A. Le Marois, D. J. Williamson, K. Suhling, C. D. Lorenz and D. M. Owen, *Phys. Chem. Chem. Phys.*, 2018, **20**, 16060–16066.
49 A. Suhaj, D. Gowland, N. Bonini, D. M. Owen and C. D. Lorenz, *J. Phys. Chem. B*, 2020, **124**, 11419–11430.
50 M. F. Martini and M. Pickholz, *Int. J. Quantum Chem.*, 2012, **112**, 3341–3345.
51 M. Pickholz, L. F. Fraceto and E. de Paula, *Synth. Met.*, 2009, **159**, 2157–2158.
52 S. J. Marrink and H. J. C. Berendsen, *J. Phys. Chem.*, 1996, **100**, 16729–16738.
53 R. M. Venable, A. Kramer and R. W. Pastor, *Chem. Rev.*, 2019, **119**, 5954–5997.
54 A. Kramer, A. Ghysels, E. Wang, R. M. Venable, J. B. Klauda, B. R. Brooks and R. W. Pastor, *J. Chem. Phys.*, 2020, **153**, 124107.
55 R.-X. Gu, S. Baoukina and D. P. Tieleman, *J. Am. Chem. Soc.*, 2020, **142**, 2844–2856.
56 P. Høyrup, J. Davidsen and K. Jørgensen, *J. Phys. Chem. B*, 2001, **105**, 2649–2657.
57 A. Arouri and O. G. Mouritsen, *Prog. Lipid Res.*, 2013, **52**, 130–140.
58 S. M. Yee and C. D. Lorenz, *J. Phys. Chem. B*, 2021, **125**, 8038–8047.
59 J. A. Hamilton and K. Brunaldi, *J. Mol. Neurosci.*, 2007, **33**, 12–17.
60 F. Kamp, D. Zakim, F. Zhang, N. Noy and J. A. Hamilton, *Biochemistry*, 1995, **34**, 11928–11937.
61 A. M. Kleinfeld, P. Chu and C. Romero, *Biochemistry*, 1997, **36**, 14146–14158.
62 E. L. Wu, X. Cheng, S. Jo, H. Rui, K. C. Song, E. M. Dávila-Contreras, Y. Qi, J. Lee, V. Monje-Galvan, R. M. Venable, J. B. Klauda and W. Im, *CHARMM-GUI membrane builder toward realistic biological membrane simulations*, 2014.
63 J. Huang, S. Rauscher, G. Nawrocki, T. Ran, M. Feig, B. L. De Groot, H. Grubmüller and A. D. MacKerell Jr., *Nat. Methods*, 2017, **14**, 71–73.
64 M. J. Abraham, T. Murtola, R. Schulz, S. Páll, J. C. Smith, B. Hess and E. Lindahl, *SoftwareX*, 2015, **1**, 19–25.
65 S. Nosé, *Mol. Phys.*, 1984, **52**, 255–268.
66 W. G. Hoover, *Phys. Rev. A*, 1985, **31**, 1695.
67 M. Parrinello and A. Rahman, *J. Appl. Phys.*, 1981, **52**, 7182–7190.
68 S. Nosé and M. L. Klein, *Mol. Phys.*, 1983, **50**, 1055–1076.

69 B. Hess, H. Bekker, H. J. Berendsen and J. G. Fraaije, *J. Comput. Chem.*, 1997, **18**, 1463–1472.
70 S. Buchoux, *Bioinformatics*, 2016, **33**, 133–134.
71 T. J. Piggot, J. R. Allison, R. B. Sessions and J. W. Essex, *J. Chem. Theory Comput.*, 2017, **13**, 5683–5696.
72 R. Gupta, Y. Badhe, S. Mitragotri and B. Rai, *Nanoscale*, 2020, **12**, 6318–6333.
73 P. Smith, P. G. Petrov and C. D. Lorenz, bioRxiv, 2021.
74 P. Smith and C. D. Lorenz, *J. Chem. Theory Comput.*, 2021, **17**, 5907–5919.
75 W. Humphrey, A. Dalke and K. Schulten, *J. Mol. Graphics*, 1996, **14**, 33–38.
76 King's College London, *King's Computational Research, Engineering and Technology Environment (CREATE)*, 2022. DOI: **10.18742/rnvf-m076**.

Chapter 4

Impact of Anti-Cancer Drugs on the structural and properties of a Lipid-based Drug Delivery Vehicles

4.1 Introduction

Over the last few decades, the development of nanomedicine has emerged as a pivotal area in nanotechnology, aiming to enhance healthcare through the creation of drug nanocarriers. Many drug delivery systems (DDSs) designed for anti-tumor drugs offer numerous benefits, such as the solubilization of hydrophobic drugs, increased cargo loading, extension of systemic circulation, improvement of tumor targeting and cellular uptake, and controlled release of cargo[153–157]. Enzymes play a crucial role in regulating intricate structural modifications of biomaterials within our bodies. Lipids, serving as a source of energy, also act as carriers for lipophilic nutrients or drugs. They are notably significant substrates for enzymes, with a wide range of phospholipases facilitating the transformation of lipids from our diet into components that can be absorbed [121, 119].

Phosphatidylcholine (PC) lipids are the primary constituents of cellular membranes and have very distinct characteristics, such as the ability to self-assemble as a result of their amphiphilic structure [158] and their excellent biocompatibility [159]. Also they show great promise in enhancing the effectiveness of drug delivery, offering a suitable approach to systematic drug administration over the recent years[160]. Lipid micelles, conjugated phospholipids or lysolipids can spontaneously self-assemble in aqueous environments when lipid concentrations exceed their critical micelle concentrations (CMCs) and are commonly utilized in formulations for DDSs [161–163].

Approximately 40% of new chemical entities in pharmaceutical research exhibit poor aqueous solubility. Consequently, drugs with limited water solubility constitute a substantial portion of global pharmaceutical sales, estimated at approximately $37 billion[164]. Doxorubicin (DOX), a widely used chemotherapy drug, belongs to a class of drugs known as anthracyclines and is commonly used in the treatment of various types of cancers, including breast cancer, leukemia, and lymphomas[165, 166]. Camptothecin (CAMPT) is a anticancer compound and known for its ability to inhibit the activity of the enzyme topoisomerase I.[167–169] Both drugs show poor water solubility, which hampers their clinical application [170, 171]. Lipid-based delivery systems are promising carriers for a range of water-insoluble drugs. When employed to transport hydrophobic drugs, lipid-based drug delivery vehicles can encapsulate or embed the drug molecules, which would improve the stability of water-insoluble drugs in aqueous environments both in vitro and in vivo [163]. While there is growing interest in utilizing self-assembling micelles for drug-delivery purposes, there is currently a limited comprehension of the specific molecular-scale mechanisms responsible for the development of their favorable properties.

In this study, we used all-atom molecular dynamics simulations to investigate both solubilization and localization in three different composition of lipid-based micelle systems for two hydrophobic small molecule therapeutics, camptothecin (CAMPT) and doxorubicin (DOX). Our simulations provide an insight into the interaction between these drugs and the micelles, shedding light on their dynamic behaviour and impact on the micellar composition and stability. Specifically, the distinct characteristics observed for CAMPT and DOX highlight the importance of considering the specific properties of drug delivery vehicles. In particular, the observed trends in this study on orientation, internal contact and hydration numbers provide a foundation for further exploration and optimization of drug delivery systems.

4.2 Methods and Analysis

Simulations The initial state for each micelle in the simulations conducted in this study was derived from the equilibrated structure described in our earlier investigations. [2, 172] The models for the two types of drugs, Camptothecin (a) and Doxorubicin (b) (Fig. 4.1), were parameterised using the Ligand Reader & Modeler, which is part of CHARMM-GUI [173, 174]. These models were then used with the micelle structures to create three different systems, whose compositions are summarised in Table 4.1. Initially, simulations were conducted with three, six and ten drug molecules to compare their behavior. However, it was observed that with six or ten numbers, the drugs tended to aggregate rather than interact with the micelles. To avoid this aggregation and have better meaningful interactions with micelles, three drug molecules were chosen for the final simulation systems. Thus, three drug molecules were placed randomly around the pre-assembled micelle in

System	**CAMPT**					**DOX**				
	C6FA	*C6LYS*	*2C6PC*	*CAMPT*	*water*	*C6FA*	*C6LYS*	*2C6PC*	*DOX*	*water*
Pure-Lipids	0	0	35	3	6085	0	0	35	3	6149
Mixed	16	12	16	3	6086	16	12	16	3	6290
Pure-Products	29	21	0	3	6292	29	21	0	3	6388

Table 4.1 **Composition of each systems** Details of six different simulated systems, including number of molecules and drugs.

each system. In each system, water molecules are subsequently introduced to fill the remaining free volume inside of a 60 Å $\times$ 60 Å $\times$ 60 Åsimulation box. All simulations were conducted using Gromacs 2019.[175] The CHARMM TIP3P model was used for water molecules and CHARMM36 force-field was used to model the interactions of the micelles and the drug molecules.[176, 175, 177] The NVT ensemble was used to thermalize the systems, in which the Nosé-Hoover thermostat [178] was used to equilibrate the systems at a temperature of 310 K. After 200 ps of thermalization, the Nosé-Hoover thermostat and the Parrinello-Rahman barostat [179, 180] were used to equilibrate the temperature to 310 K and the pressure to 1 bar, respectively, within the NPT ensemble for another 200 ps. Finally, a production simulation was performed using the NPT ensemble, employing the Nosé–Hoover thermostat and Parrinello–Rahman barostat. For each system, the production simulation ran for an adequate duration to ensure the micelle's size and shape reached equilibrium. In all simulations, the van der Waals interactions were truncated beyond a distance of 1.2 nm and the particle-mesh Ewald algorithm was used to calculated the long-range electrostatic interactions. We applied constraints to all bonds that included hydrogen atoms by utilizing the LINCS algorithm [181].

Analysis All analysis was performed with in-house developed Python scripts [182] alongside the python MDAnalysis[183], PySoftK [184] and pySoftWhere [185]. The visualizations were produced using VMD[186].

In order to determine the shape of the micelles during the course of the simulations, we calculated each systems' eccentricity (ε) of the largest micelles, defined as the Eq. 4.1 :

$$\varepsilon = 1 - \frac{I_{\text{min}}}{I_{\text{ave}}} \tag{4.1}$$

where I_{min} represents the minimum moment of inertia, while I_{ave} denotes the average of all moment of inertia values computed. To identify the number of molecules in each micelle, the Python module Networkx [187] was used to study the aggregation of the lipid molecules and the drugs. Each molecule was defined by one atom, and a distance cut-off was introduced to identify if two molecules were considered part of the same micelle. The fraction of each component that contributes to the formation of the largest micelles was calculated by dividing the total number of molecules in the largest micelle by the total initial number of molecules. The radius of gyration R_g (Eq. 4.2) was also calculated to have an indication of the size and compactness of each micelle.

$$R_g = \left(\frac{\sum_i |\mathbf{r}_i||^2 m_i}{\sum_i m_i} \right)^{\frac{1}{2}} \tag{4.2}$$

where m_i is the mass of atom i and $\mathbf{r}_i$ is the distance between atom i and the center of the mass of the bilayer. The radius of gyration was calculated by using MDAnalysis function `radius_of_gyration()`. [188]

The interactions between pairs of molecules in our simulations were analyzed by creating contact maps with MDAnalysis tools. Firstly, we calculated the radial distributions (RDFs) between the molecules that we wanted to study. The distance corresponding to the first peak in the RDFs plots was used as the first neighbour distance between two molecules. A

similar approach was used to study the hydration of molecules. Close contact was defined when the distance between heavy atoms of the molecules of interest was within 6 Å, which was representative of the first neighbour distance for the molecules of interest, and the count of contacts was calculated for each pair of heavy atoms on these molecules. This approach allows us to track how two molecules interact. If there is no preference, the number of close interactions between two molecules will be roughly uniform across all atoms within the two molecules. A larger number (darker color in this paper) of close interactions between specific atoms might indicate a preference.

Tilt angles were calculated to investigate the orientation of drug molecules as they interact with the micelles. For the drug molecule CAMPT, we measured the angle between the vector formed by the carbon atoms C20 and C6 and another vector formed between the center of mass of the micelle and the C9 arbon atom within CAMPT to represent the center of mass of the drug (see Fig. 4.1). Regarding the drug DOX, we determined the angle between the vector connecting the C2 and C25 atoms and the vector connecting the center of mass of the micelle and the C14 carbon within the DOX molecule which represents its center of mass (see in Fig. 4.1).

To accurately examine the internal structure and the interfacial properties of the micelles, we employed the intrinsic core-shell interface (ICSI) method provided by the python package pySoftWhere within PySoftK.[185, 184] We selected acyl chains of 2C6PC as the core in Pure-Lipids micelles and the hydrophobic chain of the C6FA molecules in the Mixed and Pure-Products micelles to represent the core of the micelles as they are the main component as observed from the snapshots in Figures 4.2 & 4.2. A grid of dimensions 30×30 was chosen. A comprehensive explanation of how this

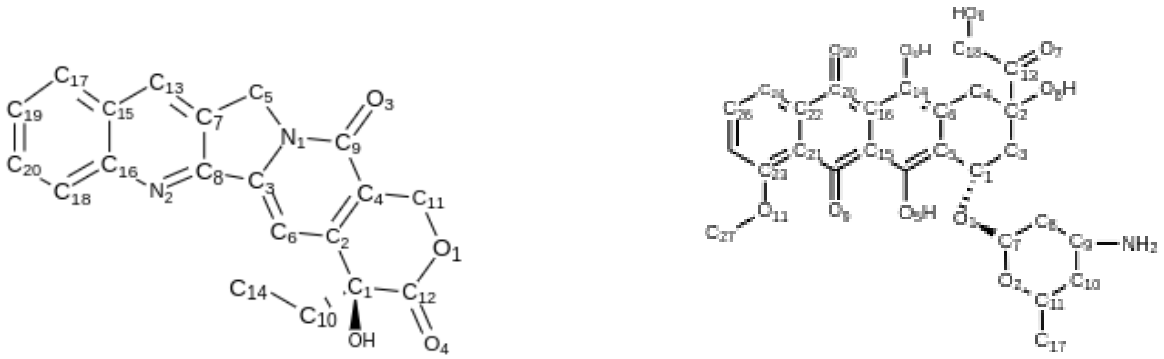

(a) (b)

Fig. 4.1 Structures of drug molecules in simulations, including (a) Camptothecin, (b) Doxorubicin. All atom labels used on contact maps.

algorithm operates can be found in the work by Ziolek et al.[189] The ICSI is defined by:

$$\rho\tilde{(}r) = \sum_i \left(\frac{\delta[r - (r_i - \xi(\theta,\phi))]}{\overline{S}_i(r)} \right) \tag{4.3}$$

where r_i is the r-position of atom i and $\xi(\theta,\phi)$ is the i-position of the ICSI. The intrinsic surface approach, denoted as $\overline{S}_i(r)$, which normalizes the intrinsic density, is given by:

$$\overline{S}_i(r) = \frac{n_i \overline{V}_{box}}{N} \tag{4.4}$$

where n_i is the number of points found in the shell containing atom i across all analyzed clusters. $\overline{V}_{box}$ denotes the average volume of the simulation box, while N corresponds to the total quantity of random coordinates utilized during the normalization process.

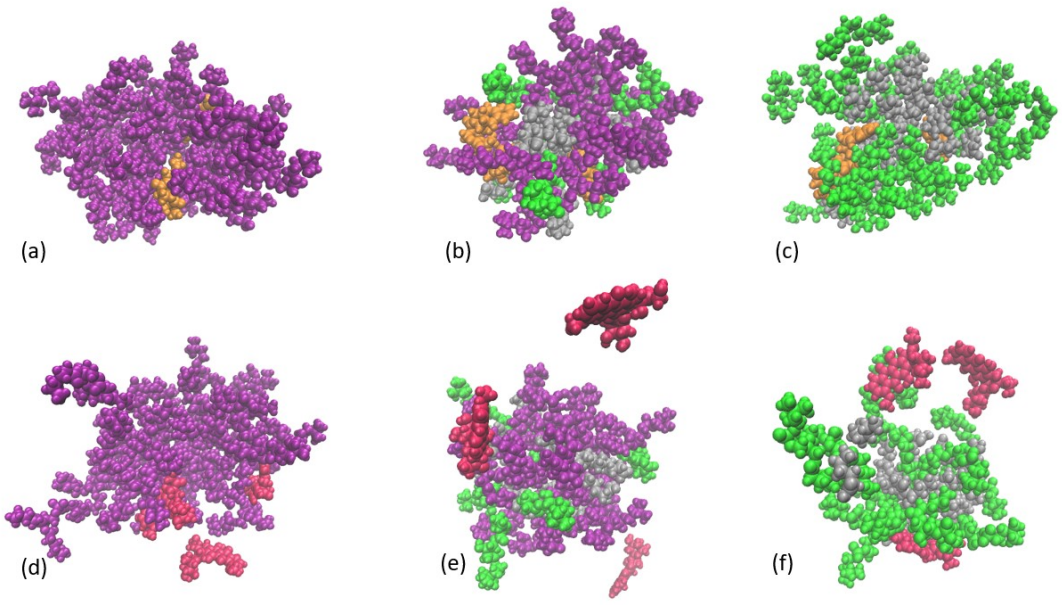

Fig. 4.2 **The interaction between drugs and different micelle systems** Representative snapshots from 2 μs production MD simulation of three different lipid-based micelles (C6PC purple, C6FA sliver, C6LYS green) with drugs CAMPT (orange) in a-c and drugs DOX (red) in d-f respectively.

4.3 Results and Discussions

4.3.1 Effect of drugs in formation of micelles

The final snapshots for each system after a 2 μs production simulation are shown in Fig. 4.2. We observed that almost all of the CAMPT molecules in orange (Fig. 4.2a-c) formed extensive contacts with the micelles. Meanwhile, isolated free DOX molecules (red) in solution are observed (Fig. 4.2d-f). We quantified the number of different molecules within each of the largest micelles in our simulations to better understand how the composition varies across the different systems. Fig. 4.3 & 4.4 display the number of the different molecule types within the largest micelles containing CAMPT and DOX drugs. Also shown in the same figures below are the probability distribution histograms for the size of micelles observed throughout the

various systems. We observed that the composition of the micelles reached equilibrium within 200 ns of the beginning of the production simulation. It is clear to see that the PP-micelle systems exhibited more fluctuations compared to PL-micelle systems so the values in histogram plots are more distributed in Fig. 4.4d-f. When comparing the distribution of micelle sizes in the systems with CAMPT (Fig. 4.3) and those with DOX (Fig. 4.4), we observe that there are more free molecules in solution in the DOX systems. As micelle molecules were observed to disassociate while interacting with drugs, we calculated the extent to which each constituent molecule contributes to the formation of the largest micelles. Fig. 4.5 illustrates the evolution of the fraction of each different molecule type in the largest micelle changes over the entire production simulation, and it is clear that the C6LYS molecules are the most dynamic within the aggregation of the lipids, as they exhibit the most significant fluctuations, particularly in Mixed-DOX systems (Fig. 4.5e). The micelles that encapsulate both drugs remain whole during the duration of our simulations.

To facilitate a clearer comparison of the composition of the various micelles, we have summarized the average total number of molecules and the fractions of each component within the largest micelles in Table 4.2. As the concentration of the product molecules from the degradation of the lipids increases within the micelles, we find that the micelles become increasingly dynamic as the standard deviation of the total number of molecules in the largest micelles increases from 1.7 to 5.1 in CAMPT encapsulated systems, and 2.2 to 4.9 in the DOX systems. There is also a decreasing total fraction of the molecules within the systems as the concentration of degradation products increases within the micelles from 95% to 80% in CAMPT systems and 92% to 75% in the DOX systems.

The number of molecules in the largest micelle in CAMPT systems is generally larger than in the DOX systems, as detailed in Table 4.2. Interestingly, C6LYS is the least probable of the various micellar components to be found in the largest micelles. Even in the Mixed-CAMPT systems, just half of C6LYS interacted with other molecules. In contrast, 2C6PC molecules exhibit the largest uptake of the molecules into the largest micelle in Table 4.2. These results align with our previous work[2, 172], indicating that C6LYS, prefer to disperse in water solutions rather than remaining intact within the largest micelles.

Similarly, the number of CAMPT drugs that are encapsulated within the largest micelle is also larger than the number of DOX molecules encapsulated in the same micelles. Particularly in the Pure-Product systems, where ~ 3 CAMPT molecules are found encapsulated in the largest micelle with time, while only ~ 2 DOX molecules are encapsulated. Figures 4.6 and 4.7 show the evolution of the number of drugs encapsulated within the largest micelle and the probability distribution of the drugs encapsulated within the micelle. The PP-CAMPT micelles (Fig. 4.6f) show that almost all drugs are in contact with micelles throughout the trajectory. However in DOX-Micelles systems, for a majority of the simulation the DOX molecules are isolated in the aqueous environment (in Fig. 4.7d-f).

To gain a general understanding of the compactness and shape of the micelles, we calculated the radius of gyration (R_g) and eccentricity ε of each system (shown in Figs. 4.8 & 4.9) and summarised in Table 4.3. Both the PP-Drugs systems form micelles that are predominately spherical in nature ($\varepsilon \sim 0.16$ (CAMPT-PP) & 0.17 (DOX-PP)). However the shape of the PL-Micelle systems underwent significant changes throughout the simulations in Fig. 4.8d & Fig. 4.9d while their compactness remained relatively stable. In the case of Mixed-Campt micelles, there is a slightly

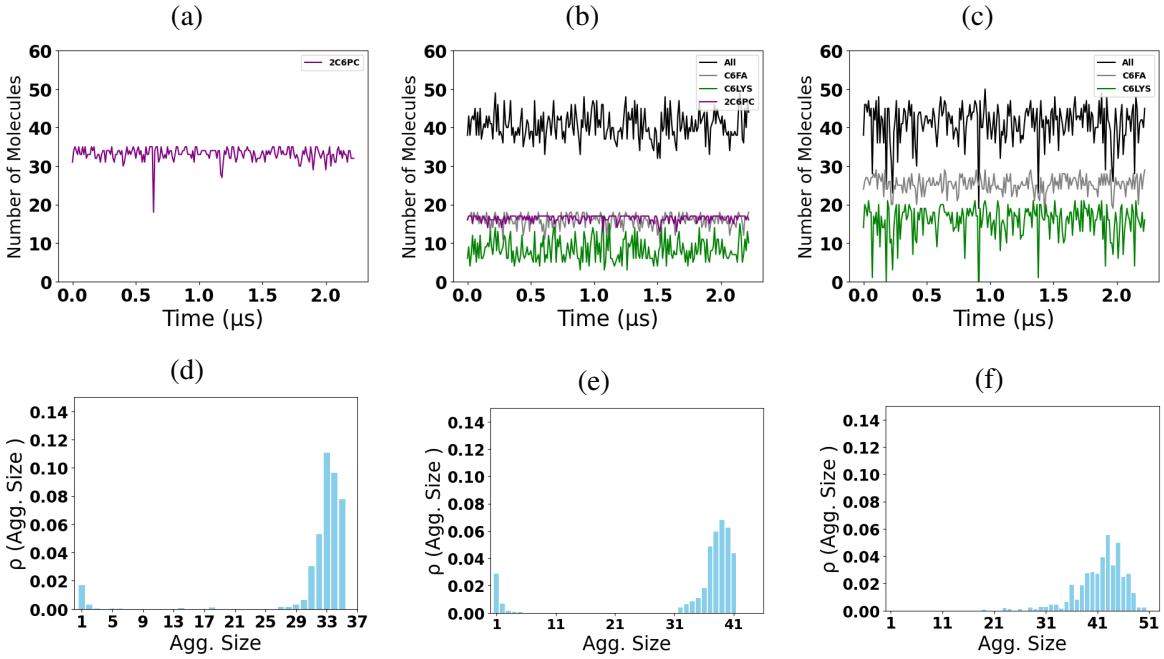

Fig. 4.3 **Largest micelle with CAMPT over the trajectory**. The aggregation numbers of the largest micelle overtime in each systems (a-c). Cluster size (i.e., the number of molecules in each largest micelles) probability distributions for (d) PL-CAMPT, (e) Mixed-CAMPT, (f) PP-CAMPT system

	CAMPT			**DOX**		
	PL	*Mixed*	*PP*	*PL*	*Mixed*	*PP*
Total #	34.1 (1.7)	40.3 (3.6)	40.6 (5.1)	33.4 (2.2)	36.8 (3.2)	37.6 (4.9)
CAMPT	2.1 (1.07)	2.4 (0.95)	2.6 (0.78)	-	-	-
CAMPT(%)	71	81	87	-	-	-
DOX	-	-	-	1.8 (1.32)	1.8 (1.20)	2.0 (0.87)
DOX(%)	-	-	-	59	60	66
2C6PC (%)	95 (0.05)	97 (0.04)	-	96 (0.06)	95 (0.05)	-
C6FA (%)	-	89 (0.09)	86 (0.08)	-	89 (0.04)	83 (0.10)
C6LYS (%)	-	56 (0.16)	78 (0.20)	-	68 (0.20)	65 (0.18)
Total Fraction (%)	95 (0.05)	81 (0.07)	80 (0.10)	92 (0.06)	82 (0.07)	75 (0.10)
Tilt Angle (°)	63.94 (1.83)	63.04 (2.00)	60.51 (1.50)	82.63 (2.71)	86.84 (2.51)	77.88 (2.33)

Table 4.2 **Effects on composition of micells with different drugs.** The mean size of the largest micelles and the average number of drugs aggregated with the largest micelle (the fraction of drugs shown in the parentheses). Then followed by the fractions of each molecules and the total number of molecules comprising the largest micelle. The last row presents the mean tilt angles for each system (standard errors in parentheses).

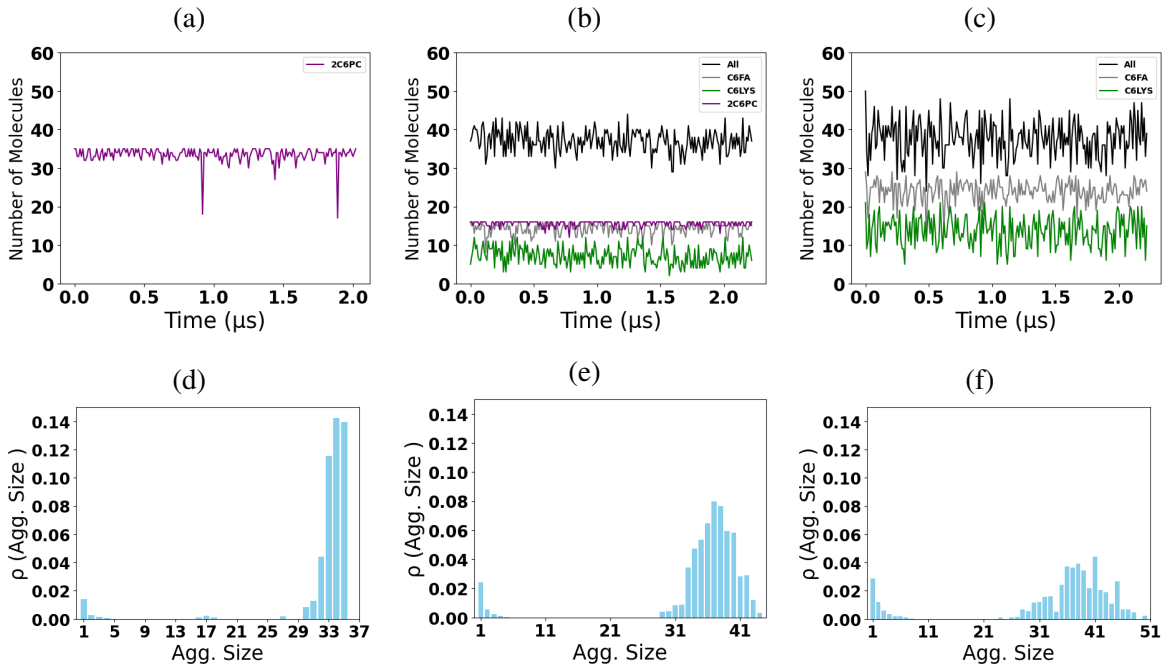

Fig. 4.4 **Largest micelle with DOX over the trajectory**. The aggregation numbers of the largest micelle overtime in each systems (a-c). Cluster size (i.e., the number of molecules in each largest micelles) probability distributions for (d) PL-DOX, (e) Mixed-DOX, (f) PP-DOX system

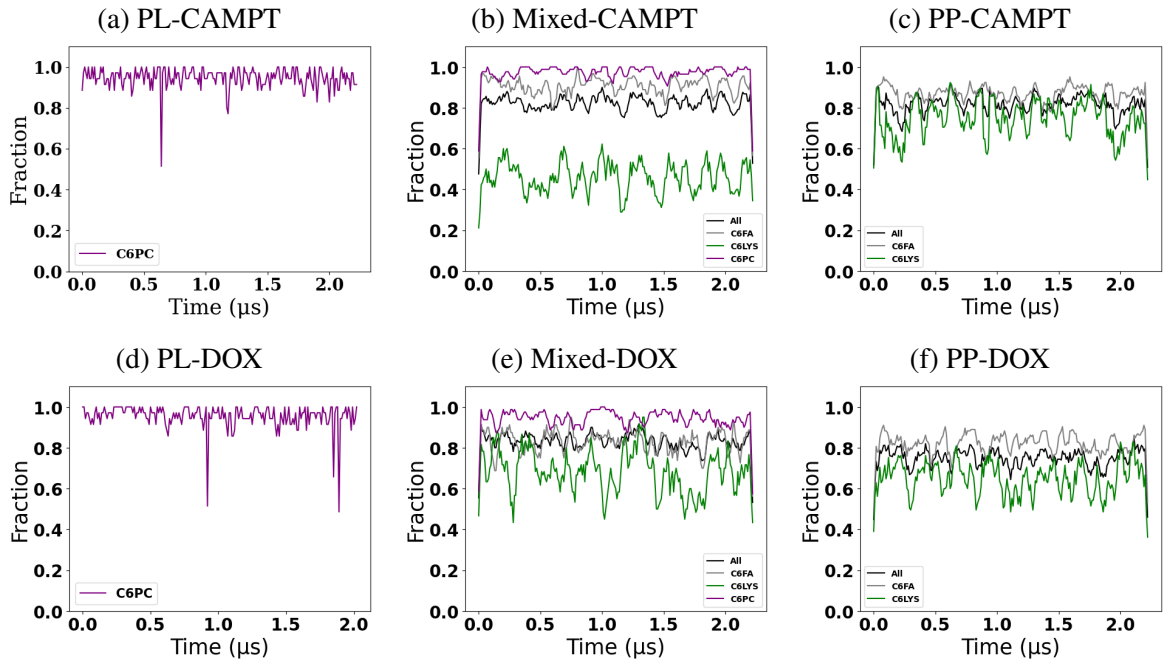

Fig. 4.5 The fractions of each molecule and the total number of molecules that formed the largest micelle in each system.

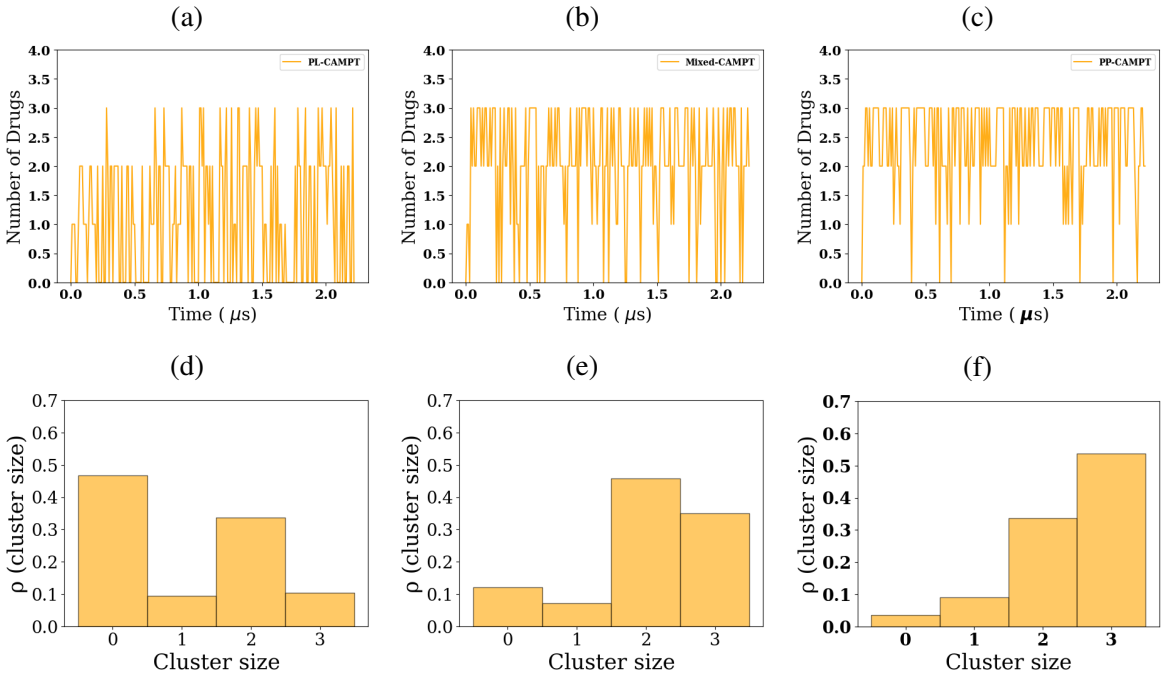

Fig. 4.6 The aggregation numbers of the drug CAMPT overtime in each systems (a-c). The probability distributions for (d) PL-CAMPT, (e) Mixed-CAMPT, (f) PP-CAMPT system

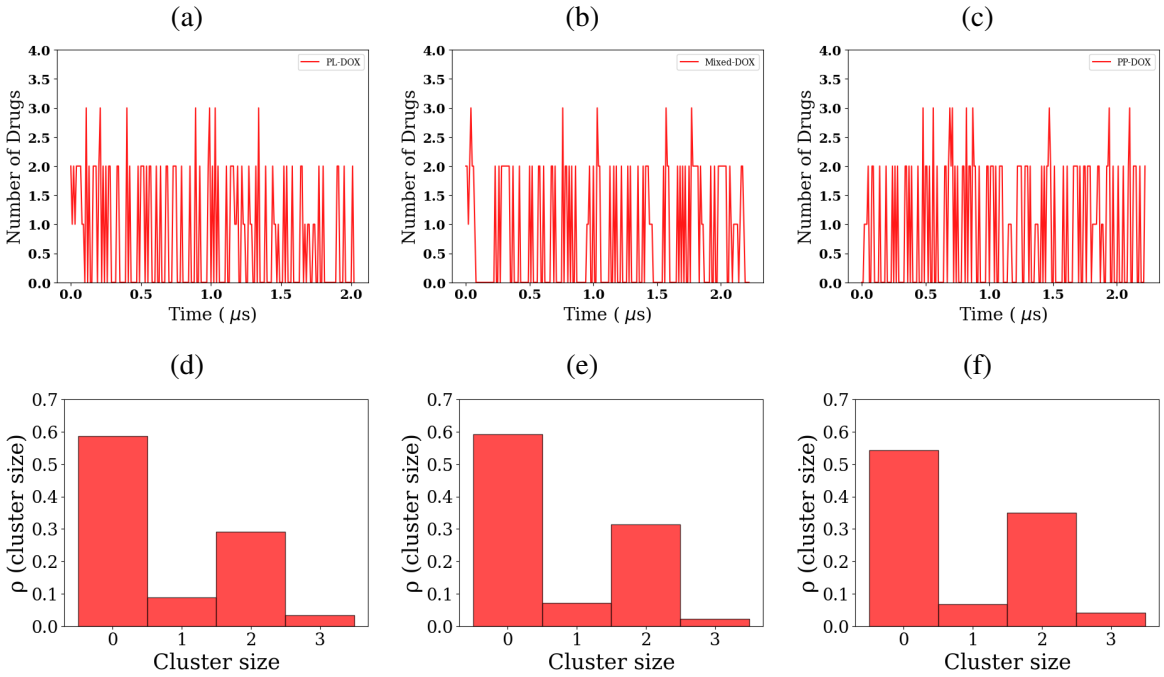

Fig. 4.7 The aggregation numbers of the drug DOX overtime in each systems (a-c). The probability distributions for (d) PL-DOX, (e) Mixed-DOX, (f) PP-DOX system

	R_g			ε		
	PL	*Mixed*	*PP*	*PL*	*Mixed*	*PP*
CAMPT	23.1 ± 3.0	29.7 ± 3.4	27.4 ± 3.2	0.30 ± 0.13	0.19 ± 0.09	0.16 ± 0.08
DOX	25.6 ± 4.1	28.9 ± 3.4	27.4 ± 3.8	0.27 ± 0.12	0.23 ± 0.11	0.17 ± 0.09
REF.	17.4 ± 0.8	18 ± 1	17 ± 1	0.34	0.25	0.23

Table 4.3 The average and standard deviation for the radius of gyration R_g, eccentricity ε and the mean size of the largest micelles over the trajectory for each systems. The values from our previous study for the pure micelles without any drugs are shown as references(REF.)[2] in the last row.

increasing trend in R_g along with a shift towards a more spherical shape over time, whereas in the Mixed-Dox micelles, a decreasing trend was observed. The DOX micelles remain approximately spherical (Table 4.3). Similar trends in eccentricity ε were observed in each system when compared to our previous reference works [2], where PP-Micelle systems exhibited the smallest values, and PL-Micelles showed the largest. However, there is a distinct increasing trend (R_g) in values when compared to the reference values. This indicates that the solubilisation of the small molecules results in a significant change of the internal structure of the micelle that results in a change in their size and shape.

4.3.2 Effect of drugs on the internal structure of micelles

We subsequently employed the corresponding radial density (Fig. 4.10)to determine the positions of different components including the drugs within each micelle and all calculations were averaged over the trajectories. The radial density profiles show that the drug CAMPT extensively inserted into micelles (indicated by the orange line in Fig. 4.10a, 4.10c and 4.10e). In contrast, (red line in Fig. 4.10b, 4.10d and 4.10f) there are not significant densities of DOX molecules within the core of the micelles. We assume this is due to the larger size of the DOX molecules and more hydrophilic

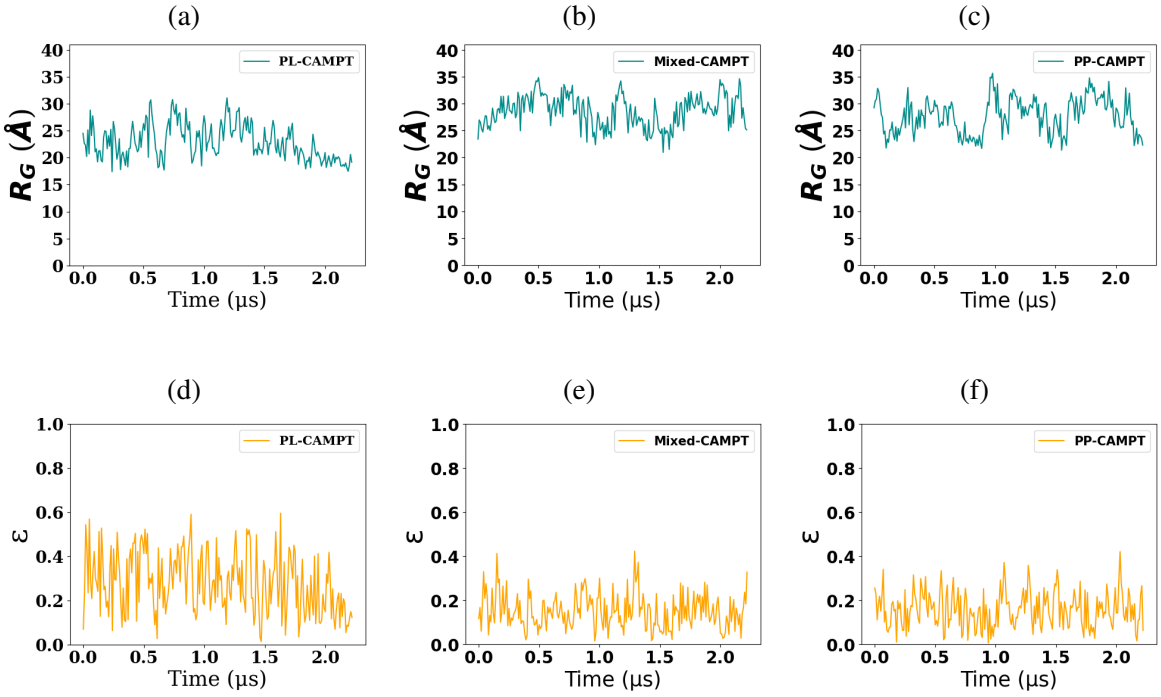

Fig. 4.8 **Size and Shape of micelles.** Plots of the R_g for the micelles with Campt drugs as a function of time shows above three in blue. The eccentricity of the micells and drugs below in yellow.

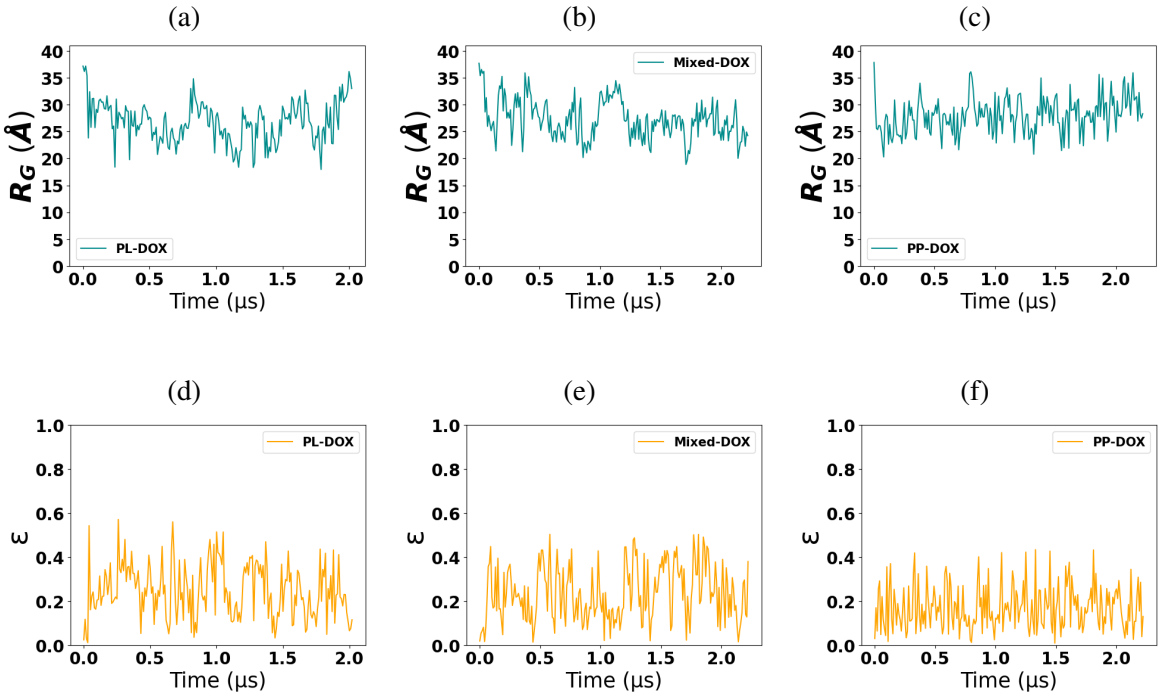

Fig. 4.9 **Size and Shape of micelles.** Plots of the R_g for the micelles with DOX drugs as a function of time shows above three in blue. The eccentricity of the micells and drugs below in yellow.

chemical function groups properties of DOX molecules, in comparison to the CAMPT molecules.

It is worth noting that we also observed an effect on the density of the water molecules within the core of the micelles. The PL-micelle system exhibits the smallest density of water within their cores, while the PP-micelles have the highest. It demonstrates that the PP-micelle system has a less stable structure, allowing water molecules to penetrate easily. Additionally, due to the hydrophobic nature of tails of 2C6PC and the tail of C6LYS, 2C6PC and C6LYS are all encapsulated inside the micelles with lower density values in Fig.4.10, which is consistant with other research works that demonstrates that amphiphilic surfactants such as 2C6PC or C6LYS prefer to accommodate their hydrophilic and hydrophobic region inside as the core.[190] These findings also aligns with our previous results, which showed that the hydrophobic region is primarily composed of C6FA and the acyl chains of lipids[2]. These results corresponds with the findings of fraction values and aggregated molecules in Table 4.2.

To investigate the orientation and localisation of drugs during their interaction with micelles, mechanism of solubilisation of the drugs within the micelles, we have measured the orientation of the drugs as they approach and are encapsulated by the micelles. We measured the angles formed by the vector connecting one side carbon (C8) atom in the benzene ring on one side of the molecule to another benzene ring carbon atom (C20) on the other side of the molecule the vector from the center of micelle mass to the center of drug mass (Fig. 4.11 and Table 4.2). The results of these calculations reiterates the observation that the DOX molecules are commonly found in the aqueous environment where they have no preferential orientation (Figs. 4.11(e)-(g)), as a result the mean orientation angle is $90\circ$ (Table 4.2). Meanwhile, the CAMPT molecules are commonly encapsulated within the

	CAMPT			**DOX**		
	PL	*Mixed*	*PP*	*PL*	*Mixed*	*PP*
O3	1.50 (0.32)	1.32 (0.32)	1.50 (0.25)	-	-	-
O4	2.13 (0.33)	2.35 (0.34)	2.13 (0.34)	-	-	-
N1	4.43 (0.52)	4.72 (0.53)	4.93 (0.54)	-	-	-
N2	0.80 (0.37)	0.94 (0.36)	1.16 (0.39)	-	-	-
O4	-	-	-	3.07 (0.28)	2.92 (0.27)	2.80 (0.28)
O8	-	-	-	3.46 (0.28)	3.46 (0.29)	3.46 (0.29)
O10	-	-	-	0.96 (0.27)	1.30 (0.27)	0.87 (0.27)
N	-	-	-	4.15 (0.29)	2.80 (0.29)	2.90 (0.28)

Table 4.4 **Hydration analysis.** The coordinate water numbers in the first shell with different drugs' oxygen atoms and nitrogen atoms. The first peak of water shell distances are shown in parentheses.

micelles and are found to have a mean orientation angle of $60\circ$ which represents the preferred orientation of the drug within the micelle.

Contact maps were constructed to help have a better understanding of the drug-drug or drug-molecules interactions. By measuring the distance between each heavy atom (except hydrogen atoms) of molecule of micelle and a neighbouring drug molecule, we can generate the distance contact maps. We then used the minimum distance between a drug molecule and a molecule within a micelle as the characteristic distance to define a contact within the system. If the distance between any two heavy atoms are within the cut-off, we considered it as a contact.

In Fig.4.13, it shows that the primary contact regions of 2C6PC with drug Campt molecues in PL-micelles are the hydrophobic tails of lipids, which corresponding to atoms C23-C26 and C32-C36 along the horizontal axis. We also observed that there is an increased number of contacts as the atom moves further away from the hydrophilic head (i.e., the larger the atom number, the greater the distance from the tail to the head). The regions of the drug CAMPT interact with lipids 2C6PC primarily via its A ring, which is part from the pyrrole[3,4-β]-quinoline moiety. It is reasonable as we have known that CAMPT is composed of a flat pentacyclic ring

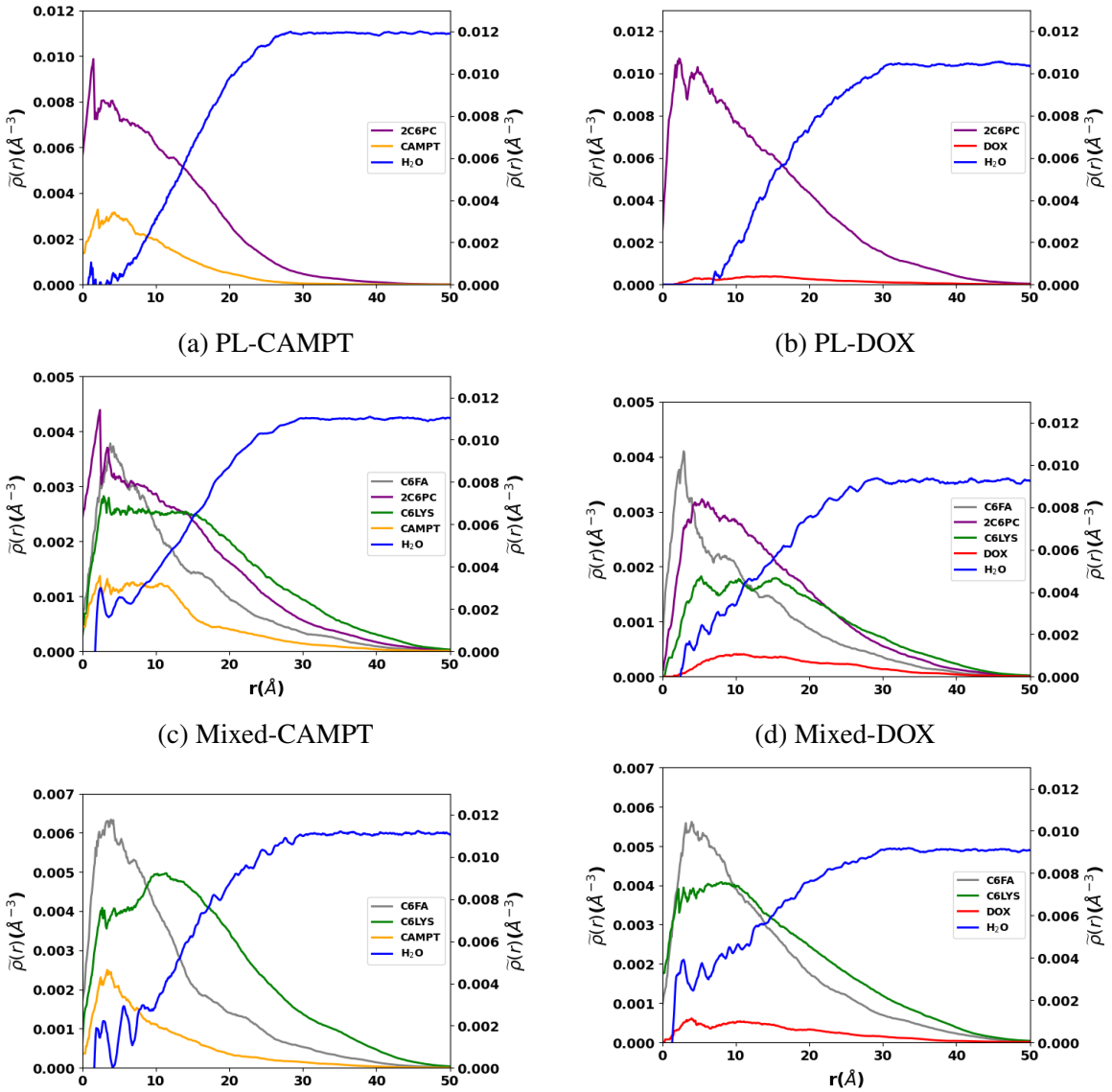

(a) PL-CAMPT

(b) PL-DOX

(c) Mixed-CAMPT

(d) Mixed-DOX

(e) PP-CAMPT

(f) PP-DOX

Fig. 4.10 Radial density of water (blue), C6LYS(green), C6FA(gray), head groups of 2C6PC(mulberry), tail groups of 2C6PC(purple), CAMPT(orange) and DOX(red) in each micelle systems as function of time.

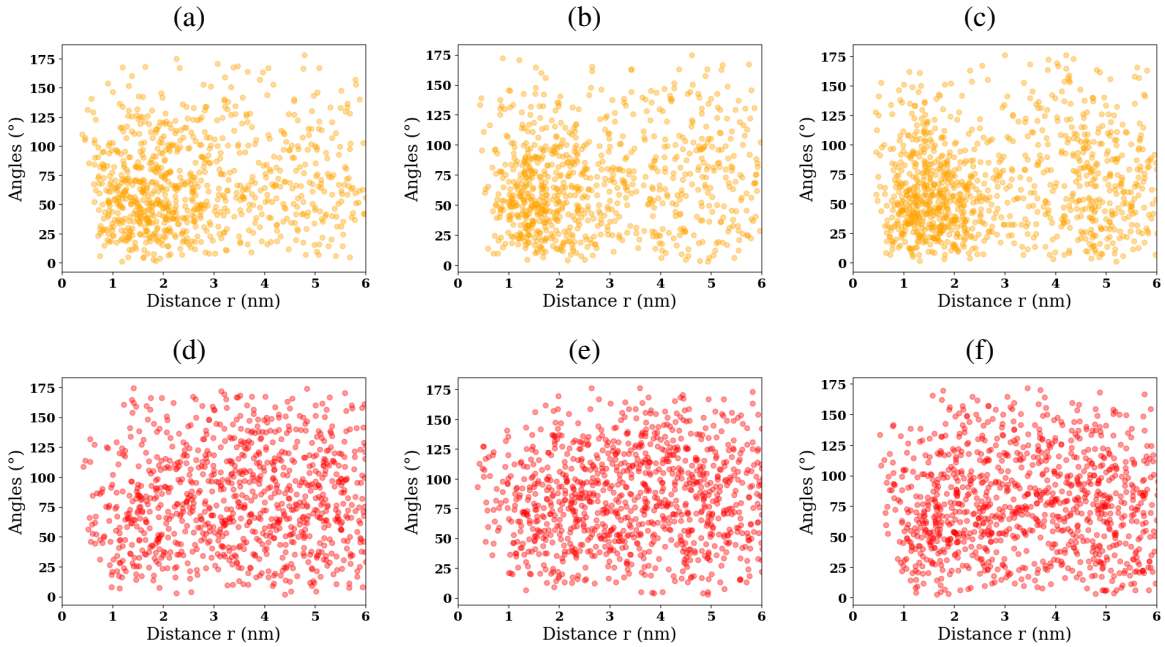

Fig. 4.11 **Orientaion of CAMPT and DOX**. The scatter plots show the distribution of the tilt angles of drugs (a-c) CAMPT in orange and DOX in red (d-f) within the PL-micelle, Mix-micelle and PP-micelle systems respectively.

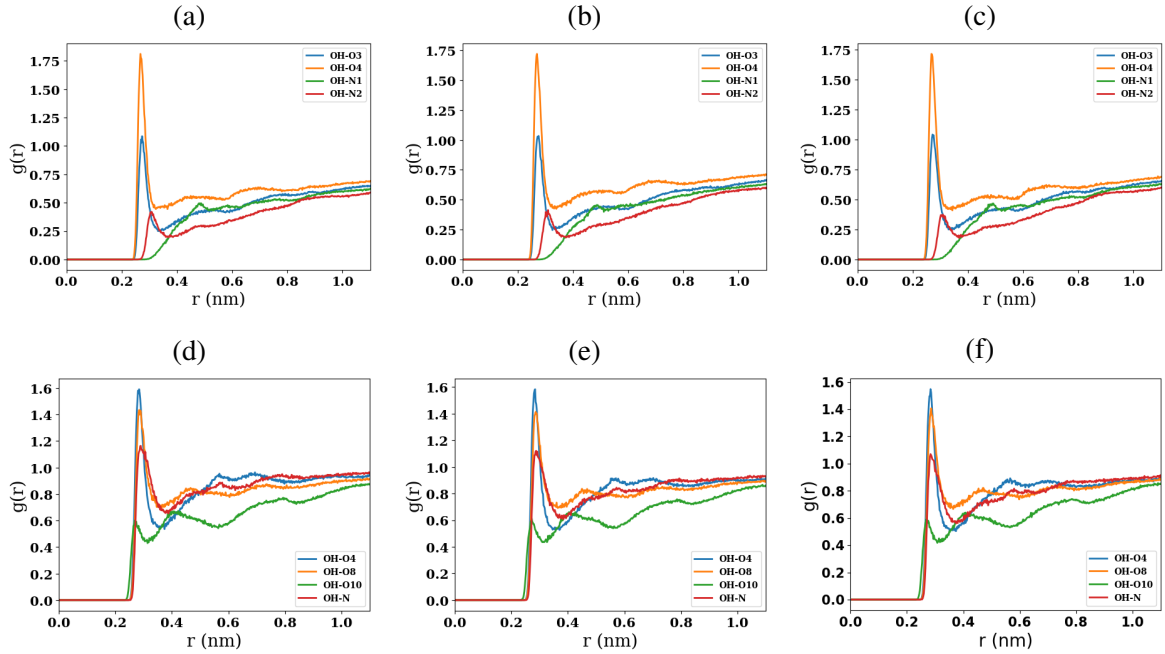

Fig. 4.12 Radial distribution functions for the different oxygen atoms and nitrogen atoms in drugs with the water oxygen (OH) (a-c) CAMPT-micelle, (d-f) DOX-micelle in the PL-micelle, Mixed-micelle, PP-micelle system respectively.

structure that includes three fused rings, specifically the the pyrrole[3,4-β]-quinoline portion (rings A, B , and C) and the A ring (atom C15-C20) is the more hydrophobic core of the CAMPT molecule. This ring plays a role in its interaction with lipid bilayers and hydrophobic regions in biological systems.[191, 192] From the chemical structure of CAMPT in Fig. 4.1a, we can observe that the left side of CAMP molecules contain three oxygen atoms and a hydroxy (-OH) group on atom C1, indicating more hydrophilic nature. The atom N2 and C7-C8 also were observed with certain amount of close contact due to it is very close to the ring A. Similarly, in Mixed-CAMPT micelle system (Fig. 4.14), the hydrophobic tail of 2C6PC has shown the tendency of interacting with ring A in CAMPT. Meanwhile, the CAMPT molecules bonded with fatty acid products of C6FA on the more hydrophobic part (atom C1-C5) and had less contact with carboxyl groups of C6FA due to the hydrophilic nature (Fig. 4.16, 4.18). It is noteworthy that not only did the pyrrole[3,4-β]-quinoline (comprising rings A, B and C with atom C13-C20) exhibited extensive close contact with C6LYS but also conjugated pyridone moiety (ring D) with atom C1-C10 and N1, N2 in Fig. 4.15 and 4.17.

Based on the chemical structure of DOX in Fig. 4.1b, we observe the presence of four hydroxy (-OH) groups located at atoms C2, C12, C14 and C18 respectively, indicating it is relativity more hydrophilic and is capable of forming more hydrogen bonds. We found that the DOX molecules exhibit a longer duration in solution (e.g. in Fig.4.4a-c), which aligns with the results obtained from contact maps that display lower contact indices (e.g., shown in Fig.4.19 - 4.24). The DOX molecules mainly have contacts with micelles through hydrophobic interactions, leading to relative large values on the contact maps, particularly on the fatty acid molecules C6FA, tail groups C6LYS and lipid of 2C6PC. These results are consistent with previous investigations that specified that DOX is considered a hydrophobic

molecule mainly because it contains several aromatic rings in its structure and hydrocarbon chains, such as the daunosamine sugar moiety etc.[193] The results indicate that atoms C19-C26, C14-C16, O5-O6, and O9-O10 formed contacts with each other. These findings are in agreement with the work conducted by Fude Sun's group, which demonstrated that the DOX head (C16-C26 in our study) is oriented toward the bilayer center, corresponding to the more hydrophobic core.[194]

We calculated the radial distribution functions (RDFs) for different drug oxygen atoms or nitrogen atoms with the oxygen atom of surrounding water molecules to analysis the hydration of the drugs in different micelle systems in Fig. 4.12. To quantify the number of water molecules surrounding the atoms within the first shell, we calculated the integral of the RDF from 0 nm to the distance of the first peak minimum as the coordination numbers in Table 4.4. Due to the insertion of CAMPT in the micelles, the CAMPT-micelle systems exhibit distinct hydration characteristics. The N2 in CAMPT has the least water number of molecules (0.80) within the closest water shell at 0.30 nm, while N1 has the highest coordination number (4.43). Interestingly, even though similar trends across all CAMPT drug atoms, the less compact PP-micelle system consistently has the highest number of water molecules for the cased of the nitrogens. This hydration of the nitrogen atom N1 in the benzene ring suggests a hydrophobic nature, consistent with its chemical properties and also consistent with contact maps. For instance, N1 in CAMPT shows larger contacts and interactions with the hydrophobic tails of lipids, as depicted in Fig. 4.13. As for the DOX-micelle systems in Fig. 4.12 d-f, it demonstrate variations in the number of water molecules surrounding specific atoms. For instance, O10 (0.96), being part of the more hydrophobic region, exhibits fewer water molecules. In contrast, atoms like O4 (3.07), O8 (3.46), and N (4.15) in systems such as PL-DOX show a higher coordination with water molecules

(see Tab 4.4). This discrepancy can be attributed to the hydrophilic nature of the DOX head. Similarly, in the contact maps regarding to DOX (for instance, Fig. 4.19 of PL-DOX system), the atom O10 shows higher contacts with the tails of C6PC, whereas the atom O4, O8 as well as N show much less close contacts. We also observed a slight decrease in the number of water molecules when fewer lipids are involved in the formation of the complete micelle. This observation is reasonable because the structure of the PL-micelle is the most compact, resulting in fewer DOX drugs being inserted into the micelle and, consequently, more water molecules surrounding it.

4.4 Conclusions

In this work, our results and analyses provided a comprehensive picture on the behavior of different drugs, specifically CAMPT and DOX, within lipid-based micelle environments. One notable observation was the distinct influence of CAMPT on lipid-based micelles, with its hydrophobic core facilitating extensive interactions, especially with the hydrophobic tails of lipids, resulting in some changes in composition of micelles. And we observed there are still some free isolated lysophosphocholine (C6LYSO) molecules in the aqueous environment, the results are align with our previous findings. On the other hand, DOX, being more hydrophilic due to the fact that it has more hydrophilic functional groups (e.g. -OH), displayed a preference for staying with water molecules over the integration into micelles, leading to fewer close contacts with micelles.

The detailed examination of lipid-based systems underscored the importance of lipid composition in micellar dynamics. The fluctuations and fewer molecules aggregated in PP-micelle systems compared to the more

stable PL-micelle systems suggest that the lipid composition significantly influences the stability and dynamics of micelles. This insight is pivotal for optimizing drug delivery systems and tailoring them to specific drug properties. The analyses of tilt angles and distance measurements offered valuable insights into the orientation and localization of drugs within micelles. CAMPT displayed a different pattern of localization at specific radii from the center of micelle mass, which is that the hydrophobic parts of the drug CAMP have shown the tendency embed into the micelle core and more close contacts with hydrophobic tails of C6PC, C6LYS. While DOX exhibited a propensity to remain in solution, influencing its overall integration with the micelles. The radial distribution functions (RDFs) for drug atoms with surrounding water molecules revealed intriguing hydration behaviors. Lipid-based micelles with the less compact PP-micelle consistently displayed fewer water coordination numbers. This finding indicates the crucial role of micelles' structure in influencing hydration dynamics.

Our simulations provide a comprehensive insight of the intricate interactions between drugs and micelles, crucial for the design and optimization of drug delivery systems. The observed behaviors of CAMPT and DOX underscore the importance of tailoring drug-micelle interactions based on the specific properties of the drug. The disparities between PP-micelle and PL-micelle systems emphasize the significance of lipid composition in dictating micellar stability and dynamics. This insight is invaluable for guiding future research in optimizing drug delivery systems, allowing for tailored approaches based on lipid composition.

In this manuscript, these findings provide a robust foundation for further exploration and optimization of drug-micelle systems. The insights gained from the detailed analyses of lipid-based micelle composition, internal structure, and hydration behaviors offer valuable knowledge for the devel-

opment of more efficient and stable drug delivery platforms. Therefor this research would contribute to the broader field of drug delivery, offering nuanced insights that can inform future studies and advancements in the design of drug delivery systems.

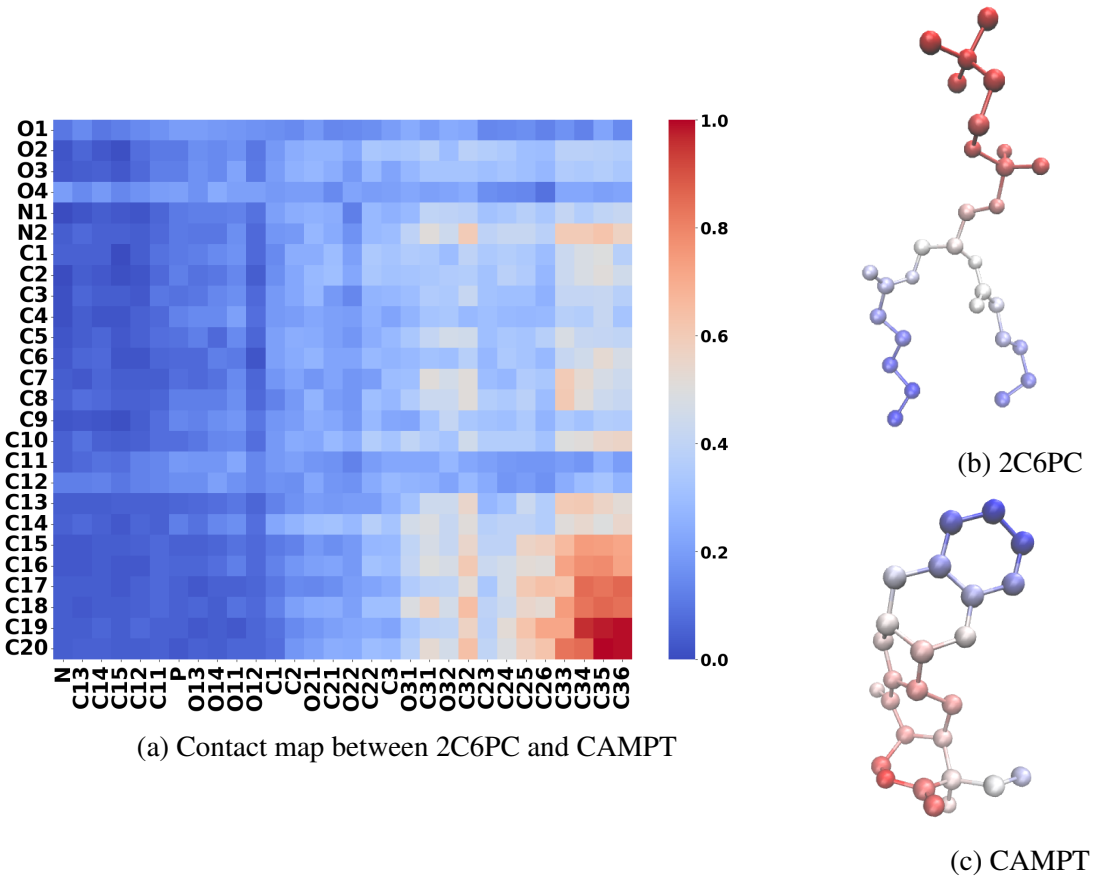

(a) Contact map between 2C6PC and CAMPT

(b) 2C6PC

(c) CAMPT

Fig. 4.13 **The contact map between pairs of CAMPT and 2C6PC in the PL-micelles system.** Contact maps (a) shows the amount of contact and interactions between two pairs of molecules. Higher values indicate closer contact. (b)(c) all coloured based on the amount of contact with each atoms. All atom labels used on contact maps are shown in Fig. 4.1.

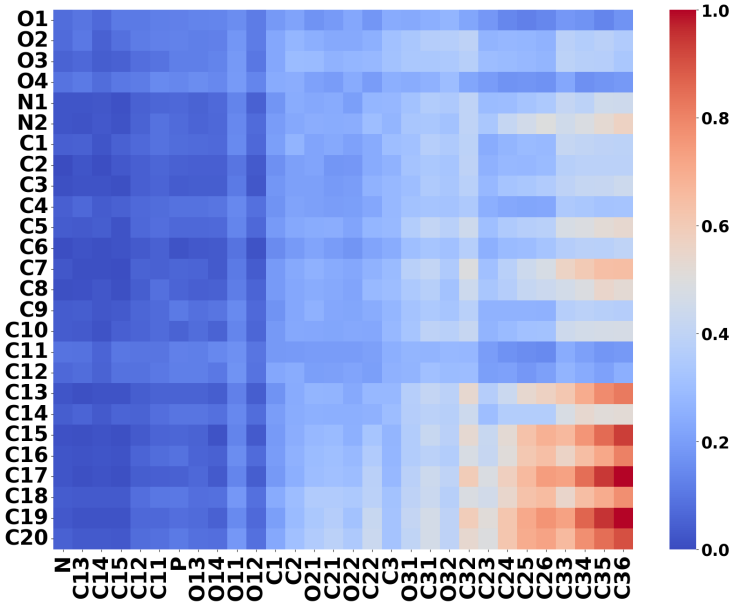

(a) Contact map between 2C6PC and CAMPT

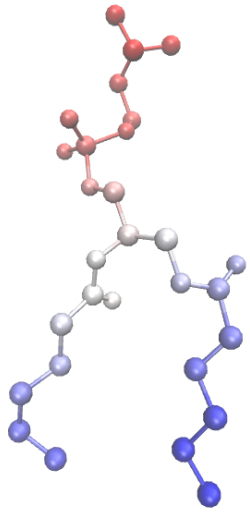

(b) 2C6PC

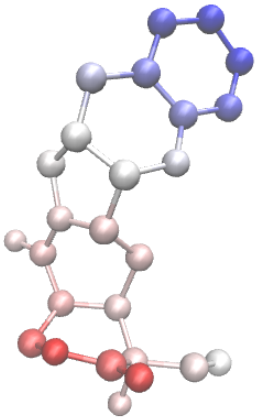

(c) CAMPT

Fig. 4.14 **The contact map between pairs of CAMPT and 2C6PC in the Mixed-micelles system.** Contact maps (a) shows the amount of contact and interactions between two pairs of molecules. Higher values indicate closer contact. (b)(c) all coloured based on the amount of contact with each atoms.

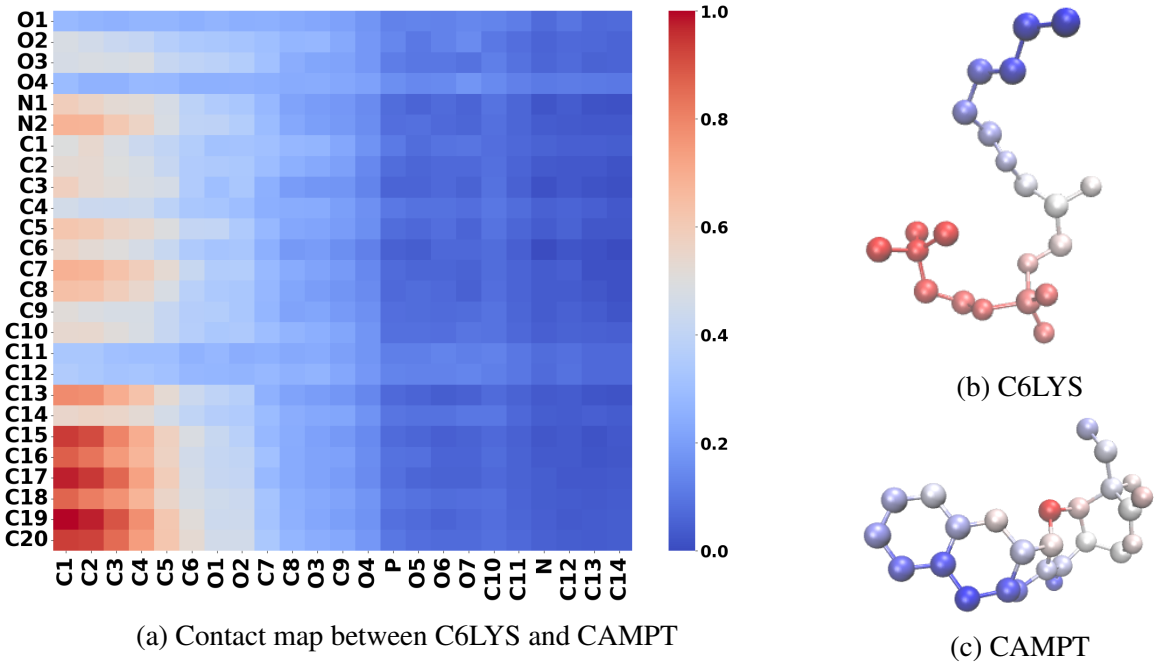

(a) Contact map between C6LYS and CAMPT

(b) C6LYS

(c) CAMPT

Fig. 4.15 **The contact map between pairs of CAMPT and C6LYS in the Mixed-micelles system.** Contact maps (a) shows the amount of contact and interactions between two pairs of molecules. Higher values indicate closer contact. (b)(c) all coloured based on the amount of contact with each atoms.

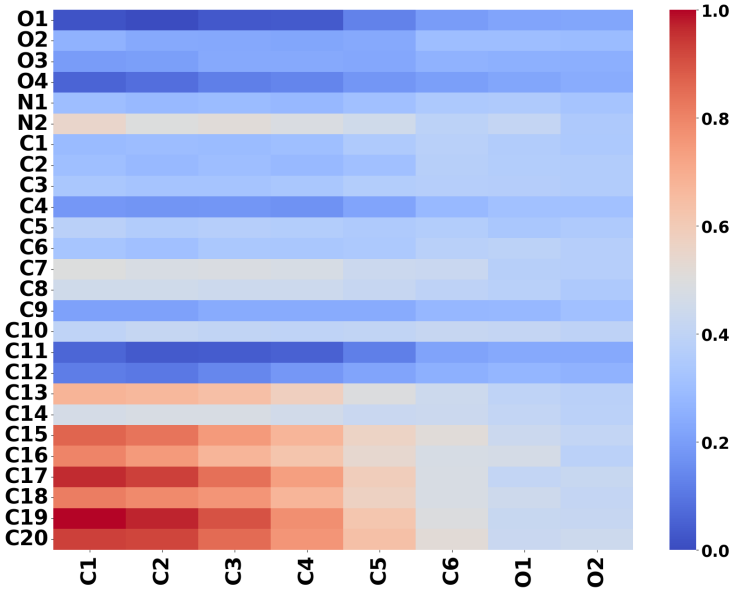

(a) Contact map between C6FA and CAMPT

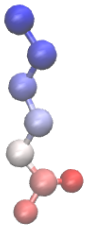

(b) C6FA

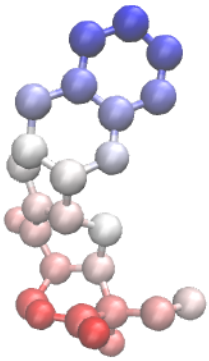

(c) CAMPT

Fig. 4.16 **The contact map between pairs of CAMPT and C6FA in the Mixed-micelles system.** Contact maps (a) shows the amount of contact and interactions between two pairs of molecules. Higher values indicate closer contact. (b)(c) all coloured based on the amount of contact with each atoms.

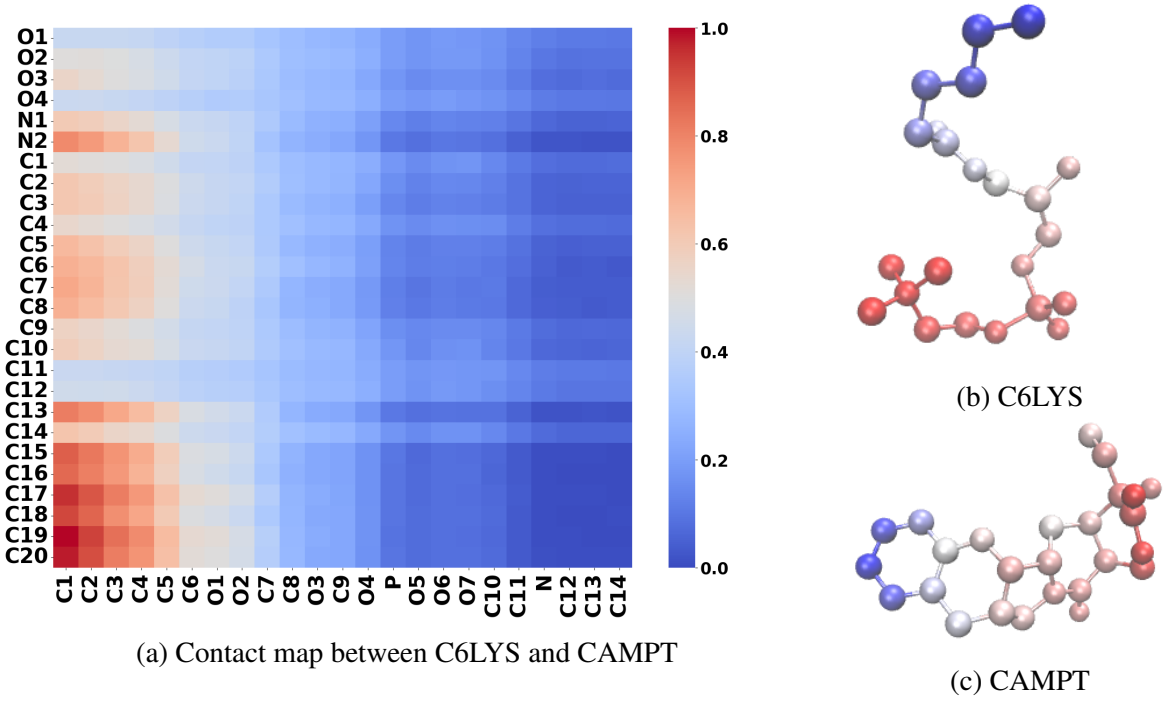

(a) Contact map between C6LYS and CAMPT

(b) C6LYS

(c) CAMPT

Fig. 4.17 **The contact map between pairs of CAMPT and C6LYS in the PP-micelles system.** Contact maps (a) shows the amount of contact and interactions between two pairs of molecules. Higher values indicate closer contact. (b)(c) all coloured based on the amount of contact with each atoms.

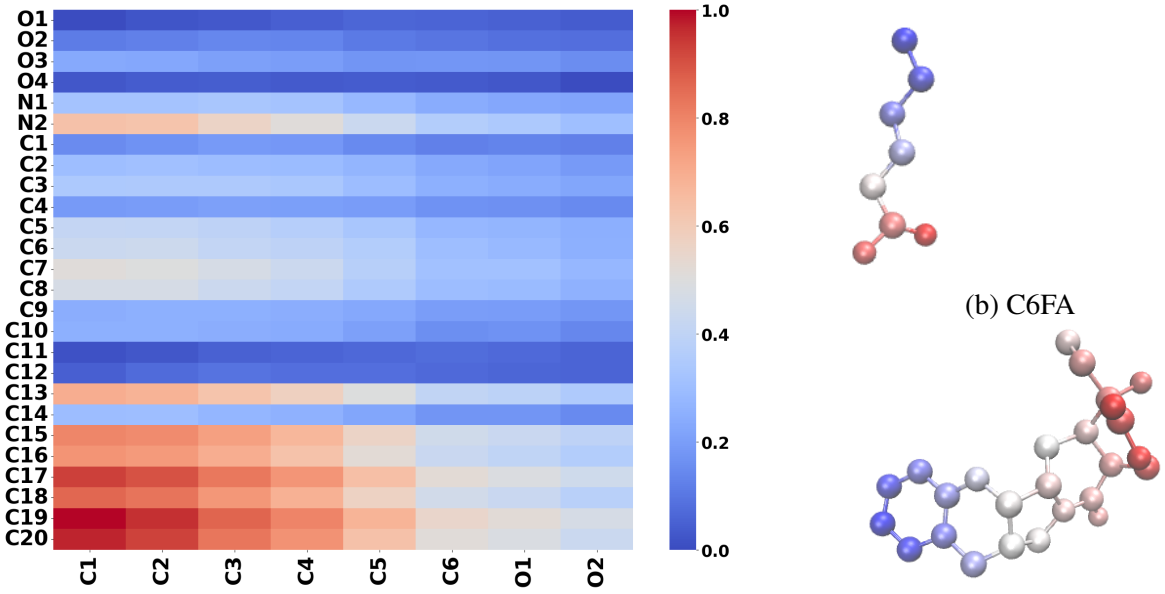

(a) Contact map between C6FA and CAMPT

(b) C6FA

(c) CAMPT

Fig. 4.18 **The contact map between pairs of CAMPT and C6FA in the PP-micelles system.** Contact maps (a) shows the amount of contact and interactions between two pairs of molecules. Higher values indicate closer contact. (b)(c) all coloured based on the amount of contact with each atoms.

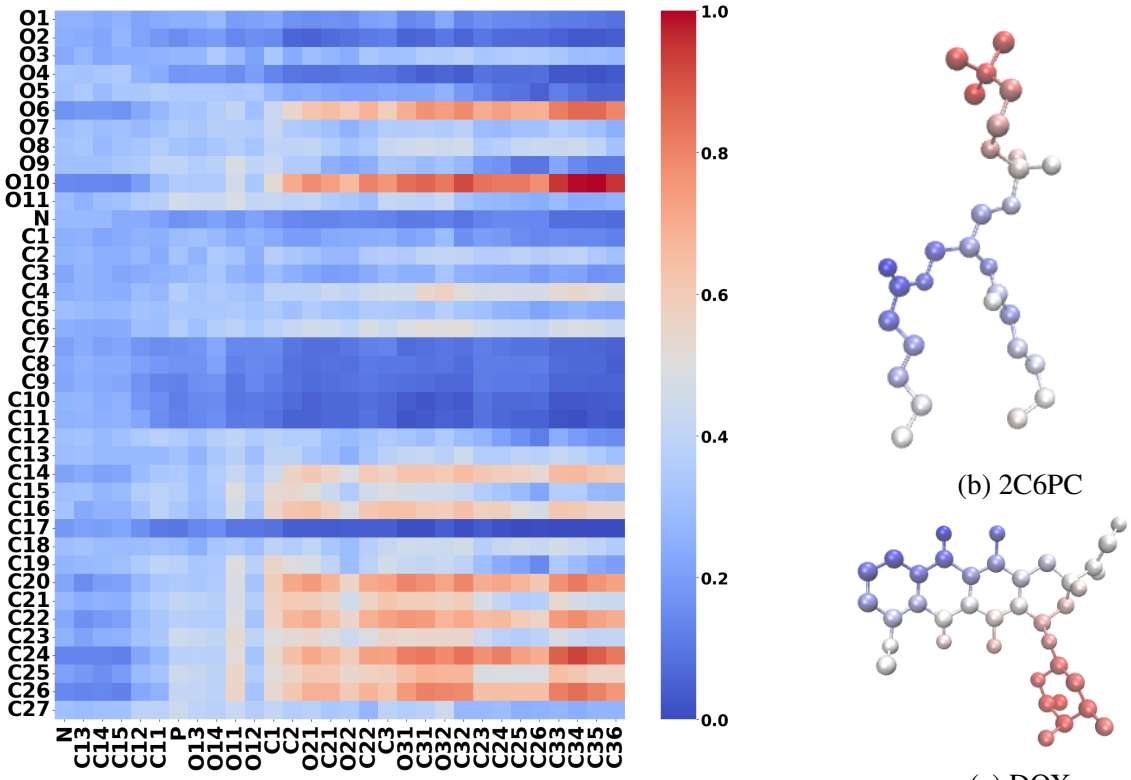

(a) Contact map between 2C6PC and DOX

(b) 2C6PC

(c) DOX

Fig. 4.19 **The contact map between pairs of DOX and 2C6PC in the PL-micelles system.** Contact maps (a) shows the amount of contact and interactions between two pairs of molecules. Higher values indicate closer contact. (b)(c) all coloured based on the amount of contact with each atoms.

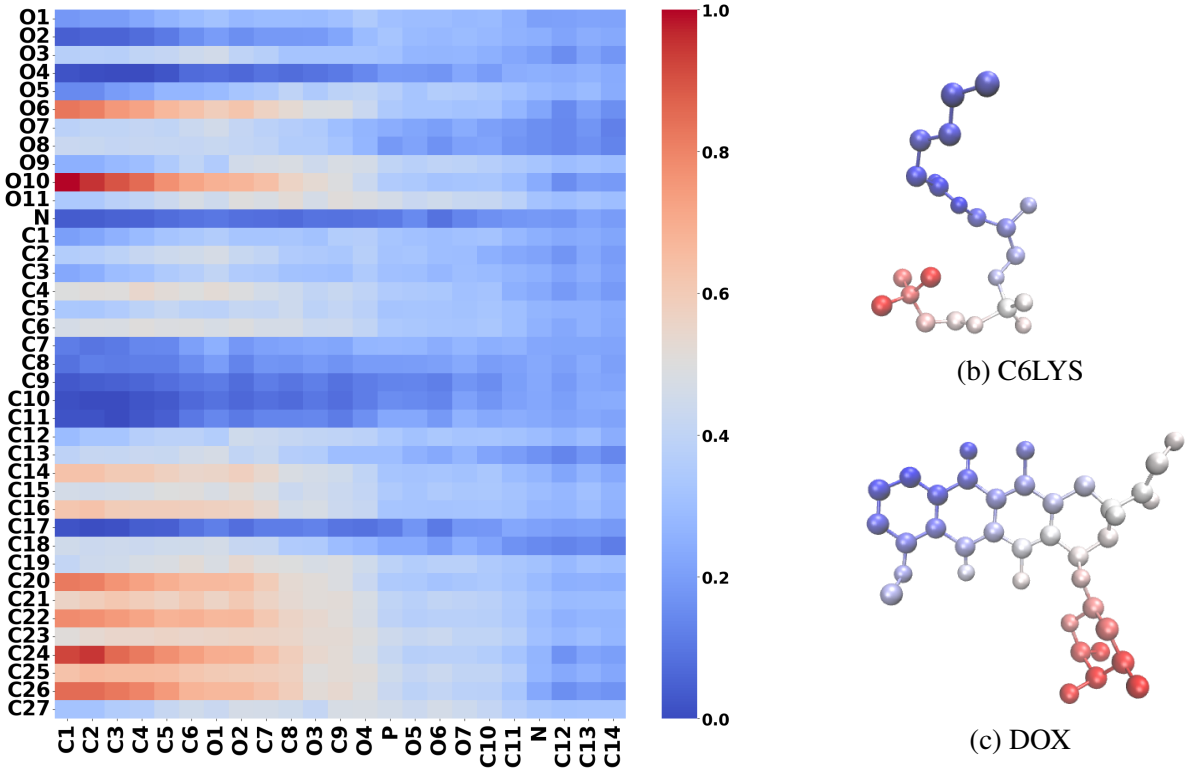

(a) Contact map between C6LYS and DOX

(b) C6LYS

(c) DOX

Fig. 4.20 **The contact map between pairs of DOX and C6LYS in the Mixed-micelles system.** Contact maps (a) shows the amount of contact and interactions between two pairs of molecules. Higher values indicate closer contact. (b)(c) all coloured based on the amount of contact with each atoms.

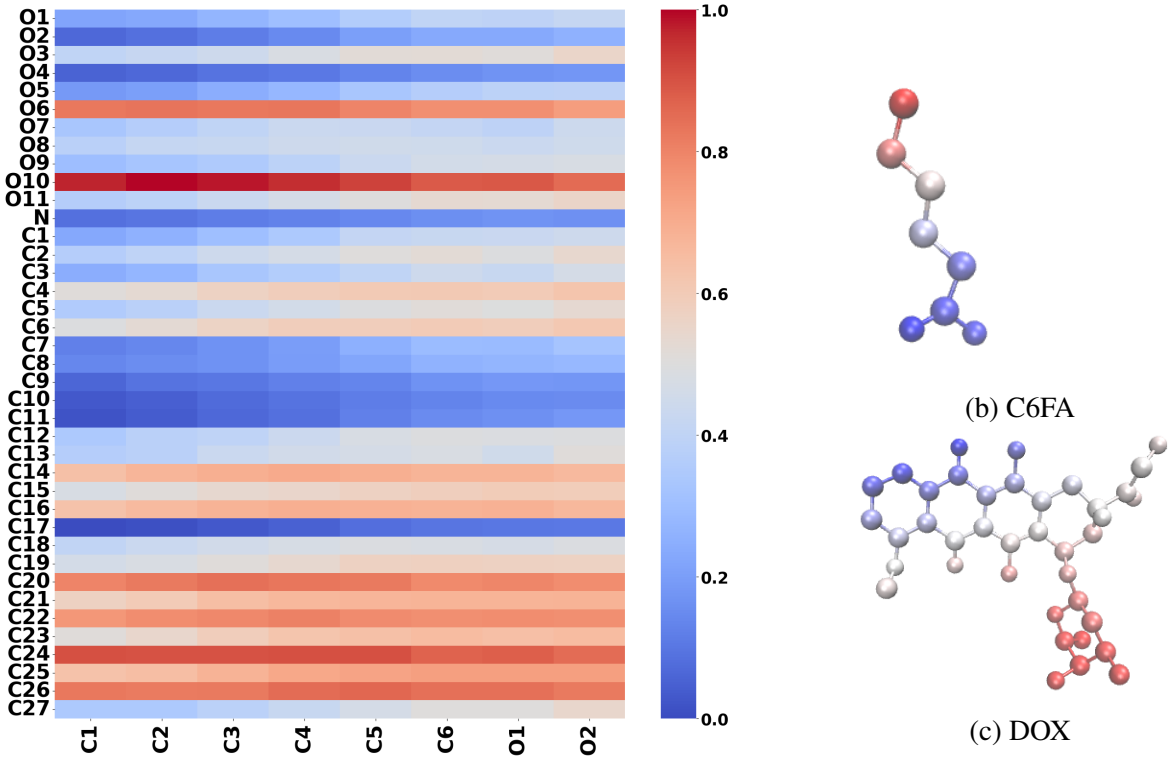

(a) Contact map between C6FA and DOX

(b) C6FA

(c) DOX

Fig. 4.21 **The contact map between pairs of DOX and C6FA in the Mixed-micelles system.** Contact maps (a) shows the amount of contact and interactions between two pairs of molecules. Higher values indicate closer contact. (b)(c) all coloured based on the amount of contact with each atoms.

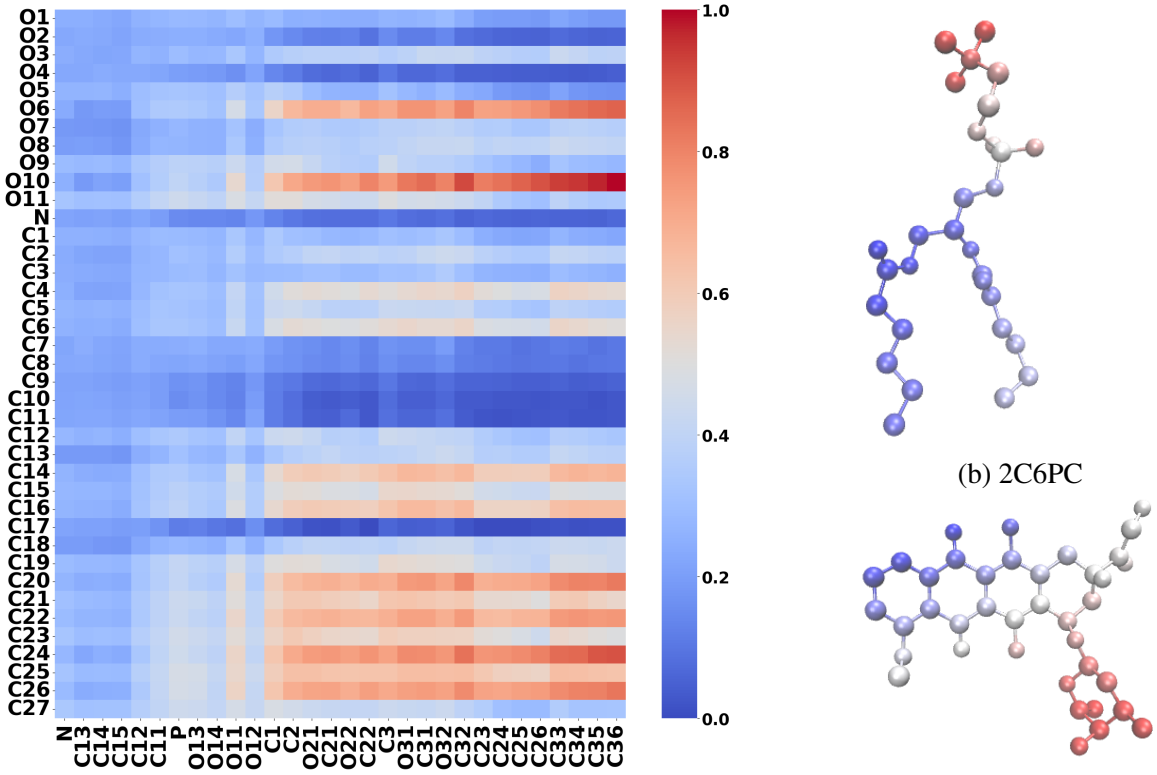

(a) Contact map between 2C6PC and DOX

(b) 2C6PC

(c) DOX

Fig. 4.22 **The contact map between pairs of DOX and 2C6PC in the Mixed-micelles system.** Contact maps (a) shows the amount of contact and interactions between two pairs of molecules. Higher values indicate closer contact. (b)(c) all coloured based on the amount of contact with each atoms.

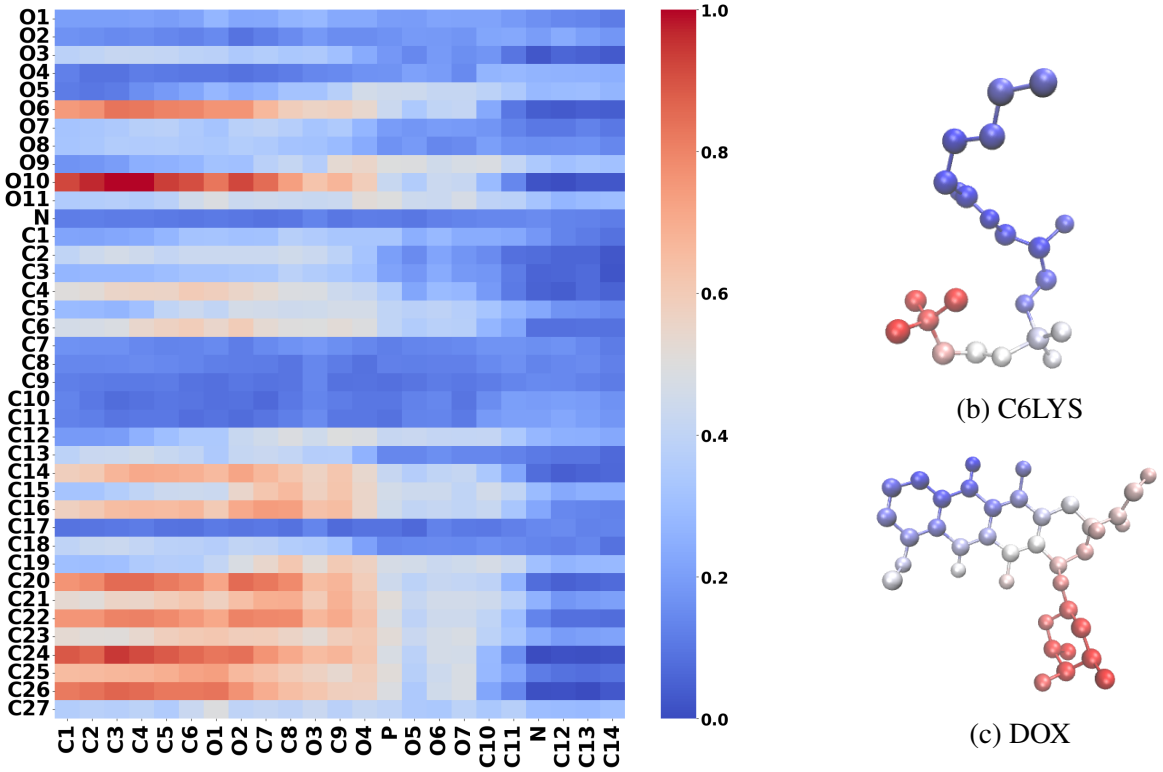

(a) Contact map between C6LYS and DOX

(b) C6LYS

(c) DOX

Fig. 4.23 **The contact map between pairs of DOX and C6LYS in the PP-micelles system.** Contact maps (a) shows the amount of contact and interactions between two pairs of molecules. Higher values indicate closer contact. (b)(c) all coloured based on the amount of contact with each atoms.

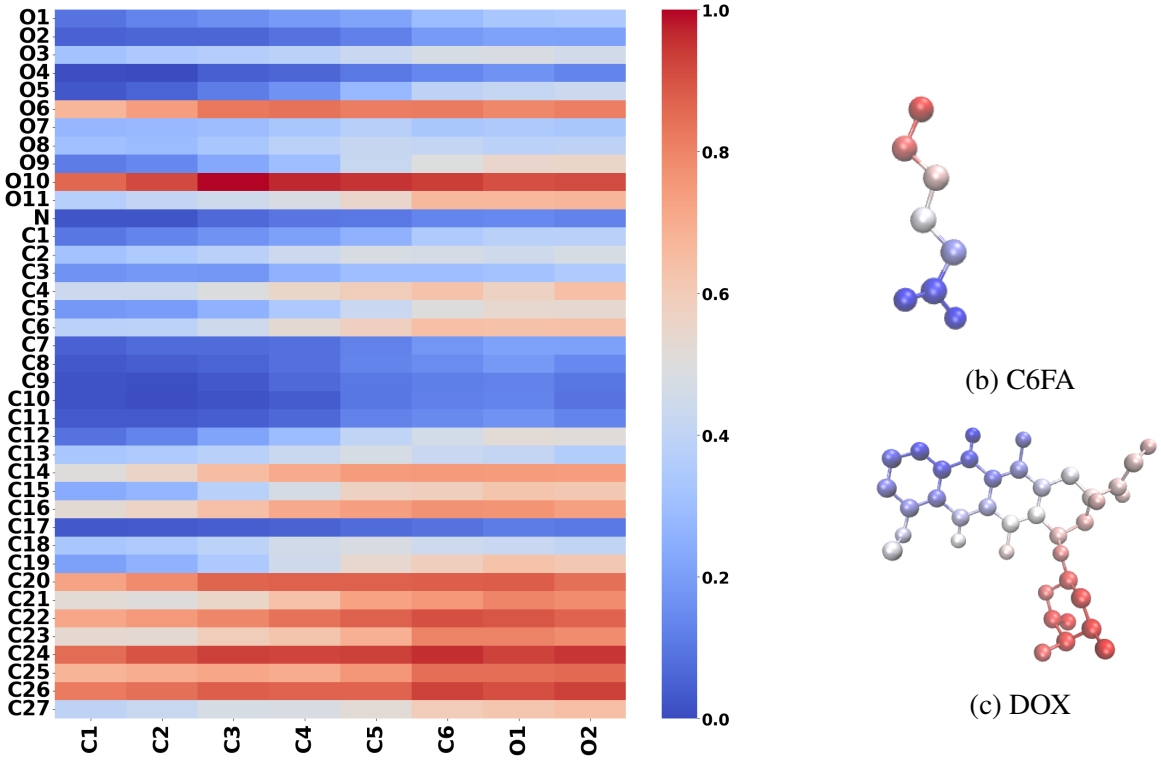

(a) Contact map between C6FA and DOX

(b) C6FA

(c) DOX

Fig. 4.24 **The contact map between pairs of DOX and C6FA in the PP-micelles system.** Contact maps (a) shows the amount of contact and interactions between two pairs of molecules. Higher values indicate closer contact. (b)(c) all coloured based on the amount of contact with each atoms.

Chapter 5

Drug localisation

5.1 Introduction

Drug delivery systems (DDS) are sophisticated technological platforms designed to package and preserve drug molecules in various formats like tablets or solutions for effective delivery. They play a pivotal role in directing drugs to specific sites within the body, maximizing therapeutic benefits while minimizing unintended effects[195, 196]. Drugs can be administered through multiple pathways, including oral, buccal, sublingual, nasal, ophthalmic, transdermal, subcutaneous, anal, transvaginal, and intravesical routes. The characteristics of drugs determine their behavior in the body and their therapeutic impacts upon ingestion[197–200].

Controlled-release drug formulations have garnered significant attention due to their advantages over traditional drugs. These formulations release drugs at predetermined rates and duration, independent of body conditions, and can offer consistent or adjustable release rates, lasting from days to years[201, 202]. They enhance drug solubility, accumulation at target sites, therapeutic efficacy, pharmacological activity, pharmacokinetic properties, patient adherence, and reduce toxicity[196]. Active targeting strategies

involve ligands or molecules that bind to target tissues, reducing side effects and improving specificity, yet challenges such as immunogenicity and degradation persist[203–205]. Responsive stimuli targeting, using factors like pH, temperature, ultrasound, magnetic fields, or electric fields, further enhance drug delivery to target cells[206, 207].

In our previous research (done by a previous PhD student Demi Pink from our group), we investigated the internal structure and conformational behavior of nanoparticles. Specifically, the SLN system studied comprised triglyceride (tripalmitin) as the lipid core and Brij O10 (C18:1E10) as the interfacial surfactant. The LLN system, on the other hand, comprised triolein (GTO) as the liquid lipid core and Brij O10 as the surfactant shell. In our study, we found that the liquid lipid aggregate consists of a lipid shell at the interface with surrounding water, with lipids primarily adopting a trident conformation to maximize contact with water molecules. Similarly, the solid lipid aggregate has a lipid shell at the interface with water, but lipids in the outer shell form various crystalline facets stabilized by interdigitation of triglyceride tails. These crystalline facets were not observed in the liquid aggregate due to the higher amount of nontrident lipid molecules present.[208, 209]

In SLNs, a crystalline lipid shell is observed at the interface with water, composed entirely of lipids in the trident conformation. The core of SLNs primarily consists of nontrident lipid conformations that crystallize with each other. Additionally, our studies revealed that the presence of a cis-double bond inhibits lipid crystallization in LLNs, leading to differences in nanoparticle morphology compared to SLNs.Our results demonstrated that Brij O10 increases ordering and crystallization in SLNs but decreases ordering in LLNs by coating the lipid surface, thus making crystallization unnecessary for shielding lipid hydrocarbon tails. Overall, our research

provides insights into the structural differences and behaviors of SLNs and LLNs, contributing to the development of more effective drug delivery vehicles.[208, 209]

The preliminary analysis conducted by Demi on LLNs and SLNs, highlighting the differences and similarities in drug localization within lipid-based nanoparticles (LLN and SLN) due to variations in lipid morphology.[1] The localization of TSTP within SLN suggests that solid lipids inhibit drug penetration into the lipid core, contrary to expectations regarding the role of the crystalline trident shell. Similarly, while more TSTP penetrates the LLN lipid core, reversible diffusion between Brij O10 and lipids indicates drug instability within both LLN and SLN. The instability observed may result from loading the drug into preformed nanoparticles or transitions in lipid states, leading to drug expulsion or difficulty in locating stable cavities within LLN's closely packed lipids.[1]

Based on this analysis, schematics (Fig. 5.1) representing testosterone propionate (TSTP) localization in SLN and LLN have been created. In SLN, a shell of crystalline trident lipids surrounds a non-trident lipid core, with most drug molecules localizing within the surfactant due to lipid crystallization. In contrast, LLN lacks a crystalline shell, with drug molecules distributed in the surfactant shell, lipid/surfactant interface, and lipid core, attributed to the absence of a trident structure and the covering of lipids by the nonionic surfactant, Brij O10 (C18:1E10). These findings highlight the complex interplay between lipid morphology and drug localization, offering insights into optimizing lipid-based nanoparticle designs for drug delivery applications.[1]

Continuing on from work discussed in our previous works, TSTP loading simulations with the SLN and LLN will be further analysised in this chapter.

The drug's orientation during the interaction into the surfactant and further hydration analysis also will be discussed.

5.2 Previous simulation setup summary

All molecular species were modeled using the CHARMM General Force Field (CGenFF), with the TSTP drug molecule's structure generated using Avogadro. The final frames representing equilibrated SLN and LLN nanoparticle structures, were used to initialize simulations. TSTP drug molecules were randomly inserted into solvent boxes based on solubilization data: 44 molecules for SLN (TPN and Brij O10) and 67 for LLN (SBO and Brij O10). Both systems were thermalized at 309 K in the NVT ensemble using the Nosé-Hoover thermostat, followed by pressure equilibration at 1 atm in the NPT ensemble using the Nosé-Hoover thermostat and Parrinello-Rahman barostat for 200 ps each. Production simulations were conducted at 309 K and 1 atm using the Nosé-Hoover thermostat and Parrinello-Rahman barostat. The SLN and LLN systems were simulated for 370 ns and 360 ns, respectively, with LINCS used for bond constraints and a timestep of 2 fs.[1]

The simulations from our previous works aimed to analyze TSTP drug molecule dynamics within SLN and LLN systems, exploring how lipid ratios influence drug localization and interactions. Insights from these simulations contribute to understanding the stability and structure-property relationships of SLNs and LLNs as drug delivery vehicles.[1]

5.3 Analysis

The tilt angle calculations were employed to have a better understanding of the atomistic mechanisms that drive the interactions of the drug molecules with the different triglycerides, which result in the previously identified distinct insertions of the drug molecules into the two nanoparticles. Specifically, for the drug molecule TSTP, the angle between the vector formed by the carbon atoms C3 and C17 were used for measurement (find the label reference atoms in Fig. 5.2). Additionally, another vector was formed between the center of mass of the nanoparticle and the C19 carbon atom within SLN systems, as well as the C22 carbon atom within LLN systems, were used to assess the orientation of the drug molecules as they approach the lipid nanoparticles. Determination of radial density functions R_g was calculated as described in previous chapters.

5.4 Results and Discussions

Tilt angle calculations were performed to analyze the orientation and localization of drugs within SLN and LLN nanoparticle systems. Additionally, the distance between the drugs and the center of nanoparticle mass was measured to assess drug penetration. The orientation angles of TSTP indicated a even distribution of drugs from cosine values from -1 to 1 within both SLN and LLN systems (Fig. 5.3(a-b)), suggesting no noticeable orientation preference. Regarding drug localization, LLN systems exhibited a higher proportion of drugs encapsulated within the nanoparticles compared to SLN systems. In contrast, in SLN systems, drugs tended to be located either inside (around 7.5 Å) or outside (around 12.5 Å - 20 Å) the systems, indicating a more compact structure with fewer drugs penetrating the nanoparticles

	O2	*O3*	*04*
SLN	0.78 (0.33)	0.02 (0.32)	0.73 (0.33)
LLN	0.35 (0.27)	0.07 (0.34)	0.65 (0.32)

Table 5.1 **Hydration analysis of drugs.** The coordinate water numbers in the first shell with TSTP drugs' oxygen atoms O2, O3 and O4 respectively. The first peak of water shell is shown in parentheses.

as a whole. In LLN systems, drug distribution was more evenly dispersed, suggesting greater system flexibility.

We calculated radial distribution functions (RDFs) to understand the hydration behavior of drugs within different lipid-based nanoparticle systems as the RDF provides information on the distribution of particles around a reference particles, showing in Fig. 5.4. To quantify the number of water molecules surrounding atoms from drug with the first shell, the integration of the RDF up to the distance corresponding to the minimum of the first peak were calculated to present the number of water molecules closely associated with the drug atoms and all values have shown in Table 5.1. In Fig. 5.4, the RDFs' for oxygen O2, O3 and O4 from drug of TSTP were used as reference atoms to see the distribution atoms from water atoms (-OH). The similar trend can be observed in Fig. 5.4 in both SLN and LLN systems, indicating that the hydration effects in these two systems might follow the similar trend. The values of coordinate water number showing in the Table 5.1 are showing relatively small, which all smaller than 1, indicating the drug molecules are around the hydrophobic environment. And the first peaks for each oxygen atoms are also very similar, with the largest value 0.33 (nm) and the smallest 0.27 (nm).

5.5 Conclusion

Based on our previous preliminary analysis, the study employed tilt angle calculations and distance measurements to elucidate the orientation, localization, and hydration behavior of drugs within SLN and LLN nanoparticle systems in this chapter. Tilt angle analysis revealed a relatively even distribution of drugs orientation within both SLN and LLN systems, suggesting no significant orientation preference. However, LLN systems exhibited a higher proportion of drugs encapsulated within nanoparticles compared to SLN systems, indicating a more compact structure with fewer drugs penetrating the nanoparticles as a whole. Conversely, in SLN systems, drugs tended to localize either inside or outside the systems, implying greater system rigidity. Additionally, the investigation into hydration behavior through radial distribution functions (RDFs) as well as coordinate water numbers showed similar trends for oxygen atoms from the drug TSTP across SLN and LLN systems. The relatively small coordination numbers and consistent first peak distances suggested that drug molecules predominantly resided within hydrophobic environments. Overall, our findings highlight differences in drug distribution and hydration behavior between SLN and LLN systems, with implications for drug delivery efficacy and nanoparticle design. These insights contribute to a deeper understanding of the complex interplay between drug molecules and lipid-based nanoparticle carriers, facilitating the development of more efficient drug delivery systems tailored to specific therapeutic needs.

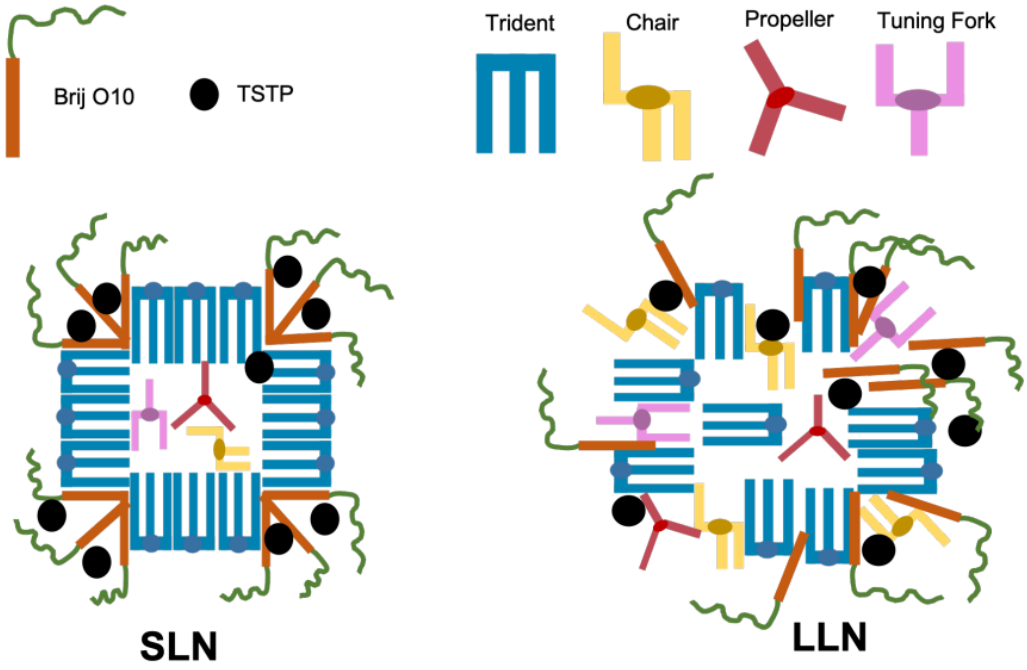

Fig. 5.1 The cartoon schematic of drug-loaded Solid Lipid Nanoparticles (SLN) and Liquid Lipid Nanoparticles (LLN) that presented in our previous works[1].

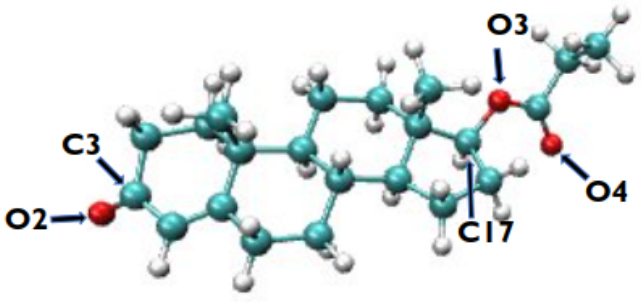

Fig. 5.2 The chemical structure of drug TSTP.

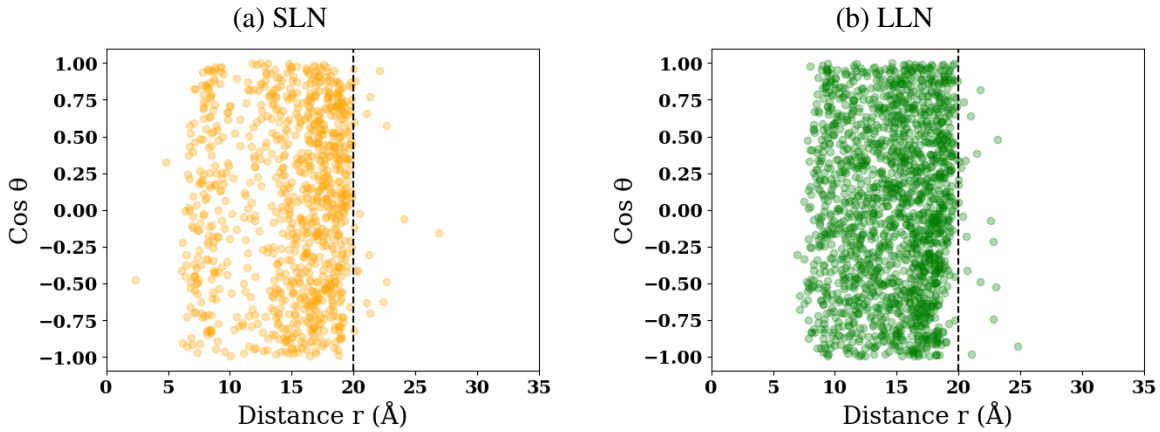

Fig. 5.3 **Orientation of drug TSTP in SLN and LLN**. The scatter plots show the distribution of the angles and localization of drugs TSTP in SLN (a) and LLN (b) systems respectively. The black dash line illustrates the probable location of the lipid core within the systems.

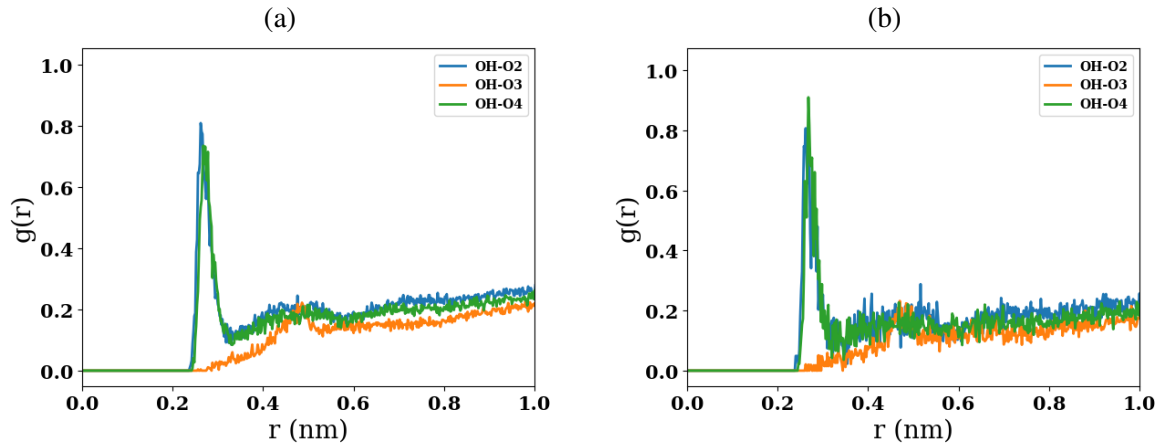

Fig. 5.4 Radial distribution functions for the drug of TSTPs' oxygen atoms O2, O3, O4 with the water oxygen (OH) in SLN (a) and LLN (b) systems respectively.

Chapter 6

Conclusions

Due to the low oral bioavailability resulting from the low water solubility of drugs, the formation of new pharmaceutical products becomes a challenge for scientists. In the field of oral drug delivery, Lipid-Based Drug Delivery Systems have garnered significant scholarly attention. Numerous researchers have contributed extensive information highlighting the utility of this delivery system in enhancing the oral bioavailability of medications. Throughout these works in this thesis, all lipid-based drug delivery systems were studied using atomistic molecular dynamics simulations to examine the underlying mechanisms between the locations, interactions and geometry of the molecules at different stages. The intention was to construct suitable drug vehicles loaded with drugs in order to understand the internal and interfacial structures and properties of micelles, and investigate the effect that could be used on its potential applications. The conducted simulations and further comprehensive analysis in the thesis have successfully provided insights of the influence of different lipid composition on micellar dynamic systems and drug localization within micelles, which providing a better understanding of lipid-based nanoformations for more effective drug delivery systems.

In chapter 3, the study employing all-atom molecular dynamics simulations has unveiled the intricate dynamics of C6 phosphocholine micelles during digestion by the sPLA2 enzyme and their subsequent interaction with disordered and ordered lipid bilayers. We observed a disassociation of micelles and release of their components, with distinctive behaviors exhibited by 2C6PC, C6LYSO, and C6FA molecules. The penetration of these molecules into different lipid bilayers revealed preferences influenced by membrane characteristics, due to the difference of free volume availability in these two membrane systems. Furthermore, our findings shed light on the diverse dynamic properties within bilayers, particularly the pronounced flip-flopping of C6FA molecules. These results contribute to the first atomistic understanding of how lipid and digestion product combinations influence model lipid membranes, offering valuable insights for the design of lipid-based drug delivery vehicles. The analysis conducted in this study also demonstrates that lysolipids and fatty acids produced during digestion enhance lipid membrane permeability, and potentially could facilitate faster diffusion of therapeutics into cancerous cells. These findings position phospholipid drug delivery vehicles as promising candidates for targeted anti-cancer formulations, providing a foundation for future advancements in cancer therapy.

In the next chapter, the study sheds light on the intricate interplay between drugs and lipid-based micelles, offering valuable insights into their behavior and interactions. Specifically, our findings highlight the distinct preferences of CAMPT and DOX within micellar environments, emphasizing the importance of tailoring drug-micelle interactions to the specific properties of the drug. The observed disparities between PP-micelle and PL-micelle systems underscore the significance of lipid composition in dictating micellar stability and dynamics. Furthermore, the detailed analyses of micelle composition, internal structure, and hydration behaviors provide

a solid foundation for the optimization of drug delivery systems. By elucidating the complex mechanisms underlying drug-micelle interactions, our research contributes to the broader field of drug delivery, offering more insights that can inform future studies and advancements in the design of more efficient and stable drug delivery platforms. In the following chapter, based on our preliminary analysis, investigations on drug orientation, localization, and hydration behavior within Solid Lipid Nanoparticles (SLN) and Liquid Lipid Nanoparticles (LLN) systems were conducted. Results show that while drug orientation is evenly distributed in both systems, LLN exhibit higher drug encapsulation compared to SLN, indicating a more compact structure. SLN systems show rigidity, with drugs localizing either inside or outside. Hydration analysis suggests drug molecules predominantly reside in hydrophobic environments.

In conclusion, the comprehensive exploration of lipid-based drug delivery systems through atomistic molecular dynamics simulations has provided valuable insights into the mechanisms governing their behavior and interactions at various stages. The study has successfully delved into the dynamics of C6 phosphocholine micelles during digestion, shedding light on their subsequent interaction with two different properties of lipid bilayers and revealing distinct behaviors exhibited by molecules. The findings emphasize the influence of lipid composition on micellar stability and dynamics, providing a foundation for the design of lipid-based drug delivery vehicles. Moreover, the investigation into the interplay between drugs and lipid-based micelles has underscored the importance of tailoring drug-micelle interactions to the specific properties of the drug. The analysis of works presented in different micelle systems highlight the significance of lipid composition in dictating micellar stability. Overall, this research contributes to the advancement of drug delivery systems, particularly in the realm of cancer therapy, offering a deeper understanding of the complex mechanisms that

can inform the design of more efficient and stable drug delivery platforms for future applications.

Based on the work conducted in this thesis, there are several studies that can be conducted to potentially improve current drug delivery system technologies. For instance, tailoring the lipid composition of drug delivery vehicles can enhance micellar stability and drug encapsulation efficiency. Specifically, the balance between hydrophilic and hydrophobic components should be adjusted to match the properties of the encapsulated drugs, ensuring better stability and targeted delivery. Specific lipid combinations, such as phospholipids and fatty acids, can be used to improve membrane permeability and facilitate faster diffusion of therapeutics into target cells, especially for cancer treatment. Designing drug delivery vehicles that can selectively target cancerous cells or specific tissues will enhance the therapeutic efficacy and reducing side effects. This could involve incorporating targeting ligands or using stimuli-responsive lipids that release drugs in response to specific biological signals. This would allow the community to investigate the potential of lipid-based systems to cross biological barriers (e.g., blood-brain barrier) and deliver drugs to hard-to-reach areas, potentially expanding the scope of treatments available for various diseases.

6.1 Further works

As simulations of the interaction between lipid-based micelles and membranes or drugs have been performed, several avenues for further research can be pursued. Additional simulations and further analysis will reveal the effect of lipid digestion on membrane permeability and enhance mechanistic insights into lipid-based formulations for drug delivery vehicles.

To build upon the works discussed in Chapter 3, further investigations can focus on how the presence of lysolipids and fatty acids resulting from phospholipid digestion affects membrane permeability to different molecules, including drugs and therapeutic agents. Although the obtained results have shown increased permeability of lipid membranes during the digestion of phospholipids, specific molecules that might potentially cause these results remain unidentified. This could involve experimental validation using in vitro models or computational simulations, such as enhanced sampling methods or free energy calculations, to predict permeability changes in the presence of lysolipids and fatty acids within membranes. Such additional work would help provide a clearer understanding of the molecular mechanisms underlying the interactions between phospholipid micelles, digestion products, and lipid membranes.

In addition to this, further exploration can also focus on strategies to optimize the design of lipid-based drug delivery vehicles based on the findings. This could involve modifying the composition of phospholipid micelles or incorporating targeting ligands to enhance their specificity towards cancer cells while exploiting the permeability-enhancing effects of lysolipids and fatty acids. This could also extend the study to include other digestive enzymes or conditions mimicking different stages of digestion. Doing so would help understand how various enzymes interact with phospholipid micelles and their subsequent effects on model membranes, providing insights into the behavior of lipid-based drug delivery systems under different physiological conditions.

As discussed in Chapter 4, simulations of CAMPT and DOX drug loading with lipid-based micelles can be explored further. The impact of the structure on drug-micelle interactions has been investigated, but different sizes and chemical properties of other drugs could also be addressed through

future works. By doing so, research can focus on their interactions with lipid-based micelles and how their hydrophobic nature influences micellar stability and composition. Examining other drugs in lipid-based micelle systems can broaden the scope of this research and provide additional insights into drug-micelle interactions.

By pursuing these research directions, as well as the many works presented in this thesis, it would be possible to further elucidate the complex interplay between lipid digestion, drug delivery, and gain a comprehensive understanding of how different drug properties and characteristics influence their interactions with micelles. Ultimately, this would advance the development of lipid-based formulations for anticancer therapeutics and potentially other biomedical applications.

References

[1] Demi L Pink. Investigating the structure of lipid-based nanoparticles for applications in drug-delivery. King's College London, 2020.

[2] Demi L. Pink, Orathai Loruthai, Robert M. Ziolek, Prawarisa Wasutrasawat, Ann E. Terry, M.J̃ayne Lawrence, and Christian D. Lorenz. On the structure of solid lipid nanoparticles. Small, 15:1903156, 2019.

[3] RAHUL Bhalla, AVINASH KUMAR Singh, SABYASACHI Pradhan, and KR Unnikumar. Lipids: structure, function and biotechnology aspects. A Textbook of Molecular Biotechnology, pages 173–209, 2009.

[4] Daryl Meyer. Lipids and biochemistry, 2022.

[5] Augustine Ikhueoya Airaodion, Uloaku Ogbuagu, Emmanuel O Ogbuagu, AP Oloruntoba, AP Agunbiade, Edith Oloseuan Airaodion, Ifeoma Pearl Mokelu, and Stella Chinonye Ekeh. Mechanisms for controlling the synthesis of lipids–review. Int. J. Res, 6(2):123–135, 2019.

[6] Niloy Kundu, Debasis Banik, and Nilmoni Sarkar. Self-assembly of amphiphiles into vesicles and fibrils: investigation of structure and dynamics using spectroscopy and microscopy techniques. Langmuir, 34(39):11637–11654, 2018.

[7] Doralicia Casares, Pablo V Escribá, and Catalina Ana Rosselló. Membrane lipid composition: effect on membrane and organelle structure, function and compartmentalization and therapeutic avenues. International journal of molecular sciences, 20(9):2167, 2019.

[8] Gaspar Banfalvi and Gaspar Banfalvi. Biological membranes. Springer, 2016.

[9] Takeshi Harayama and Howard Riezman. Understanding the diversity of membrane lipid composition. Nature reviews Molecular cell biology, 19(5):281–296, 2018.

[10] Kurt Kristiansen. Molecular mechanisms of ligand binding, signaling, and regulation within the superfamily of g-protein-coupled receptors: molecular modeling and mutagenesis approaches to receptor structure and function. Pharmacology & therapeutics, 103(1):21–80, 2004.

[11] Tomohiro Imura, Noboru Ohta, Katsuaki Inoue, Naoto Yagi, Hideyuki Negishi, Hiroshi Yanagishita, and Dai Kitamoto. Naturally engineered glycolipid biosurfactants leading

to distinctive self-assembled structures. Chemistry–A European Journal, 12(9):2434–2440, 2006.

[12] Rashmi C Desai and Raymond Kapral. Dynamics of Self-organized and Self-assembled Structures. Cambridge University Press, 2009.

[13] Hélène Barelli and Bruno Antonny. Lipid unsaturation and organelle dynamics. Current Opinion in Cell Biology, 41:25–32, 2016.

[14] Giorgio Lenaz and Giovanna Parenti Castelli. Membrane fluidity: molecular basis and physiological significance. In Structure and Properties of Cell Membrane Structure and Properties of Cell Membranes, pages 93–136. CRC Press, 2018.

[15] Rodolfo R Brenner. Effect of unsaturated acids on membrane structure and enzyme kinetics. Progress in lipid research, 23(2):69–96, 1984.

[16] Smita Pravin Soni. The effect of acyl chain unsaturation on phospholipid bilayer. 2010.

[17] Inge S Zuhorn, Udo Bakowsky, Evgeny Polushkin, Willy H Visser, Marc CA Stuart, Jan BFN Engberts, and Dick Hoekstra. Nonbilayer phase of lipoplex–membrane mixture determines endosomal escape of genetic cargo and transfection efficiency. Molecular therapy, 11(5):801–810, 2005.

[18] Rein Verbeke, Ine Lentacker, Stefaan C De Smedt, and Heleen Dewitte. The dawn of mrna vaccines: The covid-19 case. Journal of Controlled Release, 333:511–520, 2021.

[19] Sanjib Bhattacharya. Phytosomes: the new technology for enhancement of bioavailability of botanicals and nutraceuticals. International Journal of Health Research, 2(3):225–232, 2009.

[20] Theresa M Allen and Pieter R Cullis. Liposomal drug delivery systems: from concept to clinical applications. Advanced drug delivery reviews, 65(1):36–48, 2013.

[21] Abdelmoneim H Ali, Xiaoqiang Zou, Sherif M Abed, Sameh A Korma, Qingzhe Jin, and Xingguo Wang. Natural phospholipids: Occurrence, biosynthesis, separation, identification, and beneficial health aspects. Critical reviews in food science and nutrition, 59(2):253–275, 2019.

[22] Jingbo Li, Yongjin He, Sampson Anankanbil, and Zheng Guo. Phospholipid-based surfactants. In Biobased Surfactants, pages 243–286. Elsevier, 2019.

[23] Tanxi Cai and Fuquan Yang. Phospholipid and phospholipidomics in health and diseases. Lipidomics in health & disease: methods & application, pages 177–202, 2018.

[24] David N Brindley. Lipid phosphate phosphatases and related proteins: signaling functions in development, cell division, and cancer. Journal of cellular biochemistry, 92(5):900–912, 2004.

[25] Verena Kolsch, Pascale G Charest, and Richard A Firtel. The regulation of cell motility and chemotaxis by phospholipid signaling. Journal of cell science, 121(5):551–559, 2008.

[26] lipid structure. https://mibellebiochemistry.com/de/node/197.

[27] Kristine Scordo and Kim Anne Pickett. Triglycerides. The American journal of nursing, 117(1):24–31, 2017.

[28] Vigen K Babayan. Medium chain triglycerides and structured lipids. Lipids, 22(6):417–420, 1987.

[29] HW Tan, AR Abdul Aziz, and MK Aroua. Glycerol production and its applications as a raw material: A review. Renewable and sustainable energy reviews, 27:118–127, 2013.

[30] Frank D Gunstone. Fatty acids and lipids structure. In Lipid Technologies and Applications, pages 1–17. Routledge, 2018.

[31] Graham C Burdge and Philip C Calder. Introduction to fatty acids and lipids. Intravenous Lipid Emulsions, 112:1–16, 2015.

[32] Arild C Rustan and Christian A Drevon. Fatty acids: structures and properties. e LS, 2001.

[33] Helen Watson. Biological membranes. Essays in biochemistry, 59:43–69, 2015.

[34] Christina G Siontorou, Georgia-Paraskevi Nikoleli, Dimitrios P Nikolelis, and Stefanos K Karapetis. Artificial lipid membranes: Past, present, and future. Membranes, 7(3):38, 2017.

[35] David E Smith and ADJ Haymet. Free energy, entropy, and internal energy of hydrophobic interactions: Computer simulations. The Journal of chemical physics, 98(8):6445–6454, 1993.

[36] Bengt Kronberg. The hydrophobic effect. Current Opinion in Colloid & Interface Science, 22:14–22, 2016.

[37] Emilia Fisicaro, Carlotta Compari, and A Braibanti. Entropy/enthalpy compensation: hydrophobic effect, micelles and protein complexes. Physical Chemistry Chemical Physics, 6(16):4156–4166, 2004.

[38] Julian Eastoe and Rico F Tabor. Surfactants and nanoscience. In Colloidal foundations of nanoscience, pages 153–182. Elsevier, 2022.

[39] Vladimir P Torchilin. Lipid-core micelles for targeted drug delivery. Current Drug Delivery, 2(4):319–327, 2005.

[40] Zaheer Ahmad, Afzal Shah, Muhammad Siddiq, and Heinz-Bernhard Kraatz. Polymeric micelles as drug delivery vehicles. Rsc Advances, 4(33):17028–17038, 2014.

[41] Tarun Garg and Amit K Goyal. Liposomes: targeted and controlled delivery system. Drug delivery letters, 4(1):62–71, 2014.

[42] Cicera J Camilo, Debora OD Leite, Angelo RA Silva, Irwin RA Menezes, Henrique DM Coutinho, and José GM Da Costa. Lipid vesicles: Applications, principal components and methods used in their formulations. a review. Acta Biológica Colombiana, 25(2):339–352, 2020.

[43] Ole G Mouritsen. Lipids, curvature, and nano-medicine. European journal of lipid science and technology, 113(10):1174–1187, 2011.

[44] Elisabet Fuguet, Clara Ràfols, Martí Rosés, and Elisabeth Bosch. Critical micelle concentration of surfactants in aqueous buffered and unbuffered systems. Analytica Chimica Acta, 548(1-2):95–100, 2005.

[45] Saurabh Verma, Umesh K Goand, Athar Husain, Roshan A Katekar, Richa Garg, and Jiaur R Gayen. Challenges of peptide and protein drug delivery by oral route: Current strategies to improve the bioavailability. Drug development research, 82(7):927–944, 2021.

[46] Kewal K Jain. An overview of drug delivery systems. drug delivery systems, pages 1–54, 2020.

[47] Kewal K Jain. Drug delivery systems-an overview. Drug delivery systems, pages 1–50, 2008.

[48] Patrick M Glassman and Vladimir R Muzykantov. Pharmacokinetic and pharmacodynamic properties of drug delivery systems. Journal of Pharmacology and Experimental Therapeutics, 370(3):570–580, 2019.

[49] Attuluri Pavan Kumar. Optimization and Development of Enteric Coated Formulation of Gastro-Resistant Colon Specific Drug. PhD thesis, Rajiv Gandhi University of Health Sciences (India), 2013.

[50] KP Sampath Kumar, Debjit Bhowmik, Shweta Srivastava, Shravan Paswan, and Amit Sankar Dutta. Sustained release drug delivery system potential. The pharma innovation, 1(2), 2012.

[51] Sibi Raj, Sartaj Khurana, Ramesh Choudhari, Kavindra Kumar Kesari, Mohammad Amjad Kamal, Neha Garg, Janne Ruokolainen, Bhudev C Das, and Dhruv Kumar. Specific targeting cancer cells with nanoparticles and drug delivery in cancer therapy. In Seminars in cancer biology, volume 69, pages 166–177. Elsevier, 2021.

[52] Kumar Bishwajit Sutradhar and Md Lutful Amin. Nanotechnology in cancer drug delivery and selective targeting. International scholarly research notices, 2014, 2014.

[53] Sarabjeet Singh Suri, Hicham Fenniri, and Baljit Singh. Nanotechnology-based drug delivery systems. Journal of occupational medicine and toxicology, 2:1–6, 2007.

[54] Guanying Chen, Indrajit Roy, Chunhui Yang, and Paras N Prasad. Nanochemistry and nanomedicine for nanoparticle-based diagnostics and therapy. Chemical reviews, 116(5):2826–2885, 2016.

[55] Rakesh K Tekade, Rahul Maheshwari, Namrata Soni, Muktika Tekade, and Mahavir B Chougule. Nanotechnology for the development of nanomedicine. In Nanotechnology-based approaches for targeting and delivery of drugs and genes, pages 3–61. Elsevier, 2017.

[56] Camilla Hald Albertsen, Jayesh A Kulkarni, Dominik Witzigmann, Marianne Lind, Karsten Petersson, and Jens B Simonsen. The role of lipid components in lipid nanoparticles for vaccines and gene therapy. Advanced drug delivery reviews, 188:114416, 2022.

[57] Lei Yang, Liming Gong, Ping Wang, Xinghui Zhao, Feng Zhao, Zhijie Zhang, Yunfei Li, and Wei Huang. Recent advances in lipid nanoparticles for delivery of mrna. Pharmaceutics, 14(12):2682, 2022.

[58] Yu-Shiuan Wang, Monika Kumari, Guan-Hong Chen, Ming-Hsiang Hong, Joyce Pei-Yi Yuan, Jui-Ling Tsai, and Han-Chung Wu. mrna-based vaccines and therapeutics: an in-depth survey of current and upcoming clinical applications. Journal of Biomedical Science, 30(1):84, 2023.

[59] Archana Khosa, Satish Reddi, and Ranendra N Saha. Nanostructured lipid carriers for site-specific drug delivery. Biomedicine & Pharmacotherapy, 103:598–613, 2018.

[60] Hsin-I Chang and Ming-Kung Yeh. Clinical development of liposome-based drugs: formulation, characterization, and therapeutic efficacy. International journal of nanomedicine, pages 49–60, 2012.

[61] Mehran Alavi and Mehrdad Hamidi. Passive and active targeting in cancer therapy by liposomes and lipid nanoparticles. Drug metabolism and personalized therapy, 34(1):20180032, 2019.

[62] Lipid nanoparticles: The underrated invention behind the vaccine revolution. https://blog.scienceborealis.ca/lipid-nanoparticles-the-underrated-invention-behind-the-vaccine-revolution/.

[63] Jayesh A Kulkarni, Pieter R Cullis, and Roy Van Der Meel. Lipid nanoparticles enabling gene therapies: from concepts to clinical utility. Nucleic acid therapeutics, 28(3):146–157, 2018.

[64] Jayesh A Kulkarni, Johnathan Layne Myhre, Sam Chen, Yuen Yi C Tam, Adrian Danescu, Joy M Richman, and Pieter R Cullis. Design of lipid nanoparticles for in vitro and in vivo delivery of plasmid dna. Nanomedicine: Nanotechnology, Biology and Medicine, 13(4):1377–1387, 2017.

[65] Purva Khare, Sara X Edgecomb, Christine M Hamadani, Eden EL Tanner, and Devika S Manickam. Lipid nanoparticle-mediated drug delivery to the brain. Advanced Drug Delivery Reviews, page 114861, 2023.

[66] Yoshiyuki Hattori, Kyoko Tamaki, Sho Sakasai, Kei-Ichi Ozaki, and Hiraku Onishi. Effects of peg anchors in pegylated sirna lipoplexes on in vitro gene-silencing effects and sirna biodistribution in mice. Molecular Medicine Reports, 22(5):4183–4196, 2020.

[67] Varun Kumar, June Qin, Yongfeng Jiang, Richard G Duncan, Benjamin Brigham, Shannon Fishman, Jayaprakash K Nair, Akin Akinc, Scott A Barros, and Pia V Kasperkovitz. Shielding of lipid nanoparticles for sirna delivery: impact on physicochemical properties, cytokine induction, and efficacy. Molecular Therapy-Nucleic Acids, 3, 2014.

[68] Xiangsheng Liu and Huan Meng. Consideration for the scale-up manufacture of nanotherapeutics—a critical step for technology transfer. View, 2(5):20200190, 2021.

[69] Phatsapong Yingchoncharoen, Danuta S Kalinowski, and Des R Richardson. Lipid-based drug delivery systems in cancer therapy: what is available and what is yet to come. Pharmacological reviews, 68(3):701–787, 2016.

[70] Roberta Cavalli, Otto Caputo, and Maria Rosa Gasco. Solid lipospheres of doxorubicin and idarubicin. International journal of pharmaceutics, 89(1):R9–R12, 1993.

[71] Jian-Xin Wang, Xun Sun, and Zhi-Rong Zhang. Enhanced brain targeting by synthesis of 3', 5'-dioctanoyl-5-fluoro-2'-deoxyuridine and incorporation into solid lipid nanoparticles. European Journal of Pharmaceutics and Biopharmaceutics, 54(3):285–290, 2002.

[72] Loredana Serpe, Maria Graziella Catalano, Roberta Cavalli, Elena Ugazio, Ornella Bosco, Roberto Canaparo, Elisabetta Muntoni, Roberto Frairia, Maria Rosa Gasco, Mario Eandi, et al. Cytotoxicity of anticancer drugs incorporated in solid lipid nanoparticles on ht-29 colorectal cancer cell line. European Journal of Pharmaceutics and Biopharmaceutics, 58(3):673–680, 2004.

[73] Shi Cheng Yang, Li Fang Lu, Ying Cai, Jia Bi Zhu, Bing Wen Liang, and Chang Zheng Yang. Body distribution in mice of intravenously injected camptothecin solid lipid nanoparticles and targeting effect on brain. Journal of controlled release, 59(3):299–307, 1999.

[74] Gian Paolo Zara, Roberta Cavalli, ANNA FUNDARÒ, Alessandro Bargoni, OTTO CAPUTO, and MARIA ROSA GASCO. Pharmacokinetics of doxorubicin incorporated in solid lipid nanospheres (sln). Pharmacological research, 40(3):281–286, 1999.

[75] Mohammad A. Obeid, Rothwelle J. Tate, Alexander B. Mullen, and Valerie A. Ferro. Chapter 8 - lipid-based nanoparticles for cancer treatment. In Alexandru Mihai Grumezescu, editor, Lipid Nanocarriers for Drug Targeting, pages 313–359. William Andrew Publishing, 2018.

[76] Usama A. Fahmy. Augmentation of fluvastatin cytotoxicity against prostate carcinoma pc3 cell line utilizing alpha lipoic–ellagic acid nanostructured lipid carrier formula. AAPS PharmSciTech, 19(8):3454–3461, 2018.

[77] Jing Li, Shi Jin, Xue-Rong Dong, Xiao-Feng Han, and Man-Yuan Wang. Construction of artesunate nanoparticles modified by hyaluronic acid and cell-penetrating peptides and its inhibitory effect on cancer cells in vitro. Zhongguo Zhong yao za zhi= Zhongguo Zhongyao Zazhi= China Journal of Chinese Materia Medica, 43(18):3668–3675, 2018.

[78] Prasant Nahak, Rahul L Gajbhiye, Gourab Karmakar, Pritam Guha, Biplab Roy, Shila Elizabeth Besra, Alexey G Bikov, Alexander V Akentiev, Boris A Noskov, Kaushik Nag, et al. Orcinol glucoside loaded polymer-lipid hybrid nanostructured lipid carriers: potential cytotoxic agents against gastric, colon and hepatoma carcinoma cell lines. Pharmaceutical research, 35:1–10, 2018.

[79] Qiuyu Wei, Qiuxuan Yang, Qilong Wang, Congyong Sun, Yuan Zhu, Ya Niu, Jiangnan Yu, and Ximing Xu. Formulation, characterization, and pharmacokinetic studies of 6-gingerol-loaded nanostructured lipid carriers. AAPS pharmscitech, 19:3661–3669, 2018.

[80] Beatriz García-Pinel, Cristina Porras-Alcalá, Alicia Ortega-Rodríguez, Francisco Sarabia, Jose Prados, Consolación Melguizo, and Juan M López-Romero. Lipid-based nanoparticles: application and recent advances in cancer treatment. Nanomaterials, 9(4):638, 2019.

[81] Muhammad Imran, Muhammad R Shah, et al. Amphiphilic block copolymers–based micelles for drug delivery. In Design and Development of New Nanocarriers, pages 365–400. Elsevier, 2018.

[82] Amalina Bte Ebrahim Attia, Zhan Yuin Ong, James L Hedrick, Phin Peng Lee, Pui Lai Rachel Ee, Paula T Hammond, and Yi-Yan Yang. Mixed micelles self-assembled from block copolymers for drug delivery. Current Opinion in Colloid & Interface Science, 16(3):182–194, 2011.

[83] Anatoly N Lukyanov and Vladimir P Torchilin. Micelles from lipid derivatives of water-soluble polymers as delivery systems for poorly soluble drugs. Advanced drug delivery reviews, 56(9):1273–1289, 2004.

[84] Volkmar Weissig, Kathleen R Whiteman, and Vladimir P Torchilin. Accumulation of protein-loaded long-circulating micelles and liposomes in subcutaneous lewis lung carcinoma in mice. Pharmaceutical research, 15:1552–1556, 1998.

[85] Tae-You Kim, Dong-Wan Kim, Jae-Yong Chung, Sang Goo Shin, Sung-Chul Kim, Dae Seog Heo, Noe Kyeong Kim, and Yung-Jue Bang. Phase i and pharmacokinetic study of genexol-pm, a cremophor-free, polymeric micelle-formulated paclitaxel, in patients with advanced malignancies. Clinical cancer research, 10(11):3708–3716, 2004.

[86] Chunli Shi, Xing Guo, Qianqian Qu, Zhaomin Tang, Yi Wang, and Shaobing Zhou. Actively targeted delivery of anticancer drug to tumor cells by redox-responsive star-shaped micelles. Biomaterials, 35(30):8711–8722, 2014.

[87] Xun Jin, Peilan Zhang, Li Luo, Hao Cheng, Yunzu Li, Ting Du, Bingwen Zou, and Maling Gou. Efficient intravesical therapy of bladder cancer with cationic doxorubicin nanoassemblies. International journal of nanomedicine, pages 4535–4544, 2016.

[88] Preeti Kumari, Omkara Swami Muddineti, Sri Vishnu Kiran Rompicharla, Pratyusha Ghanta, Adithya Karthik BBN, Balaram Ghosh, and Swati Biswas. Cholesterol-conjugated poly (d, l-lactide)-based micelles as a nanocarrier system for effective delivery of curcumin in cancer therapy. Drug Delivery, 24(1):209–223, 2017.

[89] Stephanie Deshayes, Horacio Cabral, Takehiko Ishii, Yutaka Miura, Shutaro Kobayashi, Takashi Yamashita, Akira Matsumoto, Yuji Miyahara, Nobuhiro Nishiyama, and Kazunori Kataoka. Phenylboronic acid-installed polymeric micelles for targeting sialylated epitopes in solid tumors. Journal of the American Chemical Society, 135(41):15501–15507, 2013.

[90] Ryan N Gilbreth, Shabazz Novarra, Leslie Wetzel, Stelios Florinas, Horacio Cabral, Kazunori Kataoka, Jonathan Rios-Doria, Ronald J Christie, and Manuel Baca. Lipid- and polyion complex-based micelles as agonist platforms for tnfr superfamily receptors. Journal of Controlled Release, 234:104–114, 2016.

[91] Vladimir P Torchilin. Structure and design of polymeric surfactant-based drug delivery systems. Journal of controlled release, 73(2-3):137–172, 2001.

[92] Shan-Yang Lin and Y Kawashima. The influence of three poly (oxyethylene) poly (oxypropylene) surface-active block copolymers on the solubility behavior of indomethacin. Pharmaceutica Acta Helvetiae, 60(12):339–344, 1985.

[93] Polymeric Anticancer Drug Adriamycin-conjugated. Characterization and anticancer activity of the micelle-forming. CANCER RESEARCH, 50:1693–1700, 1990.

[94] Marie-Christine Jones and Jean-Christophe Leroux. Polymeric micelles–a new generation of colloidal drug carriers. European journal of pharmaceutics and biopharmaceutics, 48(2):101–111, 1999.

[95] JE Chung, M Yokoyama, M Yamato, T Aoyagi, Y Sakurai, and T Okano. Thermoresponsive drug delivery from polymeric micelles constructed using block copolymers of poly (n-isopropylacrylamide) and poly (butylmethacrylate). Journal of Controlled Release, 62(1-2):115–127, 1999.

[96] Wen-Yih Chen, Paschalis Alexandridis, Chia-Kai Su, Costas S Patrickios, Walter R Hertler, and T Alan Hatton. Effect of block size and sequence on the micellization of abc triblock methacrylic polyampholytes. Macromolecules, 28(25):8604–8611, 1995.

[97] Kumi Kawano, Masato Watanabe, Tatsuhiro Yamamoto, Masayuki Yokoyama, Praneet Opanasopit, Teruo Okano, and Yoshie Maitani. Enhanced antitumor effect of camptothecin loaded in long-circulating polymeric micelles. Journal of controlled release, 112(3):329–332, 2006.

[98] M Laird Forrest, Chee-Youb Won, A Waseem Malick, and Glen S Kwon. In vitro release of the mtor inhibitor rapamycin from poly (ethylene glycol)-b-poly (ε-caprolactone) micelles. Journal of Controlled Release, 110(2):370–377, 2006.

[99] Wen-Jen Lin, Lee-Wei Juang, and Chi-Chang Lin. Stability and release performance of a series of pegylated copolymeric micelles. Pharmaceutical research, 20:668–673, 2003.

[100] Gang-Biao Jiang, Daping Quan, Kairong Liao, and Haihua Wang. Novel polymer micelles prepared from chitosan grafted hydrophobic palmitoyl groups for drug delivery. Molecular Pharmaceutics, 3(2):152–160, 2006.

[101] Andrew J Beevers, Anthony Nash, Martha Salazar-Cancino, David J Scott, Rebecca Notman, and Ann M Dixon. Effects of the oncogenic v664e mutation on membrane insertion, structure, and sequence-dependent interactions of the neu transmembrane domain in micelles and model membranes: An integrated biophysical and simulation study. Biochemistry, 51(12):2558–2568, 2012.

[102] Honggang Cui, Matthew J Webber, and Samuel I Stupp. Self-assembly of peptide amphiphiles: From molecules to nanostructures to biomaterials. Peptide Science: Original Research on Biomolecules, 94(1):1–18, 2010.

[103] Ruiyun Zhang, Ruirui Xing, Tifeng Jiao, Kai Ma, Chengjun Chen, Guanghui Ma, and Xuehai Yan. Carrier-free, chemophotodynamic dual nanodrugs via self-assembly for synergistic antitumor therapy. ACS applied materials & interfaces, 8(21):13262–13269, 2016.

[104] Vitaly V Chaban and Himanshu Khandelia. Distribution of neutral lipids in the lipid droplet core. The Journal of Physical Chemistry B, 118(38):11145–11151, 2014.

[105] Vitaly V Chaban and Himanshu Khandelia. Lipid structure in triolein lipid droplets. The Journal of Physical Chemistry B, 118(35):10335–10340, 2014.

[106] Esra Tuncer and Beste Bayramoglu. Characterization of the self-assembly and size dependent structural properties of dietary mixed micelles by molecular dynamics simulations. Biophysical Chemistry, 248:16–27, 2019.

[107] Sarah L Rouse and Mark SP Sansom. Interactions of lipids and detergents with a viral ion channel protein: Molecular dynamics simulation studies. The Journal of Physical Chemistry B, 119(3):764–772, 2015.

[108] T Wymore, XF Gao, and TC Wong. Molecular dynamics simulation of the structure and dynamics of a dodecylphosphocholine micelle in aqueous solution. Journal of Molecular Structure, 485:195–210, 1999.

[109] Abhinav S Raman, Joshua Pajak, and YC Chiew. Interaction of pcl based self-assembled nano-polymeric micelles with model lipid bilayers using coarse-grained molecular dynamics simulations. Chemical physics letters, 712:1–6, 2018.

[110] Aliya O Kasimova, Giovanni M Pavan, Andrea Danani, Karine Mondon, Andrea Cristiani, Leonardo Scapozza, Robert Gurny, and Michael Moller. Validation of a novel molecular dynamics simulation approach for lipophilic drug incorporation into polymer micelles. The Journal of Physical Chemistry B, 116(14):4338–4345, 2012.

[111] Tibo Duran, Antonio Costa, Anand Gupta, Xiaoming Xu, Hailing Zhang, Diane Burgess, and Bodhisattwa Chaudhuri. Coarse-grained molecular dynamics simulations of paclitaxel-loaded polymeric micelles. Molecular Pharmaceutics, 19(4):1117–1134, 2022.

[112] Morteza Rezaeisadat, Abdol-Khalegh Bordbar, and Reza Omidyan. Molecular dynamics simulation study of curcumin interaction with nano-micelle of pnipaam-b-peg co-polymer as a smart efficient drug delivery system. Journal of Molecular Liquids, 332:115862, 2021.

[113] Sadegh Faramarzi, Brittany Bonnett, Carl A Scaggs, Ashley Hoffmaster, Danielle Grodi, Erica Harvey, and Blake Mertz. Molecular dynamics simulations as a tool for accurate determination of surfactant micelle properties. Langmuir, 33(38):9934–9943, 2017.

[114] Richard J Alsop, Adree Khondker, Jochen S Hub, and Maikel C Rheinstädter. The lipid bilayer provides a site for cortisone crystallization at high cortisone concentrations. Scientific reports, 6(1):22425, 2016.

[115] Nandhitha Subramanian, Alexandra Schumann-Gillett, Alan E Mark, and Megan L O'Mara. Understanding the accumulation of p-glycoprotein substrates within cells: The effect of cholesterol on membrane partitioning. Biochimica et Biophysica Acta (BBA)-Biomembranes, 1858(4):776–782, 2016.

[116] Timothy S Carpenter, Daniel A Kirshner, Edmond Y Lau, Sergio E Wong, Jerome P Nilmeier, and Felice C Lightstone. A method to predict blood-brain barrier permeability of drug-like compounds using molecular dynamics simulations. Biophysical journal, 107(3):630–641, 2014.

[117] Lewis J Martin, Rebecca Chao, and Ben Corry. Molecular dynamics simulation of the partitioning of benzocaine and phenytoin into a lipid bilayer. Biophysical chemistry, 185:98–107, 2014.

[118] Daniela Lopes, Sven Jakobtorweihen, Claudia Nunes, Bruno Sarmento, and Salette Reis. Shedding light on the puzzle of drug-membrane interactions: Experimental techniques and molecular dynamics simulations. Progress in lipid research, 65:24–44, 2017.

[119] Christopher JH Porter, Natalie L Trevaskis, and William N Charman. Lipids and lipid-based formulations: optimizing the oral delivery of lipophilic drugs. Nature reviews Drug discovery, 6(3):231–248, 2007.

[120] Woldeamanuel A Birru, Dallas B Warren, Ahmed Ibrahim, Hywel D Williams, Hassan Benameur, Christopher JH Porter, David K Chalmers, and Colin W Pouton. Digestion of phospholipids after secretion of bile into the duodenum changes the phase behavior of bile components. Molecular pharmaceutics, 11(8):2825–2834, 2014.

[121] Jonathan K Embleton and Colin W Pouton. Structure and function of gastro-intestinal lipases. Advanced Drug Delivery Reviews, 25(1):15–32, 1997.

[122] Jacob N Israelachvili, D John Mitchell, and Barry W Ninham. Theory of self-assembly of hydrocarbon amphiphiles into micelles and bilayers. Journal of the Chemical Society, Faraday Transactions 2: Molecular and Chemical Physics, 72:1525–1568, 1976.

[123] Jamal Khan, Adrian Hawley, Thomas Rades, and Ben J Boyd. In situ lipolysis and synchrotron small-angle x-ray scattering for the direct determination of the precipitation and solid-state form of a poorly water-soluble drug during digestion of a lipid-based formulation. Journal of pharmaceutical sciences, 105(9):2631–2639, 2016.

[124] Joerg J Moehrle, Stephan Duparc, Christoph Siethoff, Paul LM van Giersbergen, J Carl Craft, Sarah Arbe-Barnes, Susan A Charman, Maria Gutierrez, Sergio Wittlin, and Jonathan L Vennerstrom. First-in-man safety and pharmacokinetics of synthetic ozonide oz439 demonstrates an improved exposure profile relative to other peroxide antimalarials. British journal of clinical pharmacology, 75(2):535–548, 2013.

[125] Andrew J Clulow, Malinda Salim, Adrian Hawley, Elliot P Gilbert, and Ben J Boyd. The curious case of the oz439 mesylate salt: An amphiphilic antimalarial drug with diverse solution and solid state structures. Molecular Pharmaceutics, 15(5):2027–2035, 2018.

[126] Ben J Boyd, Malinda Salim, Andrew J Clulow, Gisela Ramirez, Anna C Pham, and Adrian Hawley. The impact of digestion is essential to the understanding of milk as a drug delivery system for poorly water soluble drugs. Journal of Controlled Release, 292:13–17, 2018.

[127] Malinda Salim, Jamal Khan, Gisela Ramirez, Mubtasim Murshed, Andrew J Clulow, Adrian Hawley, Hanu Ramachandruni, Stephane Beilles, and Ben J Boyd. Impact of ferroquine on the solubilization of artefenomel (oz439) during in vitro lipolysis in milk and implications for oral combination therapy for malaria. Molecular Pharmaceutics, 16(4):1658–1668, 2019.

[128] Malinda Salim, Jamal Khan, Gisela Ramirez, Andrew J Clulow, Adrian Hawley, Hanu Ramachandruni, and Ben J Boyd. Interactions of artefenomel (oz439) with milk during digestion: insights into digestion-driven solubilization and polymorphic transformations. Molecular Pharmaceutics, 15(8):3535–3544, 2018.

[129] Barnabas Wilson and Kannoth Mukundan Geetha. Lipid nanoparticles in the development of mrna vaccines for covid-19. Journal of Drug Delivery Science and Technology, 74:103553, 2022.

[130] Berni Julian Alder and Thomas Everett Wainwright. Phase transition for a hard sphere system. The Journal of chemical physics, 27(5):1208–1209, 1957.

[131] Mark E Tuckerman and Glenn J Martyna. Understanding modern molecular dynamics: Techniques and applications, 2000.

[132] Hasan Metin Aktulga, Sagar A Pandit, Adri CT Van Duin, and Ananth Y Grama. Reactive molecular dynamics: Numerical methods and algorithmic techniques. SIAM Journal on Scientific Computing, 34(1):C1–C23, 2012.

[133] Kurt Binder, Jürgen Horbach, Walter Kob, Wolfgang Paul, and Fathollah Varnik. Molecular dynamics simulations. Journal of Physics: Condensed Matter, 16(5):S429, 2004.

[134] Louis G Smith, Jianbo Zhao, David H Mathews, and Douglas H Turner. Physics-based all-atom modeling of rna energetics and structure. Wiley Interdisciplinary Reviews: RNA, 8(5):e1422, 2017.

[135] Richard M Martin. Electronic structure: basic theory and practical methods. Cambridge university press, 2020.

[136] G Andrés Cisneros, Mikko Karttunen, Pengyu Ren, and Celeste Sagui. Classical electrostatics for biomolecular simulations. Chemical reviews, 114(1):779–814, 2014.

[137] Kun Zhou and Bo Liu. Molecular dynamics simulation: Fundamentals and Applications. Academic Press, 2022.

[138] Hiqmet Kamberaj. Molecular dynamics simulations in statistical physics: theory and applications. Springer, 2020.

[139] Miguel A González. Force fields and molecular dynamics simulations. École thématique de la Société Française de la Neutronique, 12:169–200, 2011.

[140] Luca Monticelli and D Peter Tieleman. Force fields for classical molecular dynamics. Biomolecular simulations: Methods and protocols, pages 197–213, 2013.

[141] Bernard R Brooks, Robert E Bruccoleri, Barry D Olafson, David J States, S a Swaminathan, and Martin Karplus. Charmm: a program for macromolecular energy, minimization, and dynamics calculations. Journal of computational chemistry, 4(2):187–217, 1983.

[142] David A Pearlman, David A Case, James W Caldwell, Wilson S Ross, Thomas E Cheatham III, Steve DeBolt, David Ferguson, George Seibel, and Peter Kollman. Amber, a package of computer programs for applying molecular mechanics, normal mode analysis, molecular dynamics and free energy calculations to simulate the structural and energetic properties of molecules. Computer Physics Communications, 91(1-3):1–41, 1995.

[143] Thereza A Soares, Xavier Daura, Chris Oostenbrink, Lorna J Smith, and Wilfred F van Gunsteren. Validation of the gromos force-field parameter set 45a3 against nuclear magnetic resonance data of hen egg lysozyme. Journal of Biomolecular NMR, 30:407–422, 2004.

[144] Jing Huang and Alexander D MacKerell Jr. Charmm36 all-atom additive protein force field: Validation based on comparison to nmr data. Journal of computational chemistry, 34(25):2135–2145, 2013.

[145] Alexander D MacKerell Jr et al. Atomistic models and force fields. Computational biochemistry and biophysics, pages 7–38, 2001.

[146] Hannes H Loeffler and M Winn. Large biomolecular simulation on hpc platforms iii. amber, charmm, gromacs, lammps and namd. Technical report, Technical report, STFC Daresbury Laboratory, Warrington WA4 4AD, UK, 2012.

[147] Sereina Riniker. Fixed-charge atomistic force fields for molecular dynamics simulations in the condensed phase: An overview. Journal of chemical information and modeling, 58(3):565–578, 2018.

[148] Lars Meinhold. Crystalline Protein Dynamics: A Simulation Analysis of Staphylococcal Nuclease. PhD thesis, 2005.

[149] Helmut Grubmüller, Helmut Heller, Andreas Windemuth, and Klaus Schulten. Generalized verlet algorithm for efficient molecular dynamics simulations with long-range interactions. Molecular Simulation, 6(1-3):121–142, 1991.

[150] Jed W Pitera and Wilfred F van Gunsteren. A comparison of non-bonded scaling approaches for free energy calculations. Molecular Simulation, 28(1-2):45–65, 2002.

[151] Wilfred F Van Gunsteren and Herman JC Berendsen. A leap-frog algorithm for stochastic dynamics. Molecular Simulation, 1(3):173–185, 1988.

[152] Jun Xie, Demi L Pink, M Jayne Lawrence, and Christian D Lorenz. Digestion of lipid micelles leads to increased membrane permeability. Nanoscale, 16(5):2642–2653, 2024.

[153] Shixian Lv, Yuchen Wu, Kaimin Cai, Hua He, Yongjuan Li, Min Lan, Xuesi Chen, Jianjun Cheng, and Lichen Yin. High drug loading and sub-quantitative loading efficiency of polymeric micelles driven by donor–receptor coordination interactions. Journal of the American chemical society, 140(4):1235–1238, 2018.

[154] Kaimin Cai, Xi He, Ziyuan Song, Qian Yin, Yanfeng Zhang, Fatih M Uckun, Chen Jiang, and Jianjun Cheng. Dimeric drug polymeric nanoparticles with exceptionally high drug loading and quantitative loading efficiency. Journal of the American Chemical Society, 137(10):3458–3461, 2015.

[155] Ido Rosenbaum, Assaf J Harnoy, Einat Tirosh, Marina Buzhor, Merav Segal, Liat Frid, Rona Shaharabani, Ram Avinery, Roy Beck, and Roey J Amir. Encapsulation and covalent binding of molecular payload in enzymatically activated micellar nanocarriers. Journal of the American Chemical Society, 137(6):2276–2284, 2015.

[156] Rakesh K Pathak and Shanta Dhar. A nanoparticle cocktail: temporal release of predefined drug combinations. Journal of the American Chemical Society, 137(26):8324–8327, 2015.

[157] Dali Wang, Bing Liu, Yuan Ma, Chenwei Wu, Quanbing Mou, Hongping Deng, Ruibin Wang, Deyue Yan, Chuan Zhang, and Xinyuan Zhu. A molecular recognition approach to synthesize nucleoside analogue based multifunctional nanoparticles for targeted cancer therapy. Journal of the American Chemical Society, 139(40):14021–14024, 2017.

[158] Gregor Cevc. Phospholipids handbook. CRC press, 2018.

[159] PR t Cullis and B De Kruijff. Lipid polymorphism and the functional roles of lipids in biological membranes. Biochimica et Biophysica Acta (BBA)-Reviews on Biomembranes, 559(4):399–420, 1979.

[160] Christopher Rupp, Hartwig Steckel, and Bernd W Müller. Solubilization of poorly water-soluble drugs by mixed micelles based on hydrogenated phosphatidylcholine. International journal of pharmaceutics, 395(1-2):272–280, 2010.

[161] Panayiotis P Constantinides, Mahesh V Chaubal, and Robert Shorr. Advances in lipid nanodispersions for parenteral drug delivery and targeting. Advanced drug delivery reviews, 60(6):757–767, 2008.

[162] Vladimir P Torchilin. Micellar nanocarriers: pharmaceutical perspectives. Pharmaceutical research, 24:1–16, 2007.

[163] Beena Ashok, Lise Arleth, Rex P Hjelm, Israel Rubinstein, and Hayat Önyüksel. In vitro characterization of pegylated phospholipid micelles for improved drug solubilization: effects of peg chain length and pc incorporation. Journal of pharmaceutical sciences, 93(10):2476–2487, 2004.

[164] Joseph Wong, Andrew Brugger, Atul Khare, Mahesh Chaubal, Pavlos Papadopoulos, Barrett Rabinow, James Kipp, and John Ning. Suspensions for intravenous (iv) injection: a review of development, preclinical and clinical aspects. Advanced drug delivery reviews, 60(8):939–954, 2008.

[165] Richard L Momparler, Myron Karon, Stuart E Siegel, and Felicidad Avila. Effect of adriamycin on dna, rna, and protein synthesis in cell-free systems and intact cells. Cancer research, 36(8):2891–2895, 1976.

[166] Frank A Fornari, Joyce K Randolph, Jack C Yalowich, Mary K Ritke, and David A Gewirtz. Interference by doxorubicin with dna unwinding in mcf-7 breast tumor cells. Molecular pharmacology, 45(4):649–656, 1994.

[167] Qingyan Ruan, Gopal Patel, Jingyi Wang, Enhui Luo, Wei Zhou, Elwira Sieniawska, Xiaolong Hao, and Guoyin Kai. Current advances of endophytes as a platform for production of anti-cancer drug camptothecin. Food and Chemical Toxicology, 151:112113, 2021.

[168] Feihu Wang, Hao Su, Dongqing Xu, Wenbing Dai, Weijie Zhang, Zongyuan Wang, Caleb F Anderson, Mengzhen Zheng, Richard Oh, Fengyi Wan, et al. Tumour sensitization via the extended intratumoural release of a sting agonist and camptothecin from a self-assembled hydrogel. Nature biomedical engineering, 4(11):1090–1101, 2020.

[169] Elisa Checa-Chavarria, Eva Rivero-Buceta, Miguel Angel Sanchez Martos, Gema Martinez Navarrete, Cristina Soto-Sánchez, Pablo Botella, and Eduardo Fernández. Development of a prodrug of camptothecin for enhanced treatment of glioblastoma multiforme. Molecular Pharmaceutics, 18(4):1558–1572, 2021.

[170] Xiaojuan Gong, Zihan Wang, Li Zhang, Wenjuan Dong, Ruiping Wang, Yang Liu, Shengmei Song, Qin Hu, Fangfang Du, Shaomin Shuang, et al. A novel carbon-nanodots-based theranostic nano-drug delivery system for mitochondria-targeted imaging and glutathione-activated delivering camptothecin. Colloids and Surfaces B: Biointerfaces, 218:112712, 2022.

[171] Grzegorz Lapienis. Ring-opening polymerization of cyclic phosphorus monomers. 2019.

[172] Jun Xie, Demi L. Pink, M.J̃ayne Lawrence, and Christian D. Lorenz. Digestion of lipid micelles leads to increased membrane permeability. Nanoscale, 16:2642–2653, 2024.

[173] Sunwhan Jo, Taehoon Kim, Vidyashankara G. Iyer, and Wonpil Im. Charmm-gui: A web-based grapical user interface for charmm. J. Comput. Chem., 29:1859–1865, 2008.

[174] Seonghoon Kim, Jumin Lee, Sunwhan Jo, Charles L.B̃rooks III, Hui Sun Lee, and Wonpil Im. Charmm-gui ligand reader and modeler for charmm force field generation of small molecules. J. Comput. Chem., 38:1879–1886, 2017.

[175] Mark James Abraham, Teemu Murtola, Roland Schulz, Szilárd Páll, Jeremy C Smith, Berk Hess, and Erik Lindahl. Gromacs: High performance molecular simulations through multi-level parallelism from laptops to supercomputers. SoftwareX, 1:19–25, 2015.

[176] Erik Lindahl, Berk Hess, and David Van Der Spoel. Gromacs 3.0: a package for molecular simulation and trajectory analysis. Molecular modeling annual, 7:306–317, 2001.

[177] Berk Hess, Carsten Kutzner, David Van Der Spoel, and Erik Lindahl. Gromacs 4: algorithms for highly efficient, load-balanced, and scalable molecular simulation. Journal of chemical theory and computation, 4(3):435–447, 2008.

[178] Shūichi Nosé. A molecular dynamics method for simulations in the canonical ensemble. Molecular physics, 52(2):255–268, 1984.

[179] William G Hoover. Canonical dynamics: Equilibrium phase-space distributions. Physical review A, 31(3):1695, 1985.

[180] Michele Parrinello and Aneesur Rahman. Polymorphic transitions in single crystals: A new molecular dynamics method. Journal of Applied physics, 52(12):7182–7190, 1981.

[181] Berk Hess, Henk Bekker, Herman JC Berendsen, and Johannes GEM Fraaije. Lincs: A linear constraint solver for molecular simulations. Journal of computational chemistry, 18(12):1463–1472, 1997.

[182] Python documentation contents. https://docs.python.org/3/contents.html#python-documentation-contents.

[183] Naveen Michaud-Agrawal, Elizabeth J Denning, Thomas B Woolf, and Oliver Beckstein. Mdanalysis: a toolkit for the analysis of molecular dynamics simulations. J. Comput. Chem., 32(10):2319–2327, 2011.

[184] Alejandro Santana-Bonilla, Raquel López-Rios de Castro, Peike Sun, Robert M. Ziolek, and Christian D. Lorenz. Modular software for generating and modeling diverse polymer databases. J. Chem. Inf. Model., 63(12):3761–3771, 2023.

[185] pysoftwhere github. https://github.com/alejandrosantanabonilla/pysoftk.

[186] William Humphrey, Andrew Dalke, and Klaus Schulten. Vmd: visual molecular dynamics. Journal of molecular graphics, 14(1):33–38, 1996.

[187] Aric Hagberg, Pieter Swart, and Daniel S Chult. Exploring network structure, dynamics, and function using networkx. Technical report, Los Alamos National Lab.(LANL), Los Alamos, NM (United States), 2008.

[188] Oliver Beckstein, Elizabeth J Denning, Juan R Perilla, and Thomas B Woolf. Zipping and unzipping of adenylate kinase: atomistic insights into the ensemble of open closed transitions. Journal of molecular biology, 394(1):160–176, 2009.

[189] Robert M Ziolek, Paul Smith, Demi L Pink, Cecile A Dreiss, and Christian D Lorenz. Unsupervised learning unravels the structure of four-arm and linear block copolymer micelles. Macromolecules, 54(8):3755–3768, 2021.

[190] Qingrong Huang. Nanotechnology in the food, beverage and nutraceutical industries. Elsevier, 2012.

[191] Eliza de Lucas Chazin, Raisa da Rocha Reis, Walcimar Trindade Vellasco Junior, Thatyana Rocha Alves Vasconcelos, et al. An overview on the development of new potentially active camptothecin analogs against cancer. Mini reviews in medicinal chemistry, 14(12):953–962, 2014.

[192] Noura Khaiwa, Noor R Maarouf, Mhd H Darwish, Dima WM Alhamad, Anusha Sebastian, Mohamad Hamad, Hany A Omar, Gorka Orive, and Taleb H Al-Tel. Camptothecin's journey from discovery to who essential medicine: Fifty years of promise. European journal of medicinal chemistry, 223:113639, 2021.

[193] Noni Husain, Rezik A Agbaria, and Isiah M Warner. Spectroscopic analysis of the binding of doxorubicin to human. alpha.-1 acid glycoprotein. The Journal of Physical Chemistry, 97(41):10857–10861, 1993.

[194] Lina Zhao, Meina Ren, Yanjiao Wang, Hailong An, and Fude Sun. Delivering mechanism of doxorubicin by the peg-dppe micelles on membrane invasion by dynamic simulations. Physical Chemistry Chemical Physics, 2023.

[195] Bindhu Madhavi Rayaprolu, Jonathan J Strawser, and Gopal Anyarambhatla. Excipients in parenteral formulations: selection considerations and effective utilization with small molecules and biologics. Drug development and industrial pharmacy, 44(10):1565–1571, 2018.

[196] Ava M Vargason, Aaron C Anselmo, and Samir Mitragotri. The evolution of commercial drug delivery technologies. Nature biomedical engineering, 5(9):951–967, 2021.

[197] Mohammed S Alqahtani and Mohsin Kazi. Advances in oral drug delivery. Frontiers in pharmacology, 12:618411, 2021.

[198] Sharul islam Barbhuiya and Vishal Kumar. Advancement in sustain delivery drug system, chapter 9 - oral drug delivery of nanomedicine. 2023.

[199] Anuj Chauhan, Laurence Fitzhenry, and Ana Paula Serro. Recent advances in ophthalmic drug delivery. Pharmaceutics, 14(10):2075, 2022.

[200] Paramveer Sharma, Kishore Gajula, Naga Neehar Dingari, Rakesh Gupta, Sharath Gopal, Beena Rai, and Ronald G Iacocca. Subcutaneous drug delivery: A review of the state-of-the-art modeling and experimental techniques. Journal of Biomechanical Engineering, 145(2):020801, 2023.

[201] Rajan K Verma and Sanjay Garg. Drug delivery technologies and future directions. Pharm. Technol, 25(2):1–14, 2001.

[202] Rajesh A Keraliya, Chirag Patel, Pranav Patel, Vipul Keraliya, Tejal G Soni, Rajnikant C Patel, and MM Patel. Osmotic drug delivery system as a part of modified release dosage form. International Scholarly Research Notices, 2012, 2012.

[203] Chandramani Pathak, Foram U Vaidya, and Shashibhal M Pandey. Chapter 3 - mechanism for development of nanobased drug delivery system. Applications of targeted nano drugs and delivery systems, pages 35–67, 2019.

[204] Fabienne Danhier, Olivier Feron, and Véronique Préat. To exploit the tumor microenvironment: passive and active tumor targeting of nanocarriers for anti-cancer drug delivery. Journal of controlled release, 148(2):135–146, 2010.

[205] Vivek Agrahari. Novel drug delivery systems, devices, and fabrication methods, 2018.

[206] Xia Li, Myron R Szewczuk, and Cecile Malardier-Jugroot. Folic acid-conjugated amphiphilic alternating copolymer as a new active tumor targeting drug delivery platform. Drug design, development and therapy, pages 4101–4110, 2016.

[207] Vladimir P Torchilin. Multifunctional, stimuli-sensitive nanoparticulate systems for drug delivery. Nature reviews Drug discovery, 13(11):813–827, 2014.

[208] Demi L Pink, Orathai Loruthai, Robert M Ziolek, Prawarisa Wasutrasawat, Ann E Terry, M Jayne Lawrence, and Christian D Lorenz. On the structure of solid lipid nanoparticles. Small, 15(45):1903156, 2019.

[209] Demi L Pink, Orathai Loruthai, Robert M Ziolek, Ann E Terry, David J Barlow, M Jayne Lawrence, and Christian D Lorenz. Interplay of lipid and surfactant: Impact on nanoparticle structure. Journal of colloid and interface science, 597:278–288, 2021.

Appendix A

Supporting Information 1

Digestion of lipid micelles leads to increased membrane permeability

Electronic Supplementary Material (ESI) for Nanoscale.

Supporting Information for "Digestion of lipid micelles leads to increased membrane permeability"

Jun Xie,[†] Demi L. Pink,[†] M.Jayne Lawrence,[‡] and Christian D. Lorenz*,[†]

†*Department of Physics, King's College London, London*

‡*Division of Pharmacy Optometry, University of Manchester, Manchester*

E-mail: chris.lorenz@kcl.ac.uk

Phone: +44 (0)2078482639

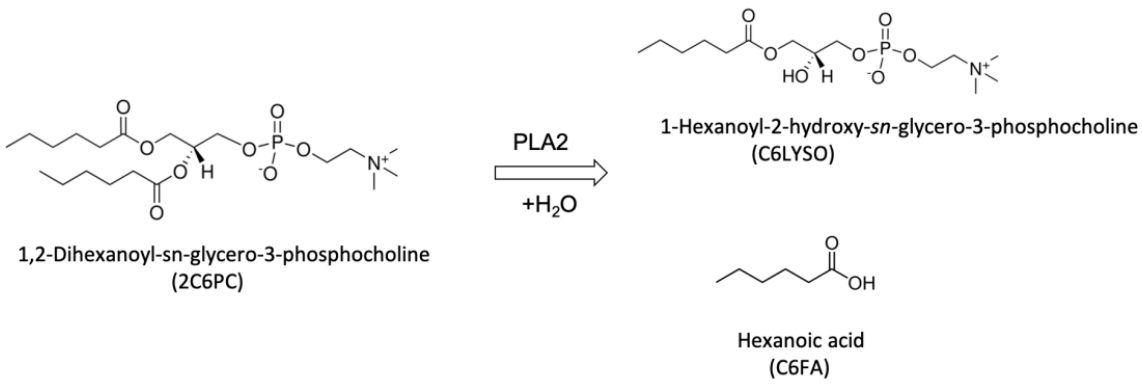

Figure S1: The chemical structure of three species. The parent 2C6PC molecules are degraded via hydrolysis alongside the C6FA and C6LYSO product molecules.

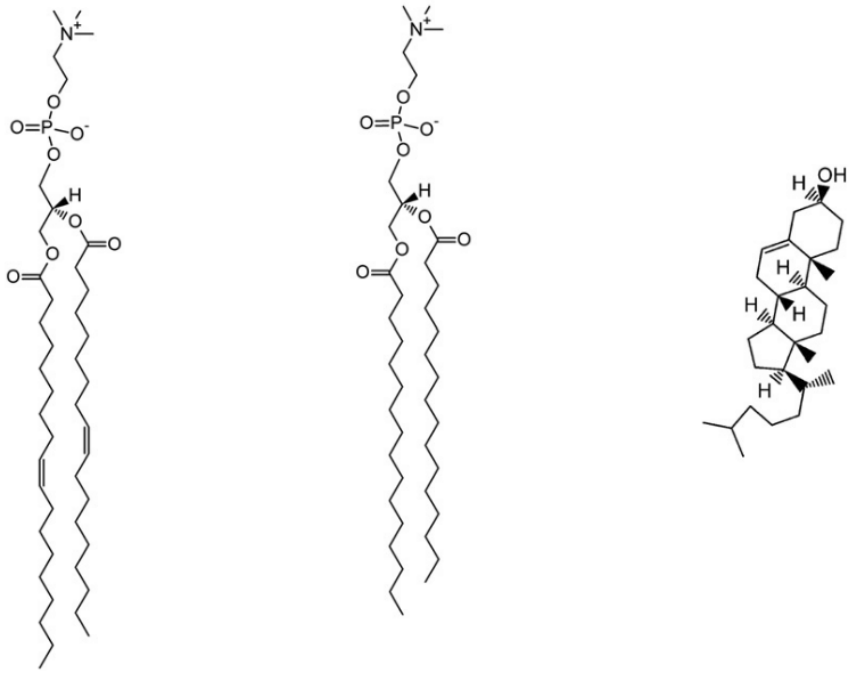

Figure S2: Chemical structures of DOPC, DPPC and cholesterol respectively.

Table S1: Detailed Description of the Composition of All of the Eight Simulated Systems.

System abbreviation	DOPC	DPPC	CHOL	C6PC	C6FA	C6LYSO	Na+	Cl-	water	MD length (ns)
DOPC	350	0	0	0	0	0	47	47	16824	200
DPPC-CHOL	0	308	132	0	0	0	43	43	15900	200
DOPC-Pure-Products	350	0	0	0	29	21	111	111	40870	1000
DOPC-Mixed	350	0	0	16	16	12	110	110	39850	1200
DOPC-Pure-Lipids	350	0	0	35	0	0	111	111	40901	1400
DPPC-CHOL-Pure-Products	0	308	132	0	29	21	58	58	21465	1000
DPPC-CHOL-Mixed	0	308	132	16	16	12	59	59	21553	1000
DPPC-CHOL-Pure-Lipids	0	308	132	35	0	0	57	57	20939	1000

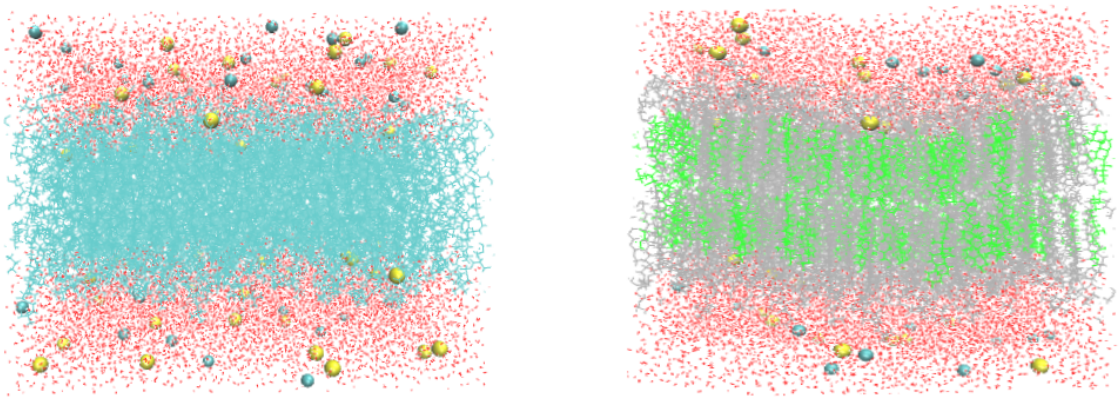

Figure S3: Snapshots of two membranes in the 200 ns time frames of trajectory. Left is the DOPC only system with ions, where Na+ is yellow, Cl- is blue, water is in red and DOPC is located in the middle of the box. Right is DPPC-CHOL membrane, where DPPC shown in grey and cholesterol in green respectively.

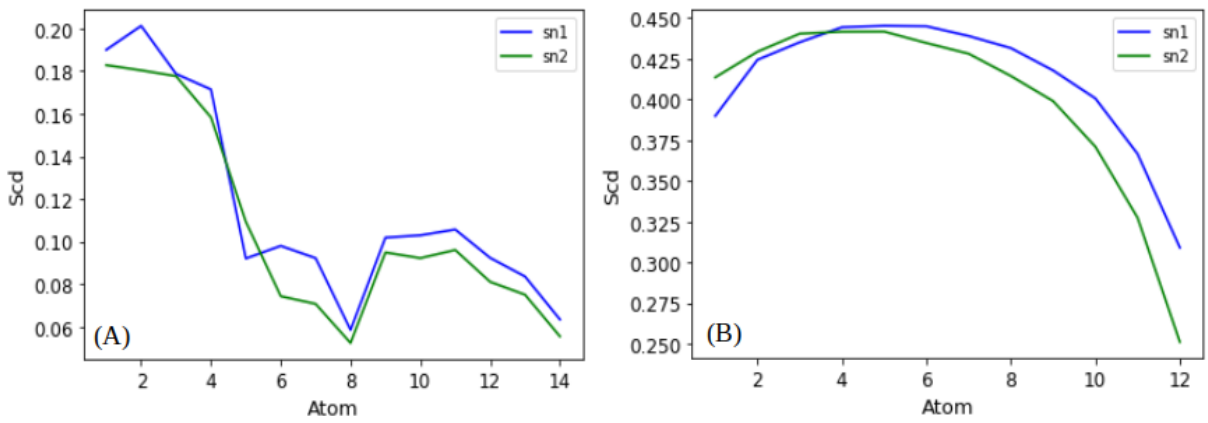

Figure S4: Absolute values of order parameters, S_{cd} , as a function of carbon number for the (A) DOPC and (B) DPPC-CHOL membrane systems interacting with micelles.

Table S2: The summary of each molecules' mean tilt angle, and the standard errors are shown in parentheses. The tilt angle reported for C6PC, DOPC and DPPC are calculated by measuring the cosine of the angle formed by the vector defined by the P and N atoms in their PC headgroups (Figs. S1 and S2) and the normal to the membrane; while the tilt angle of C6FA is calculated by measuring the cosine of the angle formed by the vector connecting the C2 and O2 atoms of the molecule (see Fig. S8) and the the normal vector of the membrane.

System	DOPC-Pure-Products	DOPC-Mixed	DOPC-Pure-Lipids	DPPC-CHOL-Pure-Products	DPPC-CHOL-Mixed	DPPC-CHOL-Pure-Lipids
C6FA	0.644 (0.008)	0.635 (0.006)	-	0.681 (0.003)	-	-
C6PC	-	0.327 (0.007)	0.301 (0.004)	-	-	-
DOPC	0.338 (0.003)	0.344 (0.002)	0.344 (0.001)	-	-	-
DPPC	-	-	-	0.341 (0.002)	0.343 (0.004)	0.391 (0.002)

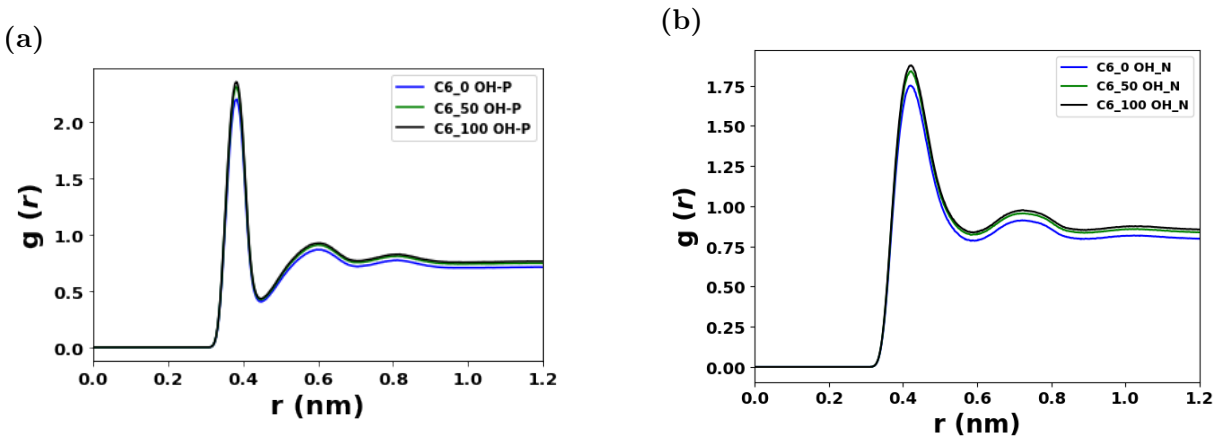

Figure S5: Radial distribution function ($g(r)$) of O_W around (a) the P and (b) N atoms in the PC head groups in the three DOPC membrane systems (Pure-Products (blue) , Mixed (green), Pure-Lipids (black)).

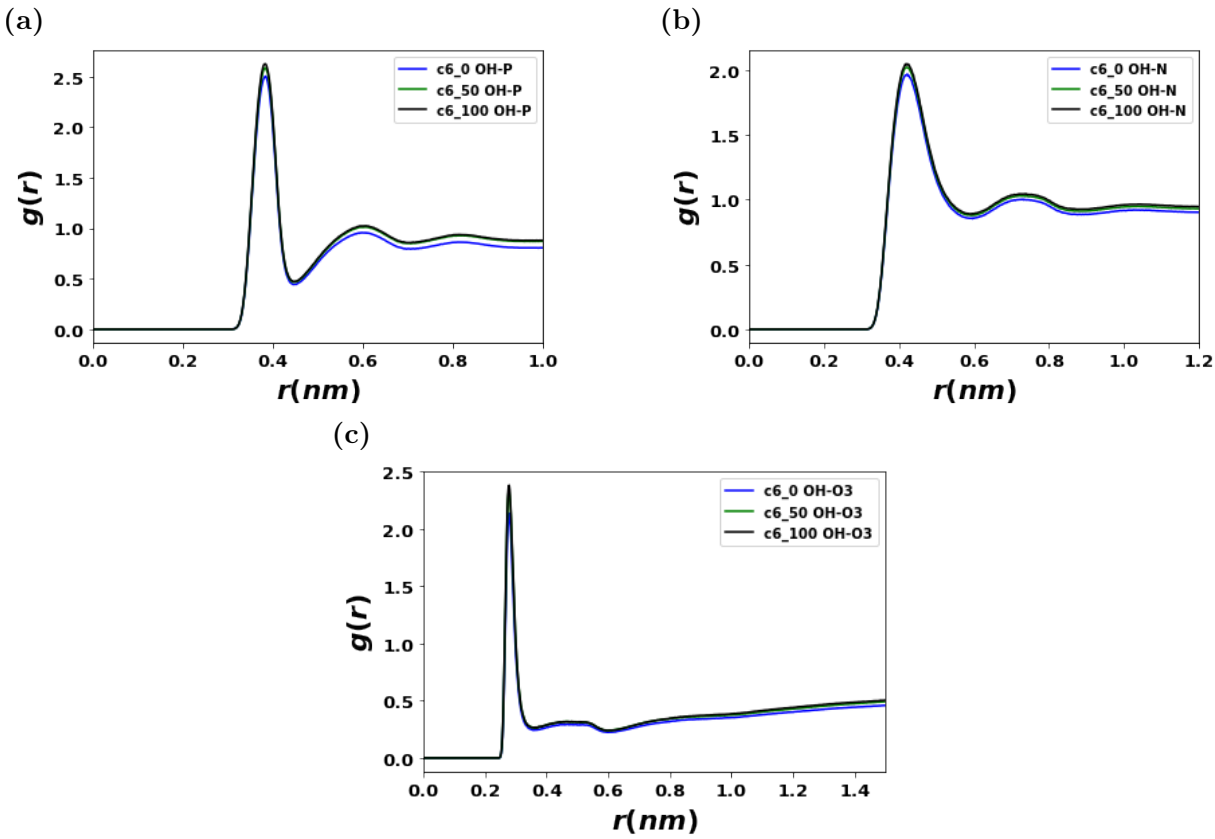

Figure S6: Radial distribution function ($g(r)$) of O_W around (a) the P and (b) N atoms in the PC head groups and (c) the O3 atom in the C6FA molecules (see Fig. S8) in the three DPPC-CHOL membrane systems (Pure-Products (blue) , Mixed (green), Pure-Lipids (black))

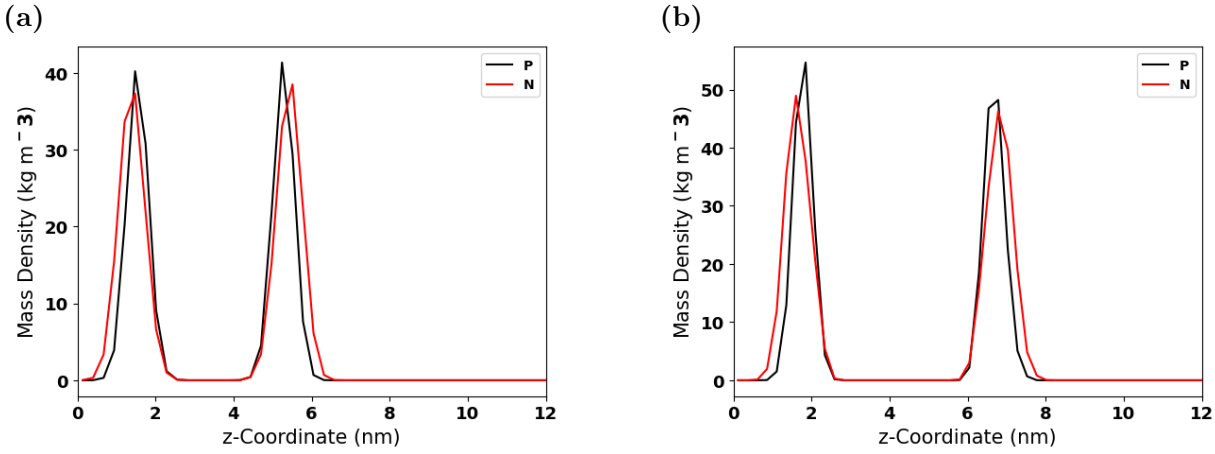

Figure S7: Mass density profiles of atom P and N in DOPC (a) or DPPC-CHOL (b) mixed membrane systems.

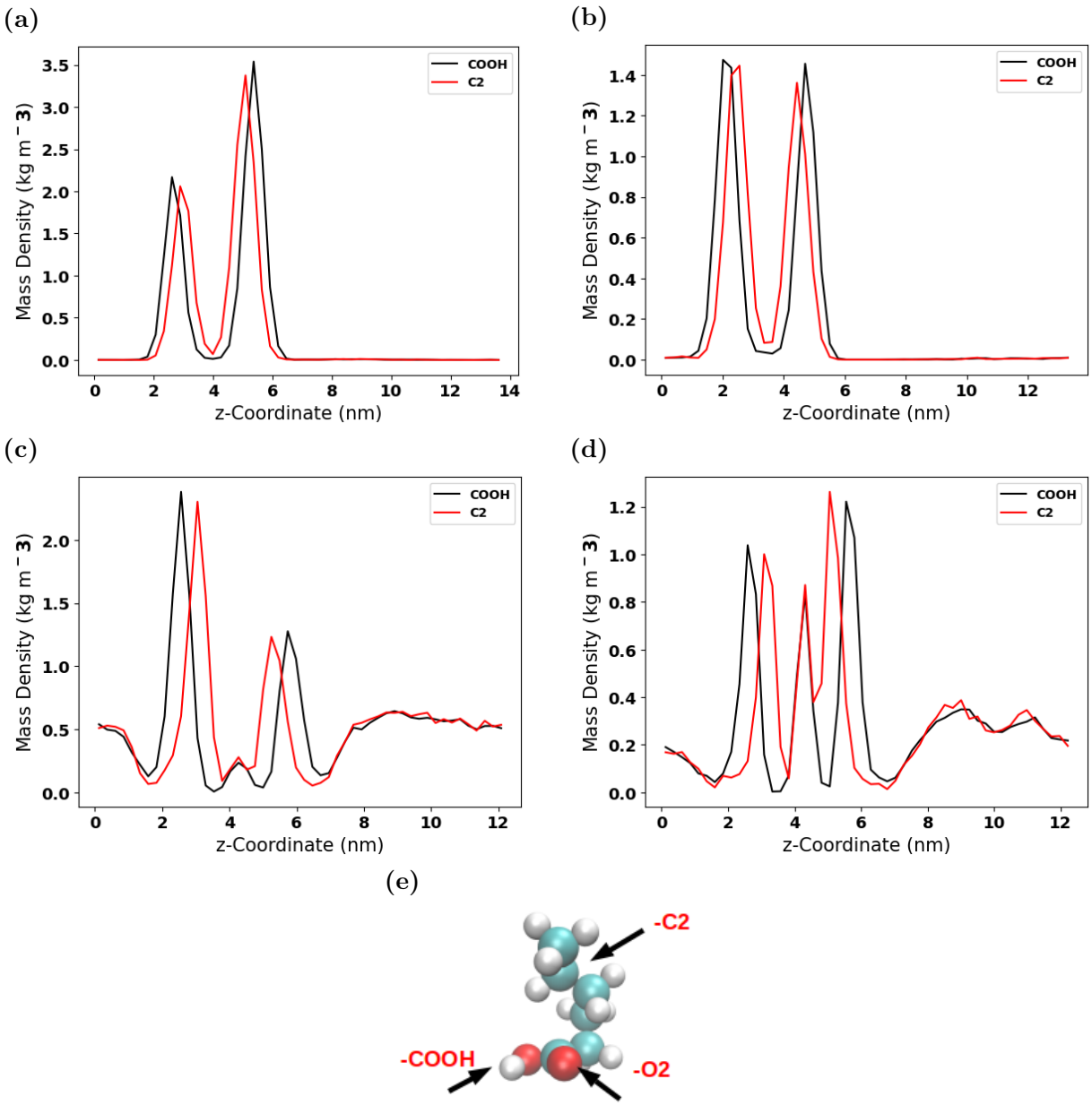

Figure S8: Mass density profiles of -COOH and C2 for C6FA in DOPC membrane systems with micelles (a) Pure-Products, (b) Mixed and DPPC-CHOL membrane systems with micelles (c) Pure-Products, (d) Mixed, (e) the structure of C6FA and atom labels that used for measuring the orientations of C6FA

Table S3: The first coordinate shell (nm) for the water oxygen atoms O_W with P, N, O3 from headgroups, glycerol ester and cholesterol respectively. The coordination number of waters is shown in parentheses.

System	Pure-DOPC	DOPC-Pure-Products	DOPC-Mixed	DOPC-Pure-Lipids	Pure-DPPC-CHOL	DPPC-CHO-Pure-Products	DPPC-CHOL-Mixed	DPPC-CHOL-Pure-Lipids
P	0.448(6.4)	0.448(6.4)	0.448(6.3)	0.448(6.3)	0.443(0.59)	0.446(5.9)	0.444(6.0)	0.446(6.0)
N	0.459(18.4)	0.604(19.4)	0.582(17.5)	0.584(17.6)	0.589(17.4)	0.596(17.4)	0.590(16.9)	0.594(17.1)
CHOL-O3	-	-	-	-	0.357(2.0)	0.358(2.0)	0.362(2.0)	0.368(2.1)

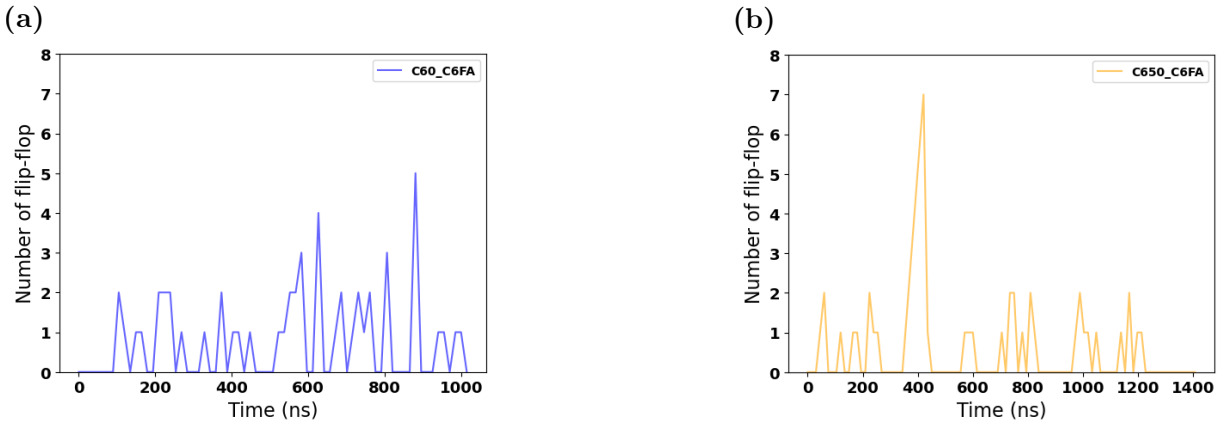

Figure S9: Number of flip-flip event for C6FA in DOPC-Pure-Products (a) and DOPC-Mixed (b) systems over time.

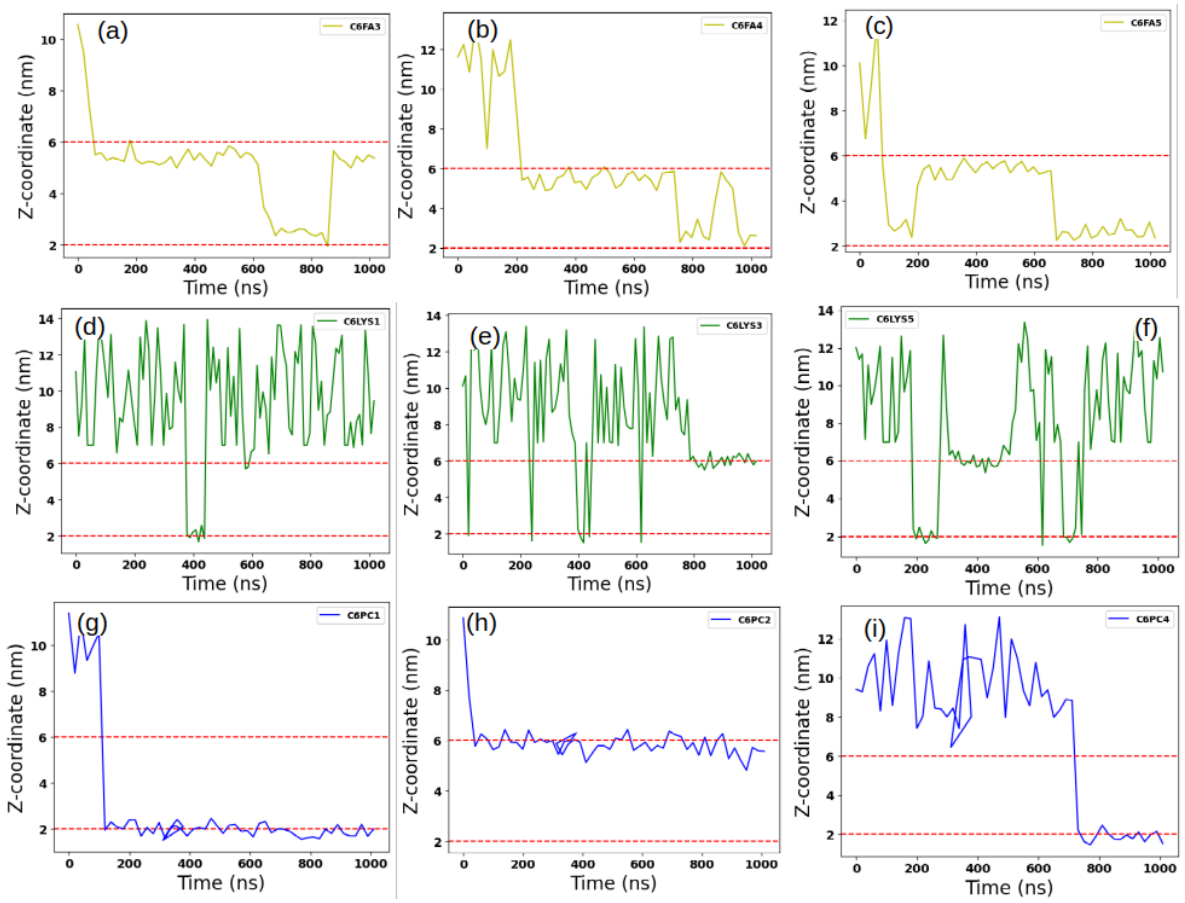

Figure S10: Z-coordinate of different molecules in DOPC membrane system profiles over time (a-c)C6FA, (d-f) C6LYS, (h-i) C6PC and the number followed after the molecule names indicate the index for different molecules. The red dashed lines represent the upper and lower limits of the bilayers.

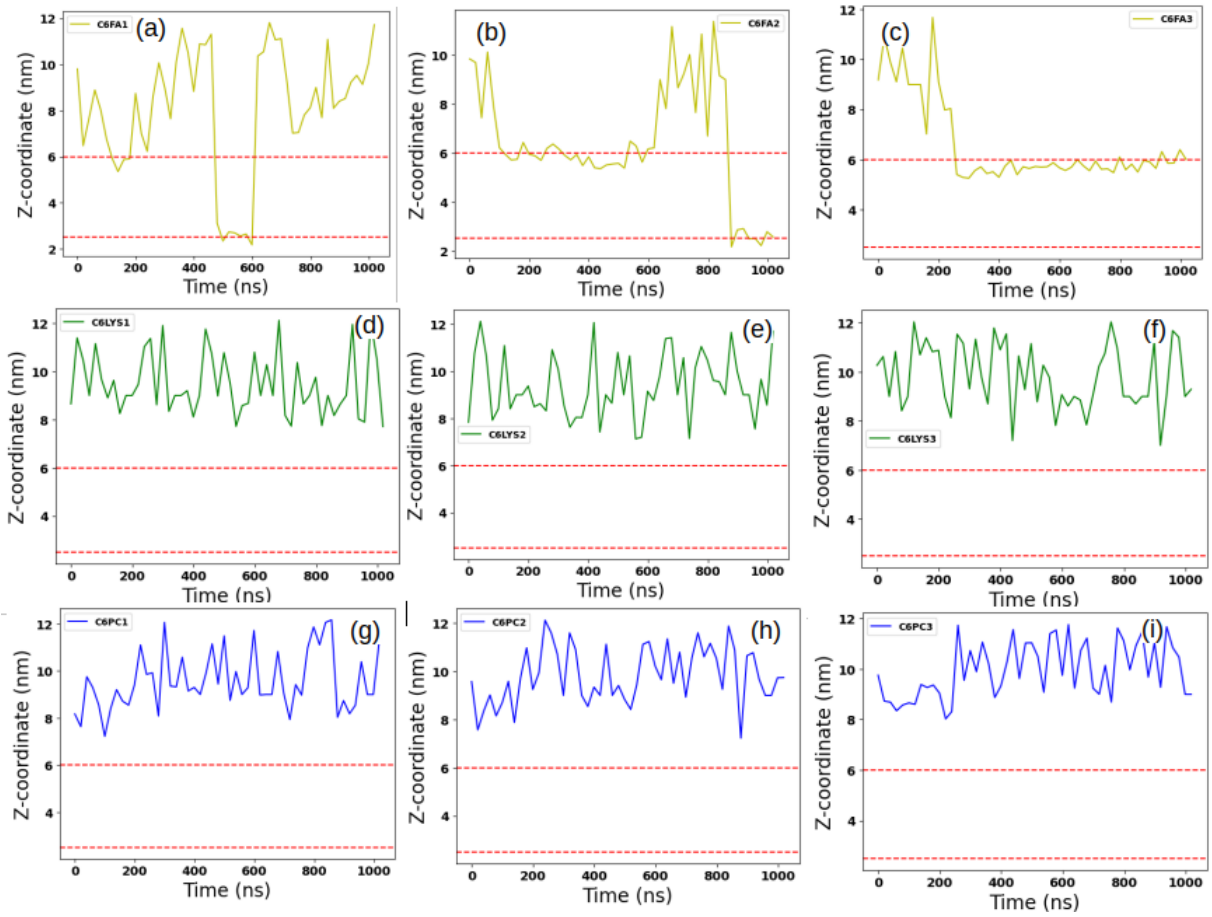

Figure S11: Z-coordinate of different molecules in DPPC-CHOL membrane system profiles over time ((a-c)C6FA, (d-f) C6LYS, (h-i) C6PC and the number followed after the molecule names indicate the index for different molecules. The red dashed lines represent the upper and lower limits of the bilayers.

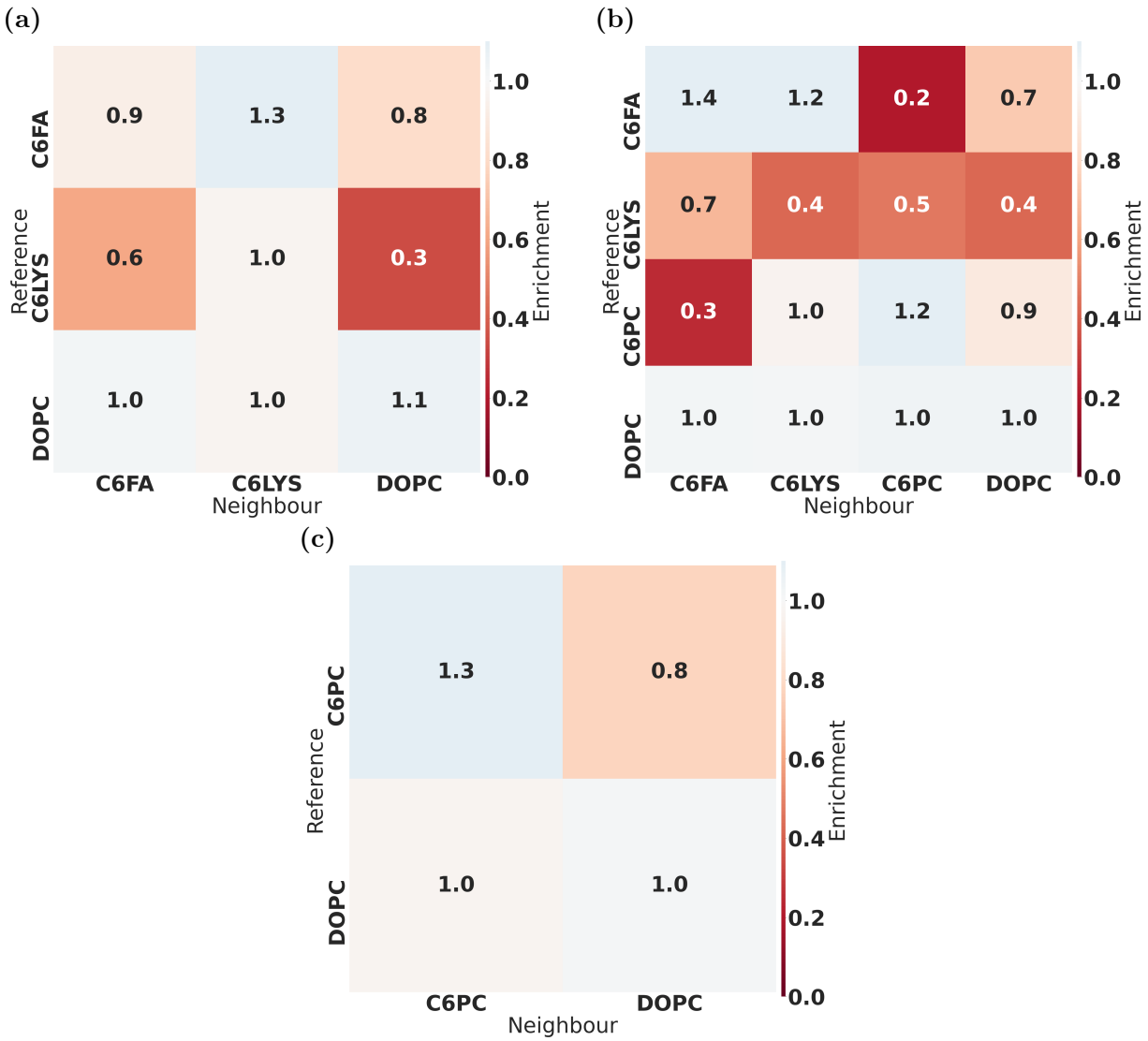

Figure S12: Enrichment/ Depletion index for DOPC-Pure-Products (a), DOPC-Mixed (b), DOPC-Pure-Lipids (c) membrane systems, calculated using the last 200 ns of each simulation. Values above and below 1 indicate enrichment and depletion, respectively.

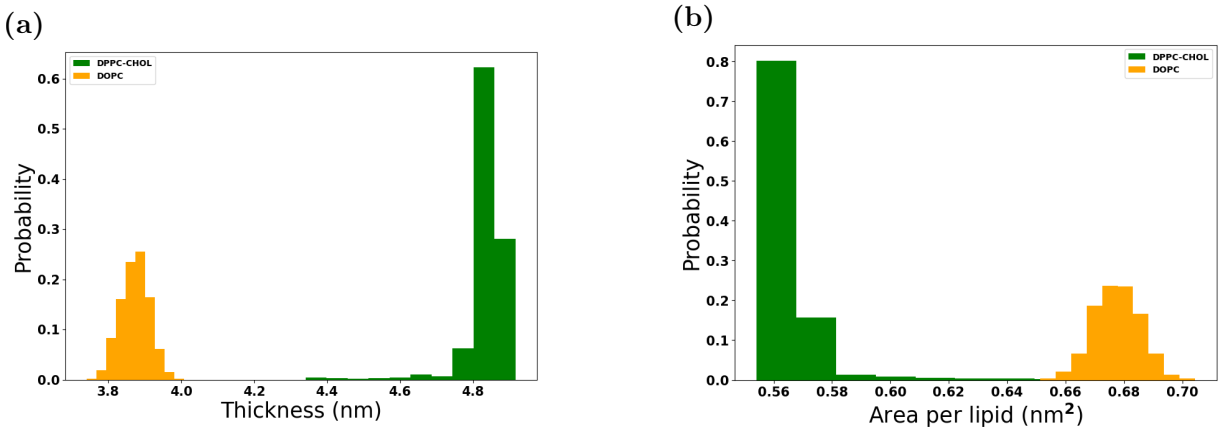

Figure S13: Membrane thickness (a) and area per lipid (b) as function of time in pure membrane systems.

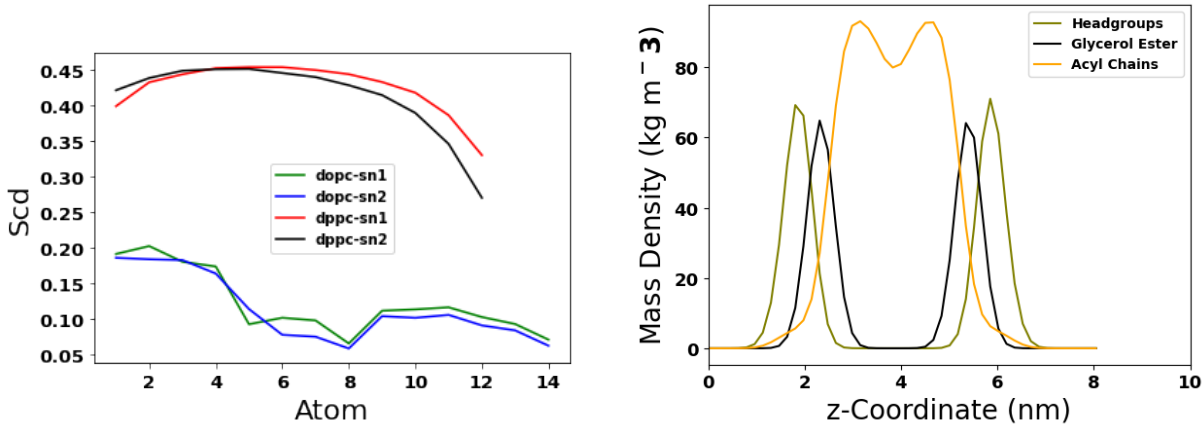

(a) order parameters **(b) mass density profile for DOPC**

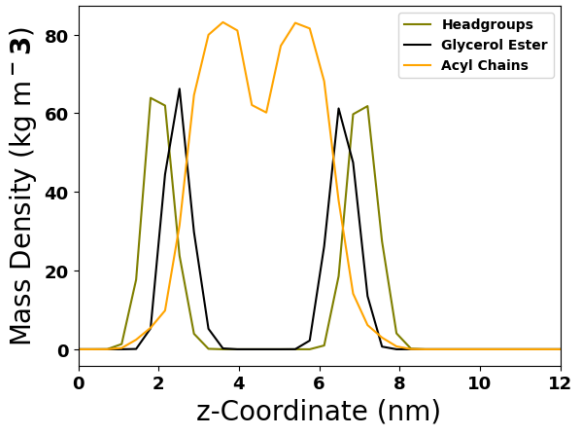

(c) mass density profile for DPPC-CHOL

Figure S14: The absolute values of (a) the lipid order parameters and mass density for the pure (b) DOPC and (c) DPPC-CHOL membranes.

Properties of Pure Membrane

Different phases of pure lipid membranes have been studied by various simulation and experimental methods.[1–3] In our study, we have measured several properties including the membrane thickness, the area per lipid and the lipid tail order parameter, to capture the differences in these two pure membrane systems and get them visualized shown in Figure S3. During the 200 ns simulation performed for the two membranes, the thickness of the DOPC system (Figure. S13(a)) fluctuates from 3.8 nm to 4.0 nm (the average value is 3.9 nm and the standard deviation is 0.04) whereas there is a increasing trend for DPPC-CHOL up to 4.87 nm. When it comes to the area per lipid, we find again that the value is more or less constant around 0.68 nm^2 (the average value is 0.68 nm^2 in DOPC membrane system (Figure. S13(b)) whereas in the DPPC-CHOL system We find that the area per lipid decreases over the first 25 ns and then reaches an approximate value of 0.57 nm^2 (the average value is 0.57 nm^2 and the standard deviation is 0.01 over the last 100 ns) . The fact that for the DPPC-CHOL membrane we have found a larger membrane thickness and a smaller area per lipid is in agreement with previous studies of similar systems which show these effects as a result of the condensing effect of cholesterol in membranes.[4–6] These results indicate that these two lipid membranes represent two distinct phases, liquid-disordered (DOPC) and liquid-ordered (DPPC-CHOL) phases. They are also in agreement with other studies that a decreased membrane thickness is normally accompanied by an increase in area per lipid.[7]

The profiles of the deuterium order parameter for DOPC and DPPC-CHOL membrane systems are shown in Figure S14(a) . The surface area of the lipids is normally inversely related to the deuterium order parameter. A more compact bilayer usually has a higher deuterium order parameter and vice versa.[8] We see that the value of order parameters for DPPC-CHOL is much larger than those for DOPC, which means the DPPC-CHOL systems are rigid in comparison with pure DOPC membrane and this trend is in agreement with the previously studied by Verde et al.[9,10] As the tails of each DOPC have two-double bonds and longer than DPPC (have two more carbon atoms), it also makes the structure of membrane

less stable and more fluid so the twisted lines can be observed as well. It has been proposed that the single bonds next to the double bond can rotate relatively easily.[11] The lowest point in DOPC membrane system (the green and blue lines) are located in the 8^{th} carbon where the position of double bond atom is and it makes it unstable. Comparing to the DPPC-CHOL membrane system (the red and black lines), each line for tails sn1 sn2 are more smooth and it means the structure of lipid changed less.

By computing mass density profiles for these two different pure membrane systems showed in Figure S14 (b) DOPC and (c) DPPC-CHOL, we can also determine the approximate positions of upper leaflet and lower leaflet with z-coordinate of headgroups on each system.

References

(1) Nagle, J. F.; Tristram-Nagle, S. Structure of lipid bilayers. *Biochim. Biophys. Acta Biomembr.* **2000**, *1469*, 159–195.

(2) Prates Ramalho, J.; Gkeka, P.; Sarkisov, L. Structure and phase transformations of DPPC lipid bilayers in the presence of nanoparticles: insights from coarse-grained molecular dynamics simulations. *Langmuir* **2011**, *27*, 3723–3730.

(3) Hakobyan, D.; Heuer, A. Phase separation in a lipid/cholesterol system: comparison of coarse-grained and united-atom simulations. *J. Phys. Chem. B* **2013**, *117*, 3841–3851.

(4) Loura, L. M.; do Canto, A. M. M.; Martins, J. Sensing hydration and behavior of pyrene in POPC and POPC/cholesterol bilayers: A molecular dynamics study. *Biochim. Biophys. Acta Biomembr.* **2013**, *1828*, 1094–1101.

(5) Shahane, G.; Ding, W.; Palaiokostas, M.; Orsi, M. Physical properties of model biological lipid bilayers: insights from all-atom molecular dynamics simulations. *J. Mol. Model.* **2019**, *25*, 1–13.

(6) Róg, T.; Pasenkiewicz-Gierula, M.; Vattulainen, I.; Karttunen, M. Ordering effects of cholesterol and its analogues. *Biochim. Biophys. Acta Biomembr.* **2009**, *1788*, 97–121.

(7) Tristram-Nagle, S.; Petrache, H. I.; Nagle, J. F. Structure and interactions of fully hydrated dioleoylphosphatidylcholine bilayers. *Biophys. J.* **1998**, *75*, 917–925.

(8) Douliez, J.-P.; Leonard, A.; Dufourc, E. J. Restatement of order parameters in biomembranes: calculation of CC bond order parameters from CD quadrupolar splittings. *Biophys. J.* **1995**, *68*, 1727–1739.

(9) Bonn, M.; Roke, S.; Berg, O.; Juurlink, L. B.; Stamouli, A.; Müller, M. A molecular view of cholesterol-induced condensation in a lipid monolayer. *The Journal of Physical Chemistry B* **2004**, *108*, 19083–19085.

(10) Leekumjorn, S.; Wu, Y.; Sum, A. K.; Chan, C. Experimental and computational studies investigating trehalose protection of HepG2 cells from palmitate-induced toxicity. *Biophys. J.* **2008**, *94*, 2869–2883.

(11) Kulig, W.; Pasenkiewicz-Gierula, M.; Róg, T. Cis and trans unsaturated phosphatidylcholine bilayers: a molecular dynamics simulation study. *Chem. Phys. Lipids* **2016**, *195*, 12–20.